



Master Thesis

Covalent Linkage of π -Extended Pt(II)-Porphyrins to Silicone Matrices

- A Convenient Way to Obtain Optical Trace Oxygen Sensors

Bernhard Müller

Zur Erlangung des akademischen Grades

"Diplom-Ingenieur"

der Studienrichtung Technische Chemie

eingereicht an der

Technischen Universität Graz

Supervisor

Univ.-Prof. Dipl.-Chem. Dr.rer.nat. Ingo Klimant

Institute of Analytical Chemistry and Food Chemistry

University of Technology, Graz

2014

Abstract

In this thesis, a new optical trace oxygen sensor material was developed. The luminescent indicator dye, Pt(II)-benzoporphyrin, was synthesized via two different synthetic routes; namely the Lindsey Condensation and the Template Method. The obtained indicator can undergo Suzuki-coupling reaction in order to get styrene-modified benzoporphyrin dyes, which can be used subsequently for covalent immobilization to a polymer matrix.

A highly gas permeable silicone matrix was obtained by the addition of a hydride- and vinyl-containing polysiloxane using hydrosilation reaction for curing. The indicator acts as crosslinker in this step and is covalently linked to the matrix, which prevents aggregation and leaching of the dye.

By applying differently substituted polysiloxanes a fine tuning of the sensitivity was achieved. The obtained sensor shows linear Stern-Volmer plots from 0 to 20 hPa O_2 with K_{SV} values between 0.183 and 0.088 hPa^{-1} . This makes them suitable for measuring trace oxygen concentrations. The new developed sensor material was tested for its suitability for oxygen measurements through colored wine bottles.

Kurzfassung

In dieser Arbeit konnte ein neues Sensormaterial für optische Sauerstoffmessung im Spurenbereich entwickelt werden. Der verwendete lumineszierende Indikatorfarbstoff, Pt(II)-Benzoporphyrin, konnte über zwei verschiedene Synthesewege, die Lindsey Kondensation und die Template Methode hergestellt werden. Der Farbstoff konnte mit Styren-Gruppen über Suzuki-Kupplung modifiziert werden, welche in weiterer Folge zur kovalenten Immobilisierung in einer Polymermatrix verwendet werden konnten.

Zur Herstellung einer hoch Gas permeablen Silikonmatrix wurden Hydrid- und Vinyl-modifizierte Polysiloxane mittels katalytischer Hydrosilierung vulkanisiert. Der Farbstoff wirkt in diesem Schritt als Vernetzer und wird kovalent in der Matrix gebunden, wodurch Aggregationen und Auswaschen des Farbstoffes verhindert wird.

Durch Verwendung unterschiedlich substituierter Polysiloxane konnte eine Feintuning der Sensitivität des Sensors durchgeführt werden. Die neuen Sensormaterialien zeigen lineare Stern-Volmer Plots in einem Bereich von 0 - 20 hPa O_2 mit K_{SV} Werten von 0,183 bis 0,088 hPa^{-1} . Sie können somit verwendet werden um Sauerstoff im Spurenbereich zu messen. Des Weiteren wurde untersucht, ob sich das neue Material zur Messung von Sauerstoff durch gefärbte Weinflaschen eignet.

Statutory Declaration

I declare that I have authored this thesis independently, that I have not used other than the declared sources / resources, and that I have explicitly marked all material which has been quoted either literally or by content from the used sources.

28 January, 2014

Date

Signature

Acknowledgement

An erster Stelle möchte ich mich bei Prof. Ingo Klimant bedanken. Die sehr lehrreichen Diskussionen, deine stets offene Bürotüre und motivierenden Besprechungen sind, genauso wie deine Art das Institut zu leiten Hauptgründe, weswegen ich so gerne hier arbeite.

Sergey - danke dass ich immer auf deine Hilfe zählen konnte, egal zu welcher Uhrzeit und an welchem Wochentag. Deine Leidenschaft für Forschung und Lehre sind für mich noch immer beeindruckend.

Ein großes Dankeschön gebührt meinem Master-Mitstreiter Christoph, von dessen unendlichen Wissen ich immer wieder profitiere.

Tobi - dank dir leide ich niemals unter Koffeinmangel und es wird durch unserer Blödelein nie langweilig. Wie du die Nerven an manchen Tagen bewahrst finde ich immer wieder Wahnsinn. Beim Rest der Arbeitsgruppe möchte ich mich gerne für die gemeinsamen Mittagessen, unterhaltsamen Kaffeepausen, Diskussionen unterschiedlichsten Niveaus, lustigen Aktivitäten usw. bedanken. Es herrscht ein so angenehmes, amüsanter Klima in unserer Arbeitsgruppe bzw. unserem Institut, dass es mir immer wieder eine Freude ist auf die Uni zu gehen. Ich hoffe, wir können das beibehalten.

Zusätzlich möchte ich mich natürlich auch bei den Menschen bedanken, die nicht zur "Fixbesetzung" gehören und nur ein paar Wochen / Monate mit der Arbeitsgruppe verbracht haben.

Weiters muss ich mich bei Klaus und Luki bedanken. Ohne euch hätte ich wohl nie diesen Weg eingeschlagen.

Danke an den 08er Jahrgang für eine unvergessliche Studienzeit. Ich finde, wir haben das außerordentlich gut gemeistert und eine gute Balance zwischen feiern und studieren gefunden. Wir haben uns gegenseitig gepusht und ohne gemeinsame Lerngruppen hätte ich das Studium nie geschafft.

Bei meinen alten Schulfreunden bedanke ich mich für tolle Besuche und spaßige Abende Zuhause im Mühlviertel.

Maria, danke für die abwechslungsreichen, lustigen, abenteuerlichen und gemütlichen letzten Jahre und für deine Unterstützung.

Der größte Dank gebührt meiner Familie, die mich nicht nur finanziell unterstützt haben sondern mich auch meinen Weg gehen lassen und dabei unterstützt haben.

Contents

1	Introduction	1
2	Theoretical Background	3
2.1	Luminescence	3
2.1.1	Non-Radiative Deactivation	6
2.1.2	Radiative Deactivation	6
2.1.3	Lifetimes	8
2.1.4	Quantum Yield	9
2.1.5	Quenching	10
2.2	Optical Oxygen Sensors	12
2.2.1	Basic Principle of Optical Sensors	12
2.2.2	Optical Oxygen Sensors	13
2.2.3	Sensitivity of a Sensor	15
2.3	Indicators	16
2.3.1	The Perfect Indicator	16
2.3.2	Commonly Used Indicators	16
2.4	Matrices	19
2.4.1	Silicone Rubbers Used for Optical Sensors	20
2.4.2	Hydrosilation	22
2.5	Covalent Immobilization Techniques of Porphyrins	23
3	Materials and Methods	25
3.1	Photophysical Measurements	25
3.1.1	Absorption	25
3.1.2	Emission and Excitation Spectra	25
3.1.3	Single Photon Counting	25

3.1.4	Photostability	25
3.1.5	Calibration of the Sensor Materials	26
3.2	Structural and Chemical Measurements	26
3.2.1	Solubility	26
3.2.2	NMR	26
3.2.3	Mass Spectrometry	26
4	Experimental	27
4.1	Lindsey Synthesis	27
4.1.1	1-Nitro-2-iodocyclohexan	27
4.1.2	1-Nitrocyclohexen	27
4.1.3	2H-Isoindol-4,5,6,7-tetrahydro-1-carboxylic acid ethyl ester	28
4.1.4	4,5,6,7-Tetrahydroisindol	29
4.1.5	H ₂ TPTCHPBr ₄	29
4.1.6	Pt-TPTCHPBr ₄	31
4.1.7	Pt-TPTBPBr ₄	32
4.1.8	Pt-TPTBPStyr ₄	33
4.2	Template Synthesis	34
4.2.1	Zn-TPTBPtBu ₄ Br ₄	34
4.2.2	H ₂ TPTBPtBu ₄ Br ₄	35
4.2.3	Pt-TPTPtBu ₄ Br ₄	36
4.2.4	Pt-TPTPtBu ₄ Br ₃ Styr	37
4.2.5	PtTPTPtBu ₄ Styr ₄	38
4.3	Optimizing of the Platination Reaction	39
4.4	Sensor Preparation	39
4.4.1	General Procedure	39
4.4.2	Sensor for Measurements Through Wine Bottles	40
5	Results and Discussion	43
5.1	Synthetic Considerations	43
5.1.1	Lindsey Condensation	43
5.1.2	Template Synthesis	46
5.1.3	Optimizing the Platination	48

5.2	Dye Characterization	55
5.2.1	Absorption- and Emissionspectra	55
5.2.2	Influence of the t-Butyl Group	56
5.2.3	Photobleaching	57
5.3	Sensor Materials	59
5.3.1	The Dye in Different Media	61
5.3.2	Influence of Pot-Time and Knife Coating	61
5.3.3	Mono and Tetra-Styrene Dyes with Different Crosslinkers	62
5.3.4	Influence of Different Amounts of Used Crosslinker	64
5.3.5	Influence of Different Backbones	66
5.3.6	Leaching Experiment	70
5.3.7	Temperature Dependency of the Sensor	72
5.3.8	Comparison with Other Trace Oxygen Sensors	73
5.3.9	Immobilisation Without Backbone	74
5.3.10	Reaction With Monohydriddopolysiloxane	75
5.4	Application of the New Sensor Material - Wine Bottles	76
5.4.1	Transmission Spectra of Wine Bottles	76
5.4.2	Excitation and Emission Spectrum	78
5.4.3	Single Photon Counting	79
5.4.4	Measuring Through Wine Bottles	80
6	Conclusion	83
7	References	85
8	Appendix	97
8.1	NMR Data	97
8.2	MALDI-TOF Data	106
8.3	List of Chemicals	113
8.4	Abbreviations	115

1 Introduction

Oxygen is one of the most important analytes on earth. It can be quantified by Winkler titration, Clark electrode and optical sensors. The latter provides the advantage of being inexpensive and miniaturizable. They do not suffer from electrical interferences and they do not consume oxygen.

Many optical oxygen sensors are available for the physiological concentration range. Their applications range from medical applications [1] over biotechnology[2] to food packaging [3].

However, measuring trace oxygen concentrations is also of interest in the food and brewing industry [4], as oxygen can have negative effects on the taste and color of foods, like beer. Oxygen is also responsible for the quality of a wine. Additionally optical sensors can be used to detect oxygen leaks or measurements in so called "oxygen-minimum-zones" in marine science[5].

The aim of this work was the development of an optical oxygen sensor, which is able to measure oxygen partial pressures between 0 and 20 hPa. A possible application of the new sensor would be the measurement of oxygen through wine bottles. Due to their coloration and the resulting low transmission of certain wavelengths in the UV-Vis region, it is necessary to use indicators which are not influenced by this. Tetrabenzoporphyrins (TBP) appear to be suitable candidates for this application as they provide unique properties like emitting in the NIR, high molar extinction coefficients and good photostability.

Usually, trace oxygen sensors are based on Pd(II)-porphyrins because of their long luminescent lifetime and the resulting high sensitivity. A shortcoming of Pd-complexes is that they are not as bright due to lower quantum yields, compared to the homologue Pt(II)-complexes. For this reason and the requirement for measuring through low transmitting glass, the sensor has to be based on a Pt(II)-complex. However, the latter has shorter lifetimes (around 60 μ s) and cannot be used for trace oxygen measurements when embedded in organic polymers like polystyrene.

Silicones are widely used as matrices for optical sensors because of their high gas permeability. Encapsulating the Pt-TBP in this matrix would increase the sensitivity tremendously. Due to the hydrophobic character of silicone, the indicator would aggregate and leach out of the ma-

trix which would compromise the sensors performance. This shortcoming could be overcome by means of covalent coupling of the indicator dye with the matrix.

To realize that, a suitable Pt-TPTBP indicator dye with functional groups which can undergo coupling reactions has to be synthesized and photophysically analysed. Also, a procedure for manufacturing silicone rubbers with a covalently linked dye has to be established. This new sensor material had to be tested for its suitability for measuring in wine bottles.

2 Theoretical Background

2.1 Luminescence

This chapter is based on reference [6]. Other references will be cited independently. The term luminescence describes the emission of photons due to relaxation of an excited system. First an electron is excited from its ground state to a higher electronically excited state. Then it falls back to the energetically lower ground state releasing energy in form of electromagnetic radiation. The emission is either called fluorescence, if the relaxation is spin-allowed or phosphorescence, if it is spin-forbidden. The excitation of the electron can be caused by several environmental influences. For instance in photoluminescence the molecule reaches the electronically excited state by the absorption of photons. This molecule can be called luminophore or dye.

Absorption

If a photon of discrete energy from the UV-Vis region is absorbed by a molecule in its ground state an electron is promoted to a higher unoccupied energy level. The energy between ground state and excited state is equal to the energy of the absorbed photon. Two types of orbitals are considered to be of importance for the absorption; the highest occupied molecular orbital (HOMO) and the lowest unoccupied molecular orbital (LUMO) in reference to the ground state. The excitation of an electron can occur from a sigma(σ), pi(π) or non-bonding orbital to an excited sigma or pi orbital (σ^* and π^*).

Excitations of σ electrons usually require high energy in the far UV light, which is not important for spectroscopic applications. Absorptions to π^* usually occur in the UV-Vis region. If the π -electron system of a molecule is extended, less energy and therefore a larger wavelength for the $\pi \rightarrow \pi^*$ transition is needed. The absorption efficiency at a certain wavelength can be described by the Lambert Beer law.

$$A = \log \left(\frac{I_0}{I} \right) = \epsilon \cdot c \cdot d \quad (2.1)$$

I_0 ... Intensity of light before the sample

I ... Intensity of light after the sample

ϵ ... Molar absorption coefficient

c ... Concentration of the dye

d ... Optical path length of the sample

Franck-Condon principle

According to the Born-Oppenheimer approximation, the electron movement is by far faster than the movement of the nuclei. A promotion of one electron to an excited molecular orbital takes about 10^{-15} seconds. This is very fast compared to the time range in which molecular vibrations take place ($10^{-10} - 10^{-12}$ seconds), indicating that the nuclei of a molecule do not change their positioning towards each other whilst electron transitions take place. This means that the atoms are equidistant to each other in the ground state as well as in the excited state.

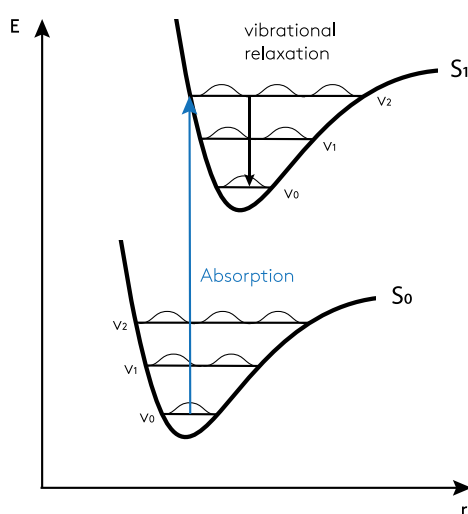


Figure 2.1: Franck-Condon principle

Two atoms in an excited state have weaker bonds; therefore the Morse potential minimum is situated at larger nuclei distance. Thus excited electrons are promoted to the energetically higher vibrational levels of the excited state. This is immediately followed by non-radiative vibrational relaxation to the lowest vibrational level of the excited state. The energy is passed

to other molecules or is transformed to heat radiation via vibration or rotation of the molecule itself. This process is faster than all other transformations in the electronic state. Information about the vibrational states of the ground state can be obtained by the emission spectra and information of the excited state by the absorption spectra.

Transitions between Electronic States

The different energy states of an electron are usually displayed in a Jablonski diagram. Spin multiplicity is horizontally and energy is vertically arranged.

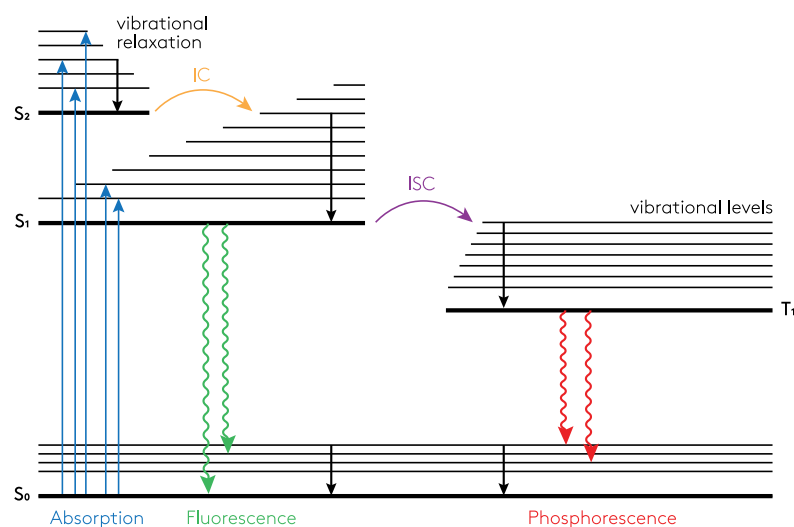


Figure 2.2: Jablonski-Diagram

S_0 is the singlet ground state, S_1 and S_2 are the excited singlet states and T_1 is the excited triplet state. The triplet state is energetically lower than the singlet state in accordance to Hunds Rule. Absorption elevates a electron to one of the vibrational levels of the excited states. Electronic transition can only occur, if the spin multiplicity does not change during excitation. This means that only singlet-singlet or triplet-triplet transitions are allowed. Singlet-triplet transitions are quantum-mechanically forbidden as the spin is changed. Nevertheless, they can occur under certain conditions. After absorption, the electron can undergo different de-excitation processes.

2.1.1 Non-Radiative Deactivation

Internal Conversion (IC)

IC is a non-radiative transition from a higher to a lower electronic state within the same multiplicity. It is usually followed by vibrational relaxation to the vibrational ground state. If the energy gap between the involved states increases, the efficiency of IC decreases. IC from $S_2 \rightarrow S_1$ can be observed in a time scale of $10^{-13} - 10^{-11}$ seconds. The energy gap from $S_1 \rightarrow S_0$ is larger and therefore other de-excitation processes can take place. An excited molecule can remain in the S_1 state between $10^{-11} - 10^{-7}$ seconds.

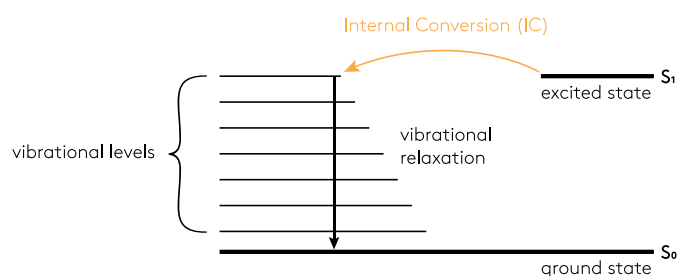


Figure 2.3: Scheme for internal conversion

Intersystem Crossing (ISC)

Intersystem crossing describes the transition from the singlet state to the triplet state of the equal vibrational level. The vibrational relaxation brings the molecule to its lowest vibrational level, T_1 . This process includes the change of the spin, which is quantum-mechanically forbidden. However, in some cases spin-orbit coupling is strong enough to provide the possibility for ISC. For example, heavy atoms like Br or Pb can increase spin-orbit coupling and therefore increase ISC. The time-rate is with $10^{-9} - 10^{-7}$ seconds fast enough to compete with other deactivation processes. Once ISC took place, the lifetime of T_1 can be up to $10^{-6} - 1$ seconds.

2.1.2 Radiative Deactivation

Fluorescence

Fluorescence is the emission of photons from S_1 to different vibrational levels of S_0 . It is independent of the excitation wavelength due to prior vibrational relaxation to the lowest vibrational

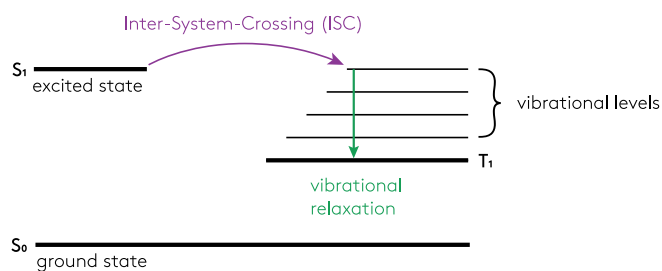


Figure 2.4: Scheme for intersystem crossing

state of S_1 before emission. This means, that the emitted light has lower energy than the absorbed light and therefore emission spectra are shifted to the red region in respect to absorption spectra. The difference of absorption and fluorescence wavelenghts is called Stokes shift. The emission a photon is as fast as absorption ($10^{-15}s$).

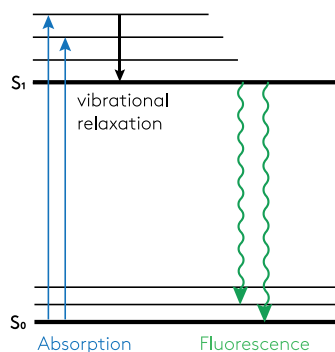


Figure 2.5: Scheme for fluorescence

Phosphorescence

The emission of photons from T_1 to S_0 is called phosphorescence and can only take place after ISC. Both processes are quantum-mechanically forbidden and rely on strong spin-orbit coupling. Thus the time rate is very slow ($10^{-6} - 1second$). Due to that non-radiative processes like reverse ISC and IC can compete with phosphorescence. At higher temperatures these deactivations outweigh, but working at low temperatures and rigid mediums can enhance phosphorescence. As the T_1 state is lower than the S_1 state phosphorescence emits at higher wavelenghts than fluorescence.

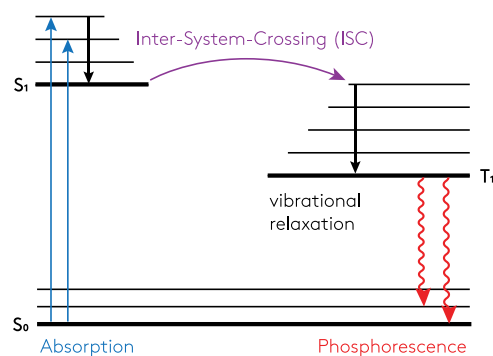


Figure 2.6: Scheme for phosphorescence

Delayed Fluorescence

Delayed fluorescence is the emission from S_1 - S_0 after intersystem crossing to T_1 and following reverse intersystem crossing back to S_1 . The emission spectrum is the same as in the fluorescence, but the luminescence lifetime is much longer. The process of delayed fluorescence is dependent on temperature since reverse intersystem-crossing occurs more likely at higher temperatures and the energy difference between T_1 and S_1 has to be small enough.

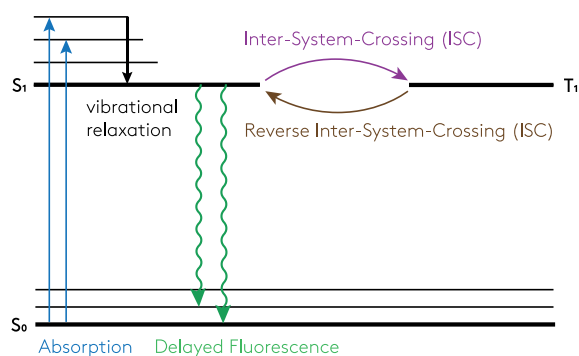


Figure 2.7: Scheme for delayed fluorescence

2.1.3 Lifetimes

If a molecule is promoted to the excited state S_1 , it can consequently undergo several different processes. There is for example deactivation via fluorescence emission and non-radiative de-excitation via IC or ISC. These processes do not occur immediately and the molecule remains in the excited state S_1 for a certain period of time. The rate of de-excitation can be described by first order kinetics.

$$-\frac{d[A^*]}{dt} = k \cdot [A^*] \quad (2.2)$$

where $[A^*]$ is the concentration of a species A in the excited state and k the sum of all possible de-activation rates.

$$k = k_{\text{radiative}} + k_{\text{non-radiative}} \quad (2.3)$$

Integration of equation 2.2 with the following definition of the excited state lifetime τ .

$$\tau = k/t \quad (2.4)$$

yields in

$$[A^*]_t = [A^*]_0 \cdot e^{-t/\tau} \quad (2.5)$$

This means that the fluorescence intensity decreases exponentially if excitation does no longer occur. The fluorescence decay time τ defines the time window for various dynamic phenomena. The lifetimes for the excited states S_1 and T_1 usually range from $10^{-11} - 10^{-7}$ s and $10^{-6} - 1$ s.

2.1.4 Quantum Yield

Not every absorbed photon is then emitted via radiation since faster non-radiative de-excitation processes accompany fluorescence and phosphorescence. The quantum yield is defined as the ratio of emitted photons compared to the number of absorbed photons. This can be calculated via formula 2.6.

$$\phi_F = \frac{\text{emitted photons}}{\text{absorbed photons}} = \frac{\tau_S}{\tau_r} = k_r \cdot \tau_S \quad (2.6)$$

τ_S lifetime of the excited state

τ_r radiative lifetime

k_r radiative rate constant

With increasing temperature the quantum yield decreases, as non-radiative processes are more likely to occur.

2.1.5 Quenching

All de-excitation processes mentioned so far are categorized as intrinsic phenomena. The term quenching describes the photo-physical interaction between an excited molecule (M^*) and a quencher (Q), which is responsible for the de-excitation of M^* . Quenching is a bimolecular reaction in which K_q is the rate constant. Intermolecular processes which cause de-excitation can be the collision with heavy atoms, electron transfer, the formation of excimer / exciplex, proton transfer or energy transfer. Due to this possible interactions, fluorescence characteristics like decay time or quantum yield are affected because intrinsic and intermolecular de-excitation processes compete.

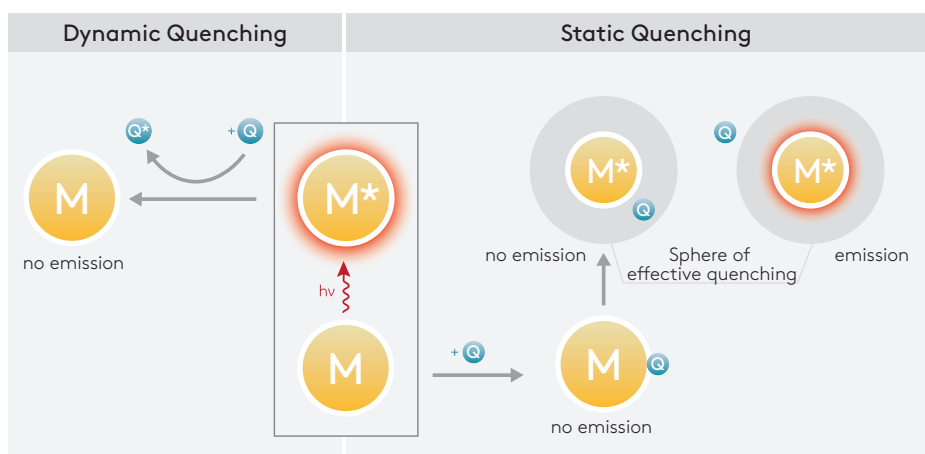


Figure 2.8: Different quenching mechanisms

Static Quenching

Static quenching results in the formation of a non-fluorescence MQ complex. This complex can be formed via M and Q in the ground states or via a sphere of effective quenching in the excited state of M . The latter requires Q and M^* to be in a small distance to each other in order for quenching to occur. Both models result in a decrease of luminophore concentration and consequently a decrease in fluorescence intensity. Nevertheless, the characteristic lifetime of the un-complexed luminophore is not effected

Dynamic Quenching

In this case the quencher interacts with the molecule while it is still in its excited state.

The collision of Q with M^* and therefore the transfer of energy in a non-radiative process to Q is more likely if the excited state lasts longer. This process is diffusion-controlled and the rate constant is therefore time dependent. The lifetime of the luminophore is reduced in the presence of a quencher. The ratio of I_0/I is proportional to τ_0/τ . If Q and M are the same molecule, self-quenching can occur. This is called an excimer, which has its own characteristic fluorescence spectrum and lifetime.

To visualize the kinetics of dynamic quenching the Stern-Volmer plot is used. It shows the correlation between the ratio I_0/I (equivalent to τ_0/τ) and the rate constant $k_q\tau_0$. Both τ_0/τ and I_0/I show a linear increase over the quencher concentration. K_{SV} represents the slope of the curve.

$$\frac{I_0}{I} = \frac{\tau_0}{\tau} = 1 + k_q \cdot \tau_0 \cdot [Q] = 1 + K_{SV} \cdot [Q] \quad (2.7)$$

I_0/τ_0 ... Fluorescence intensity/luminescence in the absence of Q

I/τ_0 ... Fluorescence intensity/luminescence in the present of Q

$k_q \cdot \tau_0 = K_{SV}$... Stern Volmer constant

2.2 Optical Oxygen Sensors

2.2.1 Basic Principle of Optical Sensors

This section is based on reference [7] and [8]. Other references will be cited independently. Sensors have become an important part of our everyday life, with their ability to measure certain environmental parameters quantitatively and qualitatively. A chemical sensor is in direct contact with the environment through a receptor, which is sensible to specific analytes or a group of analytes.

The overall purpose of a chemical sensor is responding to certain chemical, or biochemical compounds - an analyte - and process the received information into a measurable electronic signal. In order to produce this signal the analyte is neither decomposed nor compromised by the chemical sensor, which makes them suitable for long-term measurements as well as real-time monitoring. The broad range of applications is one of the major advantages of chemical sensors in comparison to many other analytical instruments. Moreover chemical sensors are not restricted to monitoring chemical reactions, but can also measure physical properties for instance and output the information as robust and easily processible data.

In general an optical sensor consists of a receptor, a transducer and a device transforming the received information into processible data. The receptor is responsible for the interaction -the bonding -with the analyte, causing an alteration of the system. A synthetically produced receptor is called a "chemosensor", but if the receptor consists of naturally occurring biological substances, like DNA, enzymes or anti-bodies it is called a biosensor [9]. The transducer usually has either a characteristic absorbance or luminescence which is sensible to those alterations, mentioned before, resulting in a measurable optical signal which is subsequently out-putted as processible data. The basic "set-up" can be changed in order to eliminate unwanted signals by preventing certain compounds from binding to the receptor. This can be achieved for example by introducing a polymer layer with specifically chosen properties functioning as a barrier to certain species. Another advantage of immobilizing the indicator dye in a polymer matrix is the even distribution of the dye, achieving better comparable and reproducible results.

There are many different types of chemical sensors, tailored to meet certain expectations and

monitor various parameters. They should be easy to use, but still provide a great accuracy. Optical sensors can be divided into two categories, the intrinsic and the extrinsic optical sensors. An intrinsic optical sensor simply responds to the optical properties of the analyte and nothing else. An extrinsic optical sensor on the other hand produces a signal based on the interaction of the analyte with an indicator (for example a dye) as the analyte itself does not give a signal. Such an indicator can interact physically as well as chemically with the analyte, resulting in a - for the optical sensor detectable - alteration of its properties, which is subsequently transformed in an electronic signal.

Optical sensors provide a huge range of applications as they are suitable for measurements of oxygen, CO₂, NH₃, pH and ionic species as they respond to optical phenomena like absorption, refractivity or luminescence.

2.2.2 Optical Oxygen Sensors

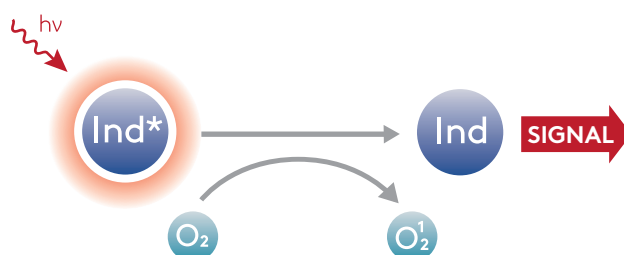


Figure 2.9: Principle of an optical oxygen sensor

The principle of optical oxygen sensors relies on dynamic quenching of a luminophore indicator dye by oxygen. Oxygen is present in a triplet state as its ground state. It is excited into a singlet state by energy transfer from the excited indicator dye. The efficiency of the quenching process increases with longer ES lifetimes of the indicator. Therefore, phosphorescent dyes are more suitable for optical oxygen sensing. Typically the luminescent indicator dye is physically entrapped in an oxygen permeable polymer matrix [10]. This matrix acts as solvent for the dye and keeps the concentration of the dye even via immobilization. Moreover, it acts as barrier for ions and other unwanted species. The quenching causes a decrease of the luminescent lifetime. The connection of lifetime and concentration is described in the Stern-Volmer-Plot (eq.2.8).

$$\frac{I_0}{I} = \frac{\tau_0}{\tau} = 1 + K_{SV} \cdot [O_2] \quad (2.8)$$

I_0/τ_0 ... Luminescence intensity/luminescence in the absence of Q

I/τ_0 ... Luminescence intensity/luminescence in the present of O_2

K_{SV} ... Stern Volmer constant

The Stern-Volmer-Plot only provides information for the ideal case that the dye is evenly accessible to quenching. However, due to the immobilization of the dye in a heterogenic matrix the plot shows a downward curvature. This curvature can be described by the Two-Site- Model, which assumes that two different quenching domains exist[11].

$$\frac{\tau_0}{\tau} = \frac{1}{\frac{f}{1+K_{SV1} \cdot [O_2]} + \frac{1-f}{1+K_{SV2} \cdot [O_2]}} \quad (2.9)$$

τ_0 ... Fluorescence lifetime in the absence of O_2

τ ... Fluorescence lifetime in the present of O_2

$K_{SV1/2}$... Different Stern-Volmer constants of individual quenching domains

f ... Influence of one domain on the observed lifetime

$[O_2]$... Oxygen concentration

In less curved calibrations plots, it is possible to use the simplified Two-Site-Model in which one of the Stern-Volmer constants is set to zero. This means, there is one domain in which quenching can occur and one in which it cannot [11].

The measurement of the intensities provides many disadvantages, as signal fluctuations or photobleaching of the dye. This can be caused by a change in the intensity of the excitation source or a concentration variability of the indicator dye in the sensor. Therefore, in order to determine the oxygen concentration, lifetime-based measurements of the luminescent dye is preferred. This is carried out by using phase-fluorimetry. The light used for excitation is modulated at a particular frequency; however, the emitted light shows the same frequency but the phase and the amplitude are shifted. The phase shift is in relation to the lifetime as described in formula

2.10.

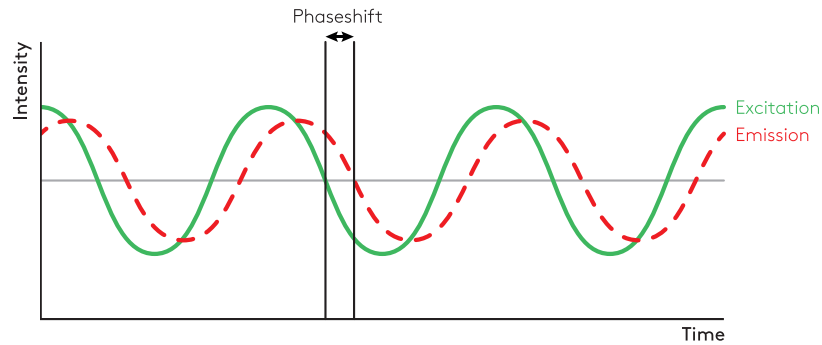


Figure 2.10: Phasefluorimetry

$$\tan\phi = \omega \cdot \tau = 2\pi f\tau \quad (2.10)$$

ω ... angular frequency

τ ... decay time in the presence of O_2

τ_0 ... decay time in the absence of O_2

ϕ ... detected phase angle

f ... adjusted frequency of the modulated light

2.2.3 Sensitivity of a Sensor

In order to develop an optical oxygen sensor for the measurement of a specific oxygen level, the choice of lumophore is of great importance. The natural lifetime of the luminescent excited state depends strongly on the type of lumophore and therefore has a great influence on the sensitivity of the sensor. The second factor, which has a tremendous impact on the sensitivity, is the gas permeability of the matrix. If the same lumophore, which can be quenched by oxygen, is used in matrices of different gas permeabilities optical oxygen sensors of different sensitivities can be produced.

2.3 Indicators

2.3.1 The Perfect Indicator

There are certain parameters which are important for oxygen indicators[12]:

- They should possess a large Stokes shift so that emission and excitation light can be separated by using optical filters.
- They should have a high extinction coefficient and a high quantum yield, as the brightness of a dye is the product of these two factors. If the dye is bright, smaller amounts of it is needed in the sensor, preventing aggregations of the dye in the polymer matrix, which can occur at higher concentrations. Another advantage of using smaller dye concentrations is the possibility to produce thinner films, which is good for the response time of the sensor.
- The luminescence decay time is of great importance for the sensitivity of the sensor. The longer the dye remains in the excited triplet state, the more likely it is quenched by oxygen.
- A high photostability and chemical stability of the indicator is important for measurements with high light intensities or prolonged times.
- A key issue is the solubility of the dye in the polymer matrix in which it is encapsulated. Due to very lipophilic matrices, the dye is prone to migrate and aggregate. Leaching of the matrix is a problem as well.
- For biological and medical applications it is important that the dye is not toxic. Entrapping the dye in a matrix reduces its toxicity, but processes like leaching can occur and toxic singlet oxygen is produced by the quenching process.
- Due to the requirement that a sensor should be inexpensive, the dye should be commercially available at an acceptable price or the synthesis should be simple and cheap.

2.3.2 Commonly Used Indicators

One of the first used groups were polycyclic aromatic hydrocarbons (PAH). They possess a relatively short luminescent lifetime and therefore have to be immobilized in highly gas permeable matrices like silicones, in which the dye is very poorly soluble. They possess high QY, but a weak brightness because of their low extinction coefficient. This group of indicators was important in

the early stages of oxygen sensors.

Another group of indicators are polypyridyl complexes with Ru(II), Os(II) or Re(II) as central atom. They suffer from a high influence of thermal quenching, have a moderate extinction coefficient and relatively short lifetimes. The absorption range of the dye is in the blue region of the electromagnetic spectrum, therefore the dye cannot be used in many applications. Due to these disadvantages, Ru-polypyridyl complexes are quite popular for oxygen sensors as their preparation is quite simple and the optical properties are readily tuneable. They possess a large Stokes shift and are highly photostable. In general, these complexes are ionic dyes and thus insoluble in hydrophobic matrices. One possibility to overcome this problem is to exchange the inorganic counter ion with an organic ion to make it more soluble [13] [14].

Metalloporphyrins with Pt(II) or Pd(II) as central atom possess high phosphorescence at RT, moderate to high extinction coefficients and large Stokes shifts. The absorption spectrum of porphyrins generally shows two distinctive regions; the Soret-band at lower wavelength but higher extinction and the Q-band at higher wavelength and lower extinction. The lifetime of the porphyrin depends on the central atom. Pd(II) has a longer lifetime than Pt(II) due to increased spin-orbit coupling [15]. Therefore, Pd(II) are more commonly used as trace oxygen sensors than Pt(II) porphyrins. However, Pt(II) has a higher QY in the magnitude of 2 to 3.

Porphyrins with Ir(III) as central atom can be used for oxygen sensing as well [16]. Tetrakis(pentafluorophenyl) porphyrin (PtTFPP) is commercially available and very photostable, as a direct result of the electron withdrawing fluorine groups. Therefore it is commonly used as indicator. All the dyes mentioned before show absorption and emission maxima in the UV-Vis region and therefore suffer from several drawbacks.

By extending the π -system at the porphyrin, the so called tetrabenzoporphyrin (TBP) can be excited with red light and emits in the NIR region [17][18]. This allows sensing through highly scattering samples.

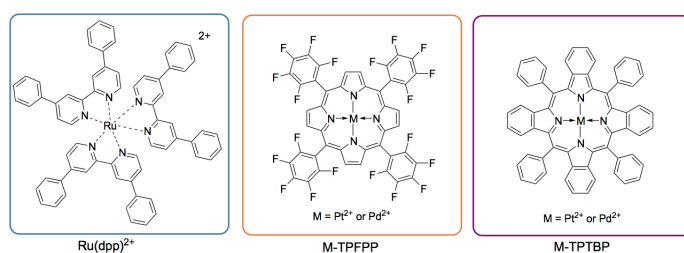


Figure 2.11: Commonly used Oxygen Indicators

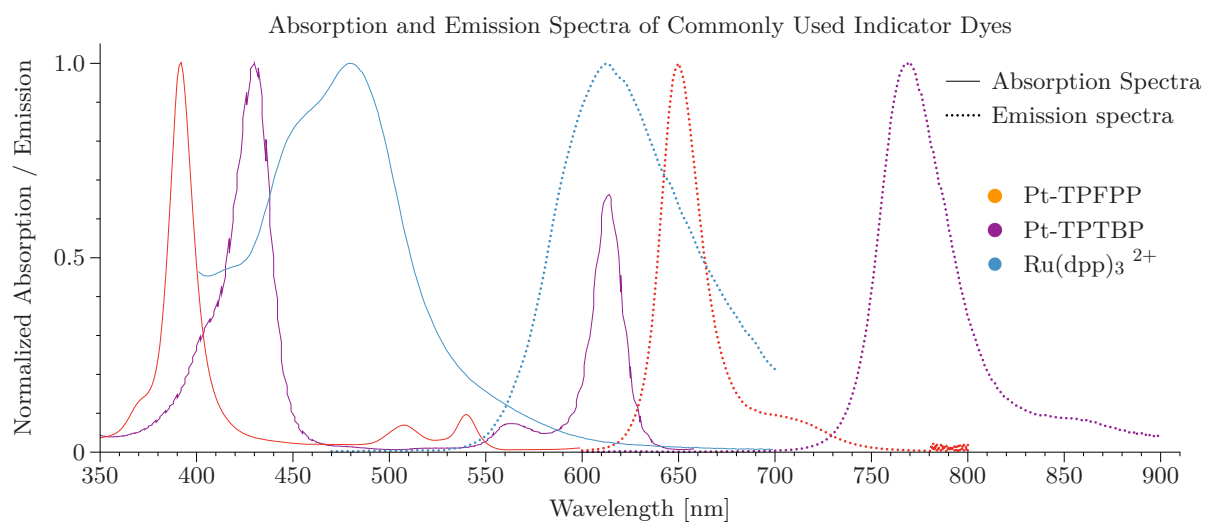


Figure 2.12: Normalized absorption and emission spectra for commonly used optical oxygen sensors

Table 2.1: Photophysical properties of different Pt-TPTBP dyes

Indicator	λ_{abs} [nm]	molar absorption $\times 10^{-3} [\text{M}^{-1}\text{cm}^{-1}]$	λ_{em} [nm]	Q.Y.	τ_0 [μs]	ref.
PtTPFPP	390, 504, 538	323, 23.2, 29.4	647, 710	0.088	60	[19]
Ru(dpp)_3^{2+}	463	28.6	618	0.37	6.4	[20]
Pt-TPTBP	430, 614	205, 136	770	0.51	47	[21]
Pd-TPTBP	443, 628	416, 173	800	0.21	286	[21]

2.4 Matrices

In order to produce an oxygen sensor, the indicator has to be immobilized in a matrix. This matrix acts as solvent for the dye; it keeps the concentration of the indicator constant and acts as barrier for unwanted species like ions or metals. The sensitivity of the sensor depends on the gas permeability of the matrix which depends on the diffusion constant and the solubility coefficient of oxygen in the matrix. Commonly used matrices are organic glassy polymers like polystyrene, poly(methylmethacrylate), fluorinated polymers, cellulose derivatives and inorganic polymers like silicones and sol gels [22]. Typical permeability coefficients are listed in table 2.2. Glassy organic polymers show lower oxygen permeabilities compared to silicone materials.

Polystyrene is very often used with $Ru(dpp)^{3+}$ and metalloporphyrin dyes because they show a high mechanical stability in thin films. However, the matrix can be destroyed by photo degradation because of singlet oxygen is produced [23].

Fluorinated polymers show a higher permeability and are highly resistant against photo degradation because of their short, strong C-F bond. They are usually used as copolymers in order to tune the properties of the polymer matrix [10].

Cellulose derivatives like ethyl cellulose show good permeabilities and provide high mechanical strengths.

Sol Gel matrices are very versatile and can be prepared for a wide sensitivity range or stability range by changing process parameters. They are often organically modified yielding in ormosils, which possess excellent optical properties. These matrices can be prepared as hydrophilic or hydrophobic matrices [24].

Silicone rubber is a commonly used matrix because of its high gas permeability. Therefore it is frequently used for highly sensitive sensors. It is also highly chemically stable and has a very good adhesion to glass supports [10][25].

Table 2.2: Permeability rates of commonly used sensor matrices [10]

Polymer matrix	Permeation rate for oxygen [$cm^2s^{-1}mmHg^{-1}$]
Poly(methylmethacrylate)	9
Polystyrene	2.63
Polyvinylchloride	0.34
Poly(2,2,2-trifluoroethylmethacrylate)	32
Ethylcellulose	11.0
Cellulose acetate	5.85
Poly(dimethylsiloxane)	695

2.4.1 Silicone Rubbers Used for Optical Sensors

As mentioned before, a lot of oxygen sensors rely on silicone matrices because of their great properties. As silicone polymers suffer from a low mechanical stability in thin films they have to be cured. Usually, a prepolymer is used in oxygen sensors and is afterwards crosslinked (vulcanized) using different methods. These silicone types are called room-temperature vulcanization silicones (RTV). RTV silicones can be classified into two types, depending on their composition[26]. RTV-1 silicones consist of only one part and cures through humidity. RTV-2 silicones consist of 2 parts which cure by the treatment with a catalyst [27].

RTV-1 silicones consist of a polysiloxane with alcohol groups, which can react with different crosslinkers. Using different crosslinkers while curing results in different by-products and can be acidic(acetic acid), basic (amines) or neutral (alcohols or oxims). The reaction can be accelerated by higher temperatures and higher degrees of humidity, but in general, depending on the thickness of the film, takes a long time. The curing time also depends on the organic substituents. A lot of oxygen sensors are based on these silicone matrices, because they are very easy to handle and provide good properties, although often the used dyes have to be modified in order to avoid aggregation [28][13][24].

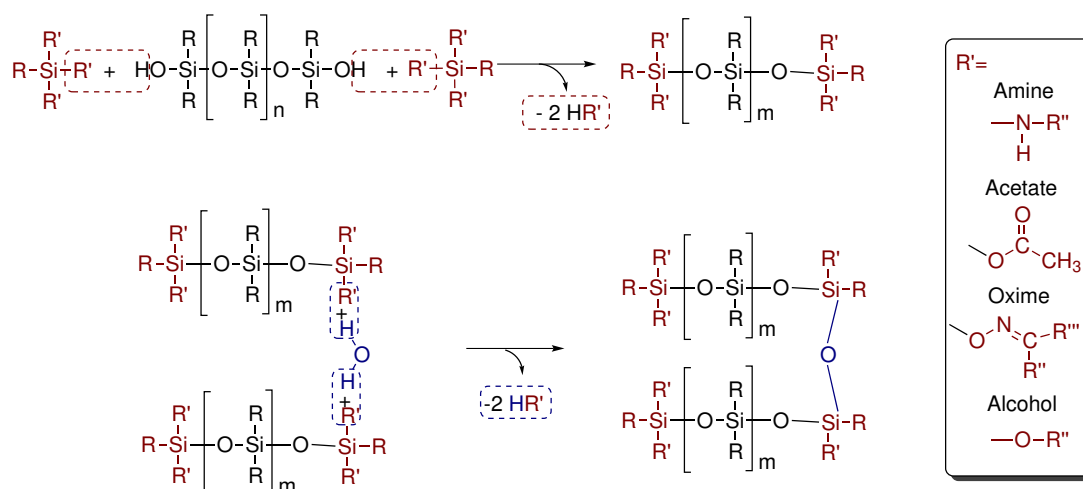


Figure 2.13: RTV1 Silicones

RTV-2 silicones are based on a two-component system. Crosslinking of the silicone polymer is usually achieved via one of those three routes: condensation reaction, addition reaction or radical reaction. The latter is standardized performed at higher temperatures [29].

The condensation reaction is carried out by a silanol system and polyalkoxysiloxanes as crosslinkers. It is catalysed by a tin catalyst like dialkyltin carboxylate. Alcohol by-products are formed during the curing process.

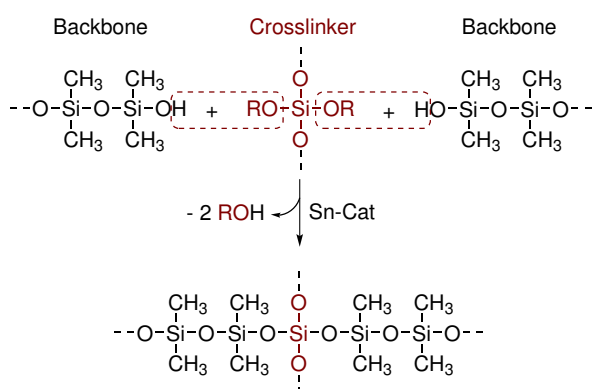


Figure 2.14: RTV2 Silicones - condensation

For addition curing the hydrosilation reaction is used, which is based on the reaction of vinyl functional siloxanes and hydride functional siloxanes. Platinum is a typical catalyst for this reaction. In this process no side reactions take place and no by-products are formed. The

cross-linking polymer is usually a methylhydrosiloxane-dimethylsiloxane copolymer. The curing can be accelerated by higher temperatures, but is usually in a minute-wide range. In order to control the work time it is possible to add retarders which are used to decelerate the platinum catalyst.

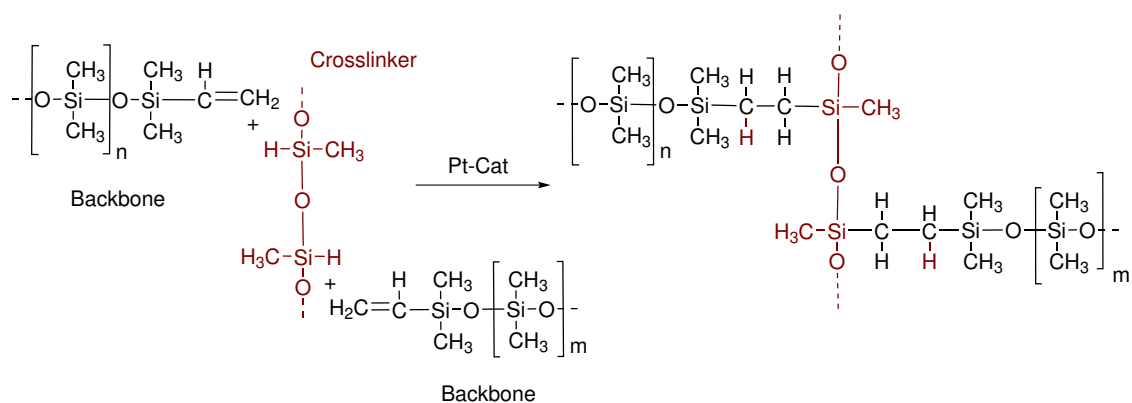


Figure 2.15: RTV2 Silicones - addition

Crosslinking through radicals is usually referred to as HCR (heat cured rubbers) as the reaction is carried out at 140-160°C. Crosslinking of vinyl and methyl groups of siloxane copolymers is usually initiated by peroxides.

These curing methods open the possibility of covalent immobilization of suitable modified indicators [25]. However, it can be used for immobilisation of particles as well [30].

2.4.2 Hydrosilation

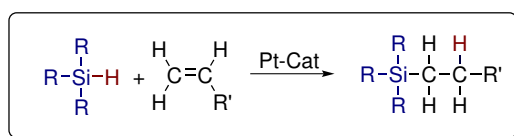


Figure 2.16: Hydrosilation

Hydrosilanes can undergo a catalysed addition reaction with the carbon-carbon double bonds of an olefin. Usually the catalyst is a late, electron-rich transition metal complex (ML_n), which can activate the hydrosilane as well as the olefin. The most important catalysts for hydrosilation reactions are the Speier and the Karstedt catalyst. The Speier catalyst (H₂PtCl₆ · 6 H₂O/iPrOH)

is widely used when handling a non-activated C=C-double bond [31]. The Karstedt catalysts contain vinyl-siloxane ligands and are also widely used. Both catalyst have an active Pt(0) centre [32].

The catalytic cycle according to Lewis (1990) is presented in scheme ??.

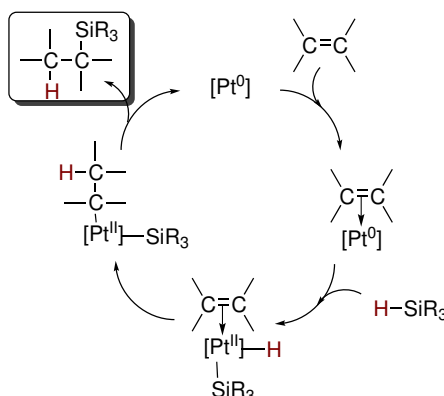


Figure 2.17: Catalytic cycle of hydrosilation reaction

Apart from the reaction with C-C double bonds hydrosilation can occur with C=O-, N=O-, N=N- and C=N multiple bonds, resulting in a broad field of applications. For instance, hydrosilation reactions are often used in the synthesis of monomers or in crosslinking-reactions. Crosslinked silicones can be used for paper release coatings, gaskets or pressure sensitive adhesives, just to name a few. Another application is liquid injection molding (LIM), where hydrosilation is responsible for curing [33].

2.5 Covalent Immobilization Techniques of Porphyrins

As mentioned before, poor solubility of the indicator dye in the matrix can cause aggregation or leaching of the dye. This raises problems of signal instability, inaccuracy of measurements, lower long-term applicability, and toxicity for cells in biological applications. Usually, the indicator is physically entrapped in the polymer matrix where the dye can migrate. Covalent coupling of the dye with matrix would improve the sensors performance and prevent leaching and aggregation

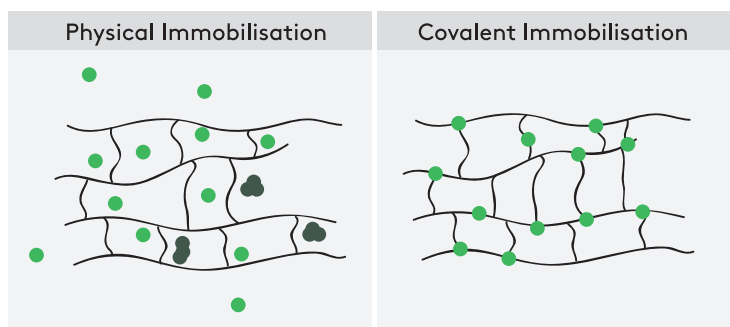


Figure 2.18: Different ways of immobilization

Covalent coupling of porphyrin dyes is not very common. However, there is the possibility to couple PtTFPP covalently via a nucleophilic reaction to the matrix, due to its labile fluorine group on the para position on the meso phenyl ring. There are various possible modifications like substituting the fluorine via nucleophilic substitution with di-thiols to a polystyrene-pentafluorostyrene copolymer [34] or the introduction of methacrylate groups with subsequent copolymerisation [35] or coupling to ormosil particles [36]. However, there is no comparable coupling approach for π -extended tetrabenzoporphyrins due to the missing chemical reactive substitutes on the porphyrin ring.

3 Materials and Methods

3.1 Photophysical Measurements

3.1.1 Absorption

Absorption measurements were performed between 800 nm and 350 nm on a "Varian Cary 50 Conc "UV-Vis spectrophotometer by Varian, Palo Alto, United States (www.varianinc.com), set at a fast scan rate using baseline correction and an adequate blank sample. Hellma 100-QS 10mm precision cuvettes or Hellma 101-OS 10mm precision cuvettes were used. Extinction coefficients were calculated using Lambert-Beers law.

3.1.2 Emission and Excitation Spectra

Emission and excitation spectra were recorded on a Hitachi-F-7000 spectrofluorometer in Hellma screw-cap fluorescence cuvettes and corrected for detector response. All emission spectra were measured in toluene.

3.1.3 Single Photon Counting

The single photon counting lifetimes were recorded on a FluoroLog Spectrofluorometer from Horiba Scientific with a DeltaHub module. Data were fitted using a mono-exponential fit.

3.1.4 Photostability

Dye solutions with an absorption of 0.3 in the Q-band were prepared in water free DMF in a Hellma screw-cap fluorescence cuvettes and illuminated with three red light emitting LEDs (617 nm) at the following settings: 7.0 W, 7.88 V, 882 mA with a photon flux of $5500 \mu\text{mol} \cdot \text{s}^{-1} \cdot \text{m}^{-2}$. The cuvette was placed in the focus of a curved mirror and the absorption spectra of the dye were recorded every 15 minutes from 300 to 900 nm. After each measurement the cuvette was unsealed shortly to ensure oxygen in the sample. The degradation was determined by calculating the average value of the three maximum absorption points in the Q-band.

3.1.5 Calibration of the Sensor Materials

Sensor calibration curves were determined by performing frequency-domain measurements of luminescence lifetimes at defined oxygen partial pressures. The phase-shift was measured using a Pyroscience Firesting Mini (www.pyro-science.com) at 10 % LED intensity, 4000 Hz modulation frequency and manual background compensation. Various controlled oxygen partial pressures were obtained using a gas-mixing device based on mass-flow controllers by mixing N₂ and 2 % O₂ gases. Constant temperature of 25 °C was achieved with a HAAKE DC50/ThermoHAAKE K10 thermostat. The sensor was fixed in a home-made stainless steel flow-through cell connected to a gas mixing device and a thermostat.

All calibrations were fitted with the modified two site model using Data Graph "www.visualdatatools.com" as plotting software.

3.2 Structural and Chemical Measurements

3.2.1 Solubility

The solvent was added to a specific amount of dye to obtain a 10 mg/ml solution assuming that the dye dissolves completely. After 10 minutes in the ultrasonic bath the solution was filtered through a syringe filter. An absorption spectrum was recorded of the filtrate. Using Lambert-Beers law the concentration of dye in the solution was calculated.

3.2.2 NMR

NMR spectra were recorded on a 300 MHz Bruker instrument (www.bruker.com). The analysis of the data was conducted with MNova NMR software (www.mestrelab.com).

3.2.3 Mass Spectrometry

Mass spectrometry was performed on a Micromass TofSpec 2E Time-of-Flight Mass Spectrometer by Dr. Robert Saf's group at the Institute for Chemistry and Technology of Materials, Graz University of Technology.

4 Experimental

4.1 Lindsey Synthesis

4.1.1 1-Nitro-2-iodocyclohexan

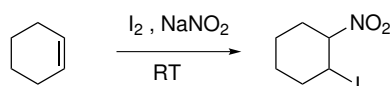


Figure 4.1: Reaction scheme for 1-nitro-2-iodocyclohexan

This reaction was conducted according to literature [37]. NaNO₂ (39.72 g, 0.575 mol, 4.00 eq) was dissolved in 60 ml H₂O and 24 ml ethylene glycol and was deoxygenated for 15 min using an Argon (Ar) flow. Cyclohexene (CH) (14.58 ml, 0.1437 mmol, 1 eq) and 150 ml ethyl acetate (EE) were added and the reaction mixture was cooled to 0 °C before adding I₂ (54.9 g, 2.16 mmol, 15.0 eq). The flask was closed and the reaction stirred for 100 hours at RT. The organic phase of the reaction was extracted with sat. Na₂S₂O₃ solution until the organic layer was colorless. The organic layer was dried over Na₂SO₄ and the solvent removed under reduced pressure.

Yield: 22.5 g $\hat{=}$ 67 %

4.1.2 1-Nitrocyclohexen

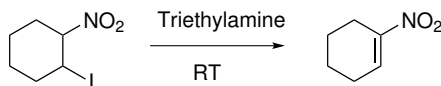


Figure 4.2: Reaction scheme for 1-nitrocyclohexen

This reaction was conducted according to literature [37]. 1-Nitro-2-iodocyclohexan (17.7 g, 0.0693 mmol, 1 eq) was dissolved in 150 ml diethylether. 10 ml Triethylamine (TEA) were added. The mixture was stirred at RT for 24 hours and then extracted with H₂O until a pH of 7 was reached. The organic layer was dried over Na₂SO₄ and the solvent removed. The crude product was cleaned using column chromatography (silica, CH/toluene 1/1) yielding a red viscous product.

Yield: 4.42 g \cong 50 %

Rf: 0.81 (silica, toluene)

4.1.3 2H-Isoindol-4,5,6,7-tetrahydro-1-carboxylic acid ethyl ester

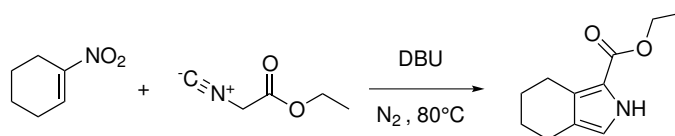


Figure 4.3: Reaction scheme for 2H-isoinidol-4,5,6,7-tetrahydro-1-carboxylic acid ethyl ester

This reaction was conducted according to literature [?]. 1-Nitrocyclohexene (0.442 ml, 3.9 mmol, 1 eq), ethylisocyanacetate (0.3389 ml, 3.9 mmol, 1 eq) and 10 ml waterfree THF were filled in a Schlenk flask under N₂ counter current. 1,8-Diazabicyclo [5.4.0] undec-7-en (DBU) (0.4642 ml, 3.9 mmol, 1 eq) was slowly added and the reaction mixture was heated to 80 °C for 18 h. The solvent was removed under reduced pressure and the crude product purified using column chromatography (silica, DCM).

Yield: 610 mg \cong 80 %

Rf: 0.52 (silica, DCM)

¹H NMR (300 MHz, CDCl₃) δ = 8.85 (s, 1 H), 6.64 (d, J = 2.9 Hz, 1 H), 4.30 (q, J = 7.1 Hz, 2 H), 2.81 (t, J = 5.9 Hz, 2 H), 2.54 (t, J = 5.7 Hz, 2 H), 1.90 - 1.57 (m, 2 H), 1.34 (t, J = 7.1 Hz, 3 H)

4.1.4 4,5,6,7-Tetrahydroisoindol

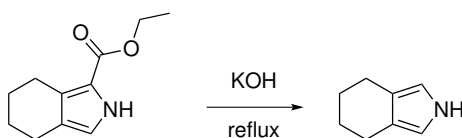
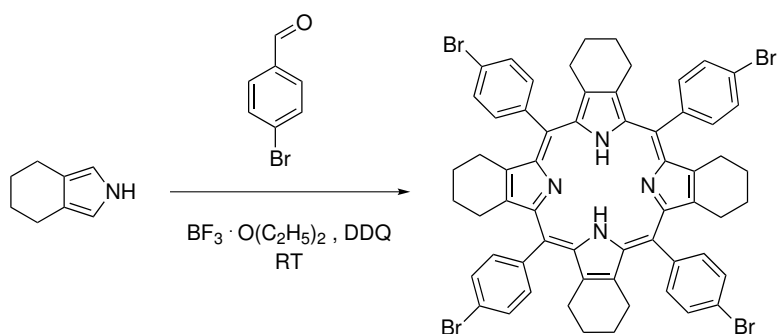


Figure 4.4: Reaction scheme for 4,5,6,7-tetrahydroisoindol

This reaction was conducted according to literature [38]. 2H-Isoindol-4,5,6,7-tetrahydro-1-carboxylic acid ethyl ester (4.339 g, 0.022 mmol, 1 eq) was dissolved in 180 ml ethylene glycol at 90°C KOH (18.860 mg, 0.336 mmol, 15 eq) was added. The heterogenous mixture was refluxed for 2 h and cooled down in an ice bath. DCM was added and the organic phase was washed with water until a pH of 7 was reached. The organic layer was dried over Na₂SO₄ and the solvent removed with rotary evaporator.

Yield: Black solid , 2.285 g \cong 83 %

¹H NMR (300 MHz, C₆D₆) δ = 7.89 (s, 1 H), 6.50 (d, 2 H), 2.70 - 2.55 (m, 4 H), 1.83 - 1.69 (m, 4 H)

4.1.5 H₂TPTCHPBr₄**meso-Tetra(4-bromophenyl)tetracyclohexenoporphyrin**Figure 4.5: Reaction scheme for H₂TPTCHPBr₄

This reaction was conducted according to literature [38]. 4,5,6,7-Tetrahydroisoindole (1.220 g, 0.010 mmol, 1 eq) and 4-bromobenzaldehyde (1.850 g, 0.010 mmol, 1 eq) were added to 1 l water

4 Experimental

free DCM, which was first degassed with Argon for 40 minutes, in a 2 l 3-neck bottle under Argon counter flow. The reaction mixture was degassed for 10 minutes. The flask was shielded from light and borontrifluoridiethyletherat ($\text{BF}_3 \cdot \text{Et}_2\text{O}$) (0.127 ml, 0.001 mmol, 0.1 eq) was added using a syringe. The reaction mixture was stirred for 3 h at room temperature before adding 0.05 ml additional $\text{BF}_3 \cdot \text{Et}_2\text{O}$ and subsequent stirring for 2 h. 2,3-Dichlor-5,6-dicyano-1,4-benzochinon (DDQ) (2.860 g, 0.0125 mmol, 1.25 eq) was added. The reaction mixture was stirred for 14 h at r.t. Remaining DDQ was quenched with 10 w% Na_2SO_3 solution and the organic phase was dried over Na_2SO_4 . The solvent was removed by rotary evaporation. The product used for the next step without further purification.

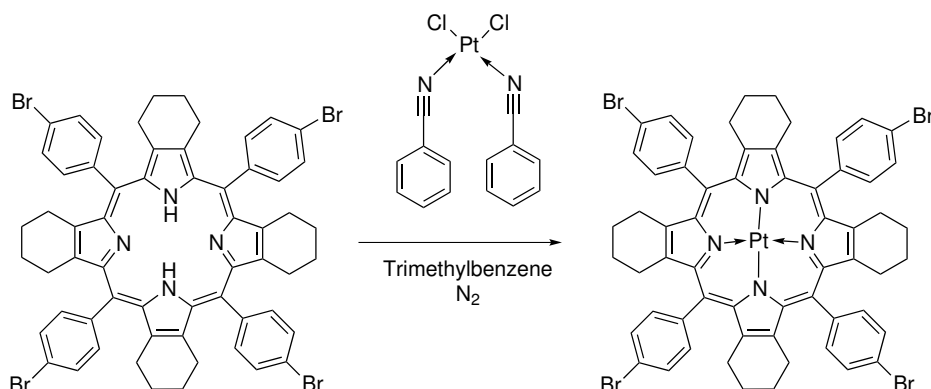
Yield: 83 % estimated via extinction

^1H NMR (300 MHz, CDCl_3) δ = 8.27 - 8.19 (m, 8 H), 8.04 - 7.95 (m, 8 H), 3.76 - 3.71 (m, 16 H), 1.88 - 1.81 (m, 16 H).

λ_{max} : acetone, 466 nm, 677 nm

4.1.6 Pt-TPTCHPBr₄

Platinum (II) meso-tetra(4-bromophenyl)tetracyclohexenoporphyrin

Figure 4.6: Reaction scheme for Pt-TPTCHPBr₄

The crude product (700 mg crude, 100 mg calculated using Lambert Beer law ($\epsilon = 250000 \text{ L}\cdot\text{mol}^{-1}\cdot\text{cm}^{-1}$) was dissolved in 60 ml 1,2,4-trimethylbenzene and heated to 150 °C. Pt(BN)₂Cl₂ (90 mg, 0.192 mmol, 2 eq) was pre-dissolved in a small volume of TMB and added to the reaction mixture. Forming HCl was removed by bubbling N₂ through the reaction mixture. The reaction progress was monitored via UV-Vis spectroscopy. After 1 h the solution was filtrated in order to remove insoluble side products. The filtrate was again refluxed with 1 eq Pt(BN)₂Cl₂. After completion of the reaction, 50 ml hexane were added and the mixture was cleaned using column chromatography (silica, hexane/DCM 2/1). Product fractions were determined via UV-Vis absorption spectra and the solvent removed under reduced pressure at 70 °C.

Yield: 52 mg, 0.045 mmol \cong 51 %

¹H NMR (300 MHz, CDCl₃) δ = 7.92 (d, J = 8.2 Hz, 8 H), 7.81 (d, J = 8.1 Hz, 8 H), 2.36 - 2.30 (m, 16 H), 1.54 - 1.50 (m, 16 H)

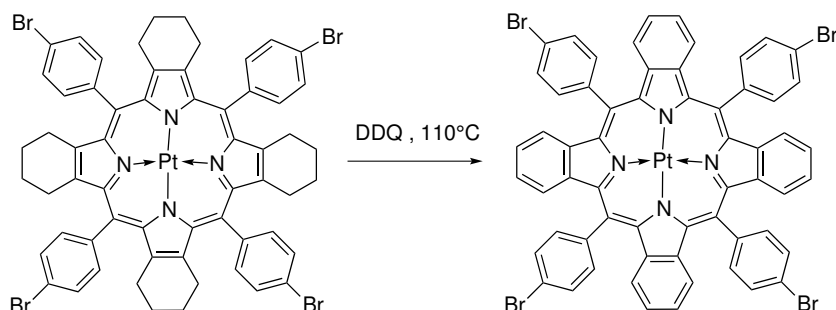
MALDI: m/z: [M⁺] calc for C₆₀H₄₈Br₄N₄Pt: 1340.0232 ; found: 1340.0132

ϵ : toluene, 412 nm, 247000 M⁻¹cm⁻¹

λ_{max} : acetone, 410 nm, 523 nm, 558 nm

4.1.7 Pt-TPTBPBr₄

Platinum (II) meso-tetra(4-bromophenyl)tetrabenzoporphyrin

Figure 4.7: Reaction scheme for Pt-TPTBPBr₄

This reaction was conducted according to literature [38]. The platinated complex (194.5 mg, 0.1692 mmol, 1 eq) was refluxed in 250 ml toluene. DDQ (385 mg, 1.696 mmol, 10 eq) was added and the red reaction mixture turned dark green after 5 minutes. The reaction progress was monitored using UV-Vis spectrometry. After completion of the reaction the green organic layer was washed three times with 10 w% Na₂SO₃ solution. The solvent was removed under reduced pressure.

Yield: 175 mg $\hat{=}$ 78 %

¹H NMR (300 MHz, C₆D₆) δ = 7.60 - 7.50 (m, 8 H), 7.48 - 7.40 (m, 8 H), 7.11 (dd, J = 6.2, 3.1 Hz, 8 H), 6.84 (dd, J = 6.2, 3.7 Hz, 8 H)

MALDI m/z: [M⁺]calc for C₆₀H₃₂Br₄N₄Pt, 1323.898; found: 1323.903

λ max: acetone, 428 nm, 615 nm

4.1.8 Pt-TPTBPStyr₄

Platinum (II) meso-tetra(4-styryl)tetrabenzoporphyrin

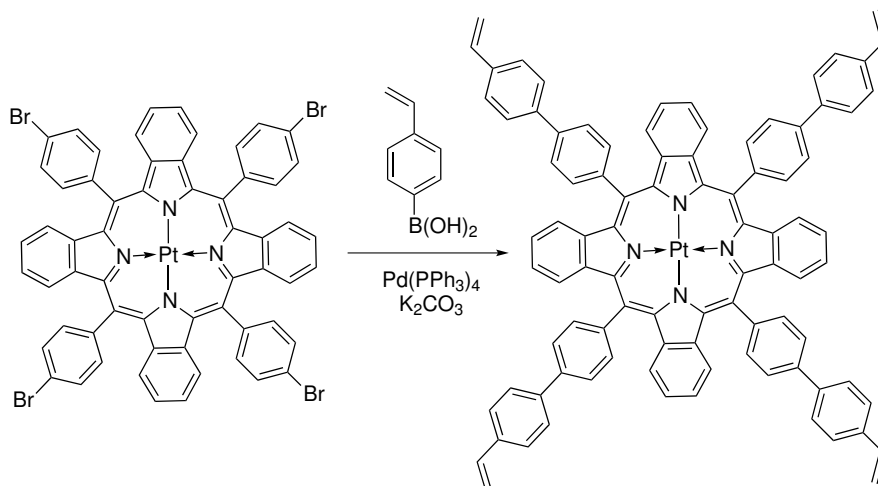


Figure 4.8: Reaction scheme for Pt-TPTBPStyr₄

Pt-TPTBPBr₄ (175 mg, 0.1326 mmol, 1 eq), 4-vinylphenylboronic acid (779 mg, 5.304 mmol, 40 eq) and K₂CO₃ (219 mg, 1.591 mmol, 12 eq) were added to a solution of THF/toluene/H₂O (20ml/20ml/10ml) under inert Argon atmosphere in a schlenk tube. The reaction mixture was deoxygenated for 20 minutes while vigorous stirring. 4 mol % Pd(PPh₃)₄ catalyst (6.12 mg) was added and the reaction mixture was heated to 75 °C for 18 h. After cooling down to RT, DCM was added and the mixture was washed with H₂O and saturated NaHCO₃ solution. The organic layer was dried under Na₂SO₄ and the solvent was removed under reduced pressure at 40 °C. The product was cleaned via silica column chromatography.

Yield: 52 mg \cong 30 %

¹H NMR (300 MHz, CDCl₃) δ = 8.42 - 8.29 (m, 8 H), 8.26 - 7.99 (m, 14 H), 7.96 - 7.89 (m, 4 H), 7.73 - 7.65 (m, 8 H), 7.43 - 7.28 (m, 8 H), 7.23 - 7.12 (m, 6 H), 6.89 (dd, J = 17.7, 10.9 Hz, 4 H), 5.92 (d, J = 17.4 Hz, 4 H), 5.38 (d, J = 11.0 Hz, 4 H).

MALDI: m/z: [M⁺] calc for C₉₂H₆₀N₄Pt, 1416.4491 ; found: 1416.4557.

4.2 Template Synthesis

4.2.1 Zn-TPTBPtBu₄Br₄

Zinc (II) meso-tetra(4-bromophenyl)tetra(*tert*-butyl)benzoporphyrin

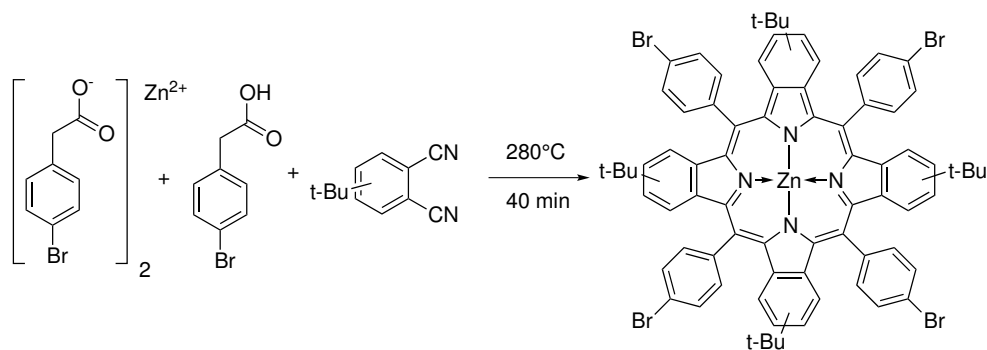


Figure 4.9: Reaction scheme for Zn-TPTBPtBu₄Br₄

Zn-(4-bromophenyl)acetate (12.50 g, 25.33 mmol, 1 eq), 4-bromophenylacetic acid (27.23 g, 126.6 mmol, 5 eq) and 4-*tert*-butylphthalonitrile (18.64 g, 101.3 mmol, 4 eq) were homogenized with a mortar and 700 mg of the mixture were weighed in a 2.5 ml Supelco-Vial and compressed. A magnetic stirrer was placed inside and the vial was sealed with a metal cap. The vials were placed into a preheated heating block at 150 °C and heated to 280 °C. The stirrer was started at 170 °C and the reaction mixture was kept to react for 40 min at 280 °C. After completion the vials were removed in order to let cool. Afterwards the product was dissolved in acetone to a volume of 500 ml. The product was precipitated two times in EtOH/H₂O/sat.NaHCO₃ (1500ml/300ml/10ml). The crude product was purified by Al₂O₃ column chromatography. Blue colored side products were removed with cyclohexane +10% DCM. The product was eluted with DCM and product containing fractions were determined via absorption spectra. The solvent was removed using rotary evaporator and again purification via column chromatography (silica, CH+20%DCM) was conducted. The solvent was removed and the product dried in the oven at 60 °C.

Yield: 3.986 g, 2.810 mmol \cong 7.12 %

ϵ : toluene, 460 nm, 319000 M⁻¹cm⁻¹ ; 656 nm, 97000 M⁻¹cm⁻¹

λ_{max} : acetone, 455 nm, 656 nm

4.2.2 $\text{H}_2\text{TPTBPtBu}_4\text{Br}_4$

meso-Tetra(4-bromophenyl)tetra(o-*t*-butyl)benzoporphyrin

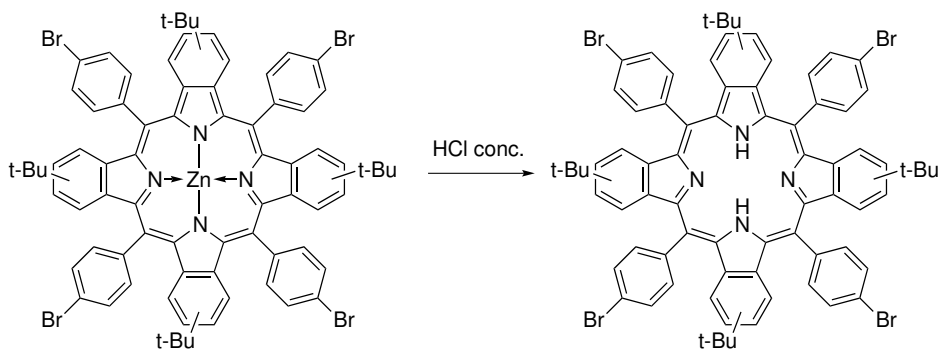


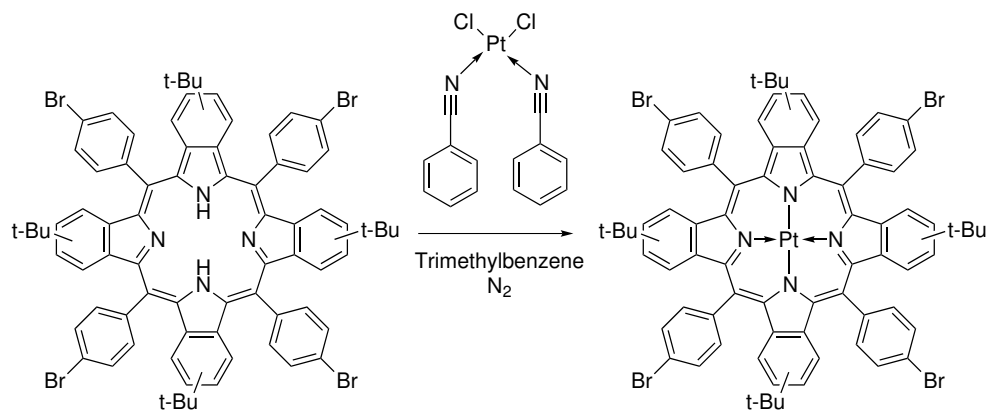
Figure 4.10: Reaction scheme for $\text{H}_2\text{TPTBPtBu}_4\text{Br}_4$

$\text{Zn-TPTBPtBu}_4\text{Br}_4$ (1.000 g, 0.7050 mmol, 1 eq) was dissolved in 500 ml DCM. 50 ml HCl conc. was slowly added. The protonated ligand could be determined by absorption spectrum in acetone. The mixture was extracted with H_2O and sat. NaHCO_3 until only free ligand was observed. The organic layer was dried over Na_2SO_4 and the solvent removed under reduced pressure.

Yield: 0.939 mg, 0.694 mmol, 98.44 %

Extinction coefficient: DCM, 464 nm, $325000 \text{ M}^{-1}\text{cm}^{-1}$

λ_{max} : acetone, 464 nm

4.2.3 Pt-TPTPtBu₄Br₄Platinum (II) meso-tetra(4-bromophenyl)tetra(*tert*-butyl)benzoporphyrinFigure 4.11: Reaction scheme for Pt-TPTPtBu₄Br₄

H₂TPTPtBu₄Br₄ (500 mg, 0.369 mmol, 1 eq) was dissolved in 250 ml TMB and heated to 155 °C in a 2-neck round bottle. N₂ was bubbled through the reaction mixture and Pt(BN)₂Cl₂ (260 mg, 0.554 mmol, 1.5 eq) was added in small pre-dissolved portions (0.3 eq) over 4 hours. The reaction was monitored via absorption spectra. The solvent was removed using a rotary evaporator at 70 °C and the crude product was purified using column chromatography (Al₂O₃, CH/DCM 5/1). The solvent was removed and the product was placed in a 2-neck round-bottle with cold finger. The viscous product was heated to 350 °C under high vacuum to remove side products.

Yield: 403.7 mg, 0.2632 mmol $\hat{=}$ 71.33 %

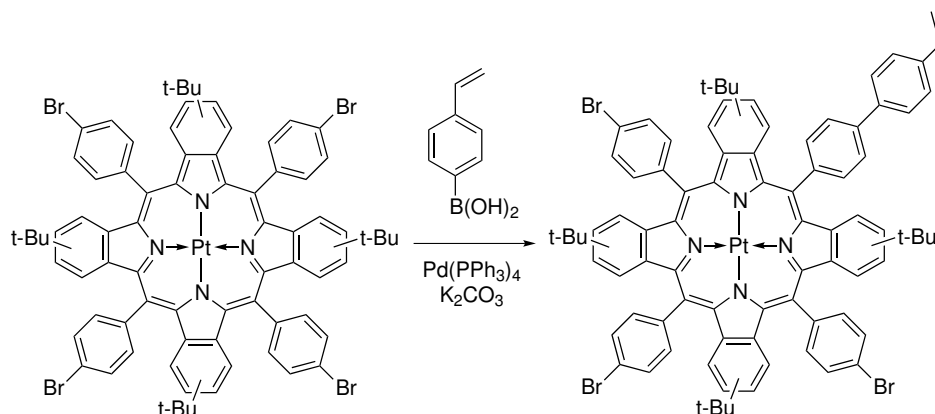
Rf: 0.44 (silica, CH+DCM 4+1)

¹H NMR (300 MHz, CDCl₃) δ = 8.26 - 8.12 (m, 8H), 8.11 - 8.01 (m, 8H), 7.49 - 7.39 (m, 4H), 7.38 - 7.34 (m, 2H), 7.21 - 7.14 (m, 2H), 7.10 - 7.04 (m, 2H), 1.29 (s, 36H).

MALDI-TOF: C₇₆H₆₄Br₄N₄Pt calc. 1548.149, found: 1548.155

ϵ : toluene, 428 nm, 245000 M⁻¹cm⁻¹, 610 nm, 174000 M⁻¹cm⁻¹

λ_{max} : acetone, 428 nm, 619 nm

4.2.4 Pt-TPTPtBu₄Br₃StyrPlatinum (II) meso-(4-styryl)-tri(4-bromophenyl)tetra(*tert*-butyl)benzoporphyrinFigure 4.12: Reaction scheme for Pt-TPTPtBu₄Br₃Styr

Pt-TPTPtBu₄Br₄ (88 mg, 0.057 mmol, 1 eq), 4-vinylphenylboronic acid (8.43 mg, 0.057 mmol, 1 eq) and K₂CO₃ (23.59 mg, 0.171 mmol, 3 eq) were dissolved in toluene/THF/H₂O (6ml/6ml/3ml) in a schlenk tube. The mixture was degassed for 20 minutes by vigorously stirring and heavy Ar flow. The catalyst Pd(PPh₃)₄ (0.6 mg, 1 mol%) was added under counter current Ar flow. The schlenk was closed and heated to 70 °C for 24 hours. After completion of the reaction, the mixture was diluted with 30 ml DCM, extracted with H₂O and sat. NaHCO₃ (3 x 50ml), dried over Na₂SO₄ and the solvent removed. The crude product was purified with silica column chromatography (CH/toluene 3/1).

Educt: 37.7 mg, 0.024 mmol, 42.1 %

Mono-styrene: 29.3 mg, 0.018 mmol, 26.3 %

Di-styrene: 18.7 mg, 0.012 mmol, 21.0 %

Rf Educt: 0.81 (silica, CH/EE 10/1)

Rf Mono-styrene: 0.72 (silica, CH/EE 10/1)

RF Di-styrene: 0.60 (silica, CH/EE 10/1)

¹H NMR (300 MHz, CDCl₃) δ = 8.36 - 7.88 (m, 21 H), 7.72 - 7.61 (m, 2 H), 7.49 - 7.26 (m, 8 H), 7.20 - 6.97 (m, 4 H), 6.87 (dd, J = 17.6, 10.9 Hz, 1 H), 5.91 (d, J = 17.6 Hz, 1 H), 5.37 (d, J = 10.8 Hz, 1 H), 1.29 - 1.22 (m, 36 H)

MALDI-TOF Mono-styrene: $C_{84}H_{71}Br_3N_4Pt$ Calc.: 1571.2871, found: 1571.2823

4.2.5 PtTPTPtBu₄Styr₄

Platinum (II) meso-tetra(4-styrene)tetra(*tert*-butyl)benzoporphyryn

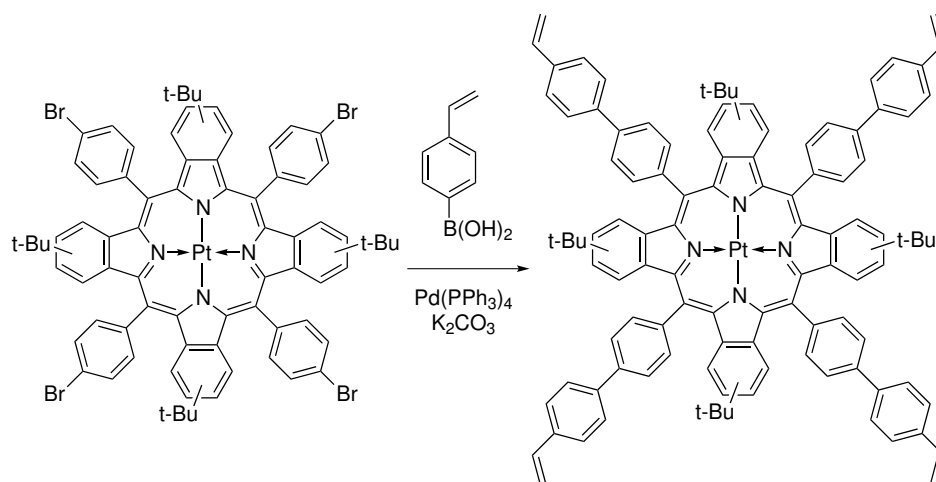


Figure 4.13: Reaction scheme for PtTPTPtBu₄Styr₄

Pt-TPTBPtBu₄Br₄ (200 mg, 0.129 mmol, 1 eq), 4-vinylphenylboronic acid (372 mg, 2.58 mmol, 20 eq) and K₂CO₃ (213 mg, 1.55 mmol, 12 eq) were dissolved in toluene/THF/H₂O (10ml/10ml/5ml) in a schlenk tube. The mixture was degassed for 20 minutes by vigorously stirring and heavy Ar flow. The catalyst Pd(PPh₃)₄ (6.0 mg, 4 mol%) was added under counter current Ar flow. The schlenk was closed and heated to 70 °C for 24 hours. After completion of the reaction, the mixture was diluted with 150 ml DCM, extracted with H₂O and sat. NaHCO₃ (3 x 200ml), dried over Na₂SO₄ and the solvent removed. The crude product was cleaned with silica column chromatographie. UV-active side product was removed with CH/toluene (3/1) and the products were eluted with CH/toluene(1/1).

Yield: 122 mg, 0.0749 mmol, 58,1 %

Rf Educt: 0.81 (silica, CH/EE 10/1)

Rf Tri-styrene: 0.52 (silica, CH/EE 10/1)

Rf Tetra-styrene: 0.45 (silica, CH/EE 10/1)

¹H NMR (300 MHz, CDCl₃) δ = 8.41 - 8.29 (m, 8 H), 8.26 - 8.00 (m, 14 H), 7.96 - 7.90 (m, 4 H),

7.75 - 7.63 (m, 8 H), 7.48 - 7.28 (m, 8 H), 7.18 - 7.09 (m, 4 H), 6.89 (dd, $J = 17.7, 10.9$ Hz, 4 H), 5.92 (d, $J = 17.4$ Hz, 4 H), 5.38 (d, $J = 11.0$ Hz, 4 H), 1.25 (s, 36 H)

MALDI-TOF: Tri-styrene: $C_{100}H_{85}BrN_4Pt$ calc: 1617.562 ; found: 1617.553 ; Tetra-styrene: $C_{108}H_{92}N_4Pt$ calc: 1640.700 ; found: 1640.689

4.3 Optimizing of the Platination Reaction

Five different reactions (A,B,C,D,E) were set up. Absorption spectra were recorded in the same dilution every 15 minutes in acetone. In reaction A,B and C $H_2TPTBP-tBu_4-Br_4$ (150 mg, 0.110 mmol, 1 eq) was dissolved in 150 ml TMB and heated to 150 °C. Small portions of $Pt(BN)_2Cl_2$ (20.9 mg, 0.044 mmol, 0.4 eq, 3x) were pre-dissolved in TMB (2 ml) and added after the recorded spectra at 0, 90 and 180 minutes. In reaction D and E $Pt(BN)_2Cl_2$ (62.8 mg, 1.32 mmol, 1.2 eq) was dissolved in 50 ml TMB and heated to 150 °C. The ligand (150 mg, 0.110 mmol, 1 eq) was dissolved in 100 ml TMB and added drop-wise over a period of 210 minutes to the reaction mixture. N_2 was bubbled through the reaction mixture B and D. Tri-n-butylamine (TBA) (52.3 μ l, 0.22 mmol, 2 eq) was added to the ligand in reaction E and in reaction C.

Table 4.1: Summary of different set ups for the platination reaction

	A	B	C	D	E
Adding $Pt(BN)_2Cl_2$	✓	✓	✓		
Adding Ligand				✓	✓
N_2 bubbling		✓		✓	
Base (tri-n-butylamine)			✓		✓

4.4 Sensor Preparation

4.4.1 General Procedure

1 mg dye (0.5 w% $Pt-TPTBPtBu_4Br_xStyr_y$) were dissolved in 400 mg chloroform (HPLC-grade) in a Supelco-Vial. The platinum catalyst was diluted with chloroform to provide appropriate con-

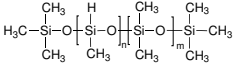
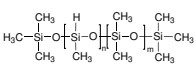
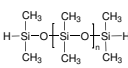
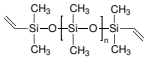
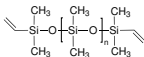
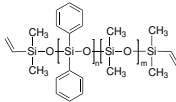
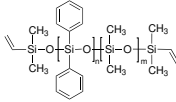
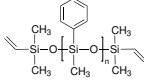
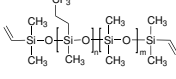
centrations. The crosslinker and the catalyst (Karstedt Catalyst, platin-divinyltetramethylsiloxan) were added and the reaction mixture and was stirred with a magnetic stirrer for 30 minutes at RT. The vial was cooled down in the freezer for 10 minutes. The backbone (different substituted polysiloxanes) was added and stirred on the vortex before storing it again in the freezer for a minimum of 30 minutes. The cocktail was knife-coated on a cleaned glass slide with 25 μm thickness. The sensor was dried in the drying cabinet at 60 °C for 24 hours. The used quantities for each sensor material are listed in table 4.2.

4.4.2 Sensor for Measurements Through Wine Bottles

4 mg tetra-styrene dye were dissolved in 800 mg chloroform (HPLC-grade) in a Supelco-Vial. The cross-linker 25-35 % MeH (108 μl , 12 eq per vinyl group) and 4 mg catalyst were added and the reaction mixture was stirred with a magnetic stirrer for 30 minutes at RT. The cocktail was cooled down in the freezer to -18 °C for 10 minutes. The backbone PDMS-2 (400 mg) was added and stirred on the vortex before storing it again in the freezer for 30 minutes. The cocktail was then knife-coated on a SiO₂ modified Mylar foil with 75 μm thickness. The sensor was dried in the drying cabinet at 60 °C for 24 hours.

The silicone rubber was covered with a TiO₂ layer in order to increase signal intensity. 1 g TiO₂ was dispersed in 5 ml CH under heavy stirring and 1 g Silicone E4 was dissolved in 3 ml CH. Both mixtures were combined and stirred for 60 min. The cocktail was knife coated on the silicone rubber foil with 75 μm thickness and dried in the drying cabinet at 60 °C for 24 hours.

Table 4.2: Used quantities for each sensor material

<p>→ Crosslinker (CL)</p> <p>↓ Backbone (BB)</p>	 <p>25-35% MeH</p>	 <p>50-55% MeH</p>	 <p>Dihydrid</p>
 <p>PDMS-1</p>	(14) 22.9µl CL, 180mg BB	(20) 25.3µl CL, 180mg BB	(25) 46µl CL, 160mg BB
 <p>PDMS-2</p>	(3,30,31) 5.6µl CL, 200mg BB (6,7,15) 6.8µl CL, 200mg BB (8) 13.6µl CL, 200mg BB (9,32-34) 108µl CL, 400mg BB	(4) 3.2µl CL, 200mg BB (5) 3.4µl CL, 200mg BB (21) 6.8µl CL, 200mg BB	(1) 26.4µl CL, 200mg BB (2) 30.0µl CL, 200mg BB (26) 15µl CL, 200mg BB
 <p>PDPDMS-1</p>	(17) 27.1µl CL, 200mg BB	(22) 2.7µl CL, 200mg BB	
 <p>PDPDMS-2</p>	(13,18) 10.0µl CL, 200mg BB (12) 5.0µl CL, 200mg BB	(24) 5.6µl CL, 200mg BB	(10) 10.9µl CL, 200mg BB (11,27) 22.0µl CL, 200mg BB
	(19) 56.0µl CL, 150mg BB	(23) 61.7µl CL, 150mg BB	(28) 92.7µl CL, 110mg BB
 <p>PFMDMS</p>	(16) 4.9µl CL, 200mg BB		(29) 30.4µl CL, 200mg BB

5 Results and Discussion

5.1 Synthetic Considerations

The first approach was to synthesize a Pt-tetraphenyl-tetrabenzoporphyrin with bromine substituents at the meso position Pt-TPTBPBr₄. These bromines can then undergo the Suzuki Cross coupling reaction with 4-vinylboronic-acid to give a styrene modified porphyrin indicator dye for covalent immobilization. This was first conducted by Lukas Hutter in his master thesis 2012 [39]. Basically, there are two different widely used methods for the synthesis of tetrabenzoporphyrins. The conventional method called Lindsey-Condensation usually yields very pure products and allows the introduction of various functional groups due to the mild conditions which can be used [40]. The starting materials for the reaction are commercially available but very expensive considering moderate yields and many follow-up reaction steps to reach the final porphyrin dye. An alternative to the sophisticated Lindsey method is the so called template synthesis which consists of three reaction steps in order to get the final Pt-TPTBP dye [41]. This reaction usually suffers from low yields and a complex product mixture, but considering the used low cost materials and the smaller synthetic effort it is a good alternative to the Lindsey Method. However, in order to obtain pure products, the Lindsey method was chosen for the first experiments.

5.1.1 Lindsey Condensation

Starting Materials

One of the starting materials (1-nitrocyclohexen) was synthesized in the lab via two simple reactions using relatively cheap chemicals in order to reduce the costs of the synthesis. The synthesis steps towards 4,5,6,7-tetrahydroisoindol were conducted according to literature.

Lindsey-Condensation to H₂TPTCHPBr₄

All reaction steps were monitored using UV-Vis spectrometry.

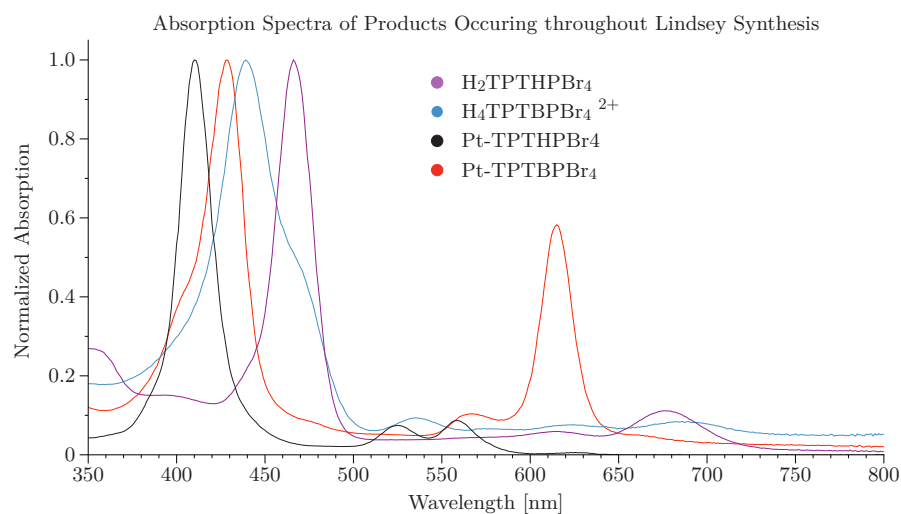


Figure 5.1: Normalized absorption spectra of the different products occurring during Lindsey method

One key step is the reaction of 4, 5, 6, 7-tetrahydroisindole with 4-bromobenzaldehyde resulting in the porphyrin. The forming of the porphyrin was monitored via UV-Vis spectrometry. Due to solubility problems arising as a consequence of aggregation of the product, the yield could not be directly determined and had to be estimated using Beers Law. Assuming an extinction coefficient of $250000 \text{ M}^{-1}\text{cm}^{-1}$ at the Soret-band and knowing the volume in the reaction flask, a yield of $\approx 80\%$ could be calculated for the end of the synthesis. Further purification proved difficult, hence the crude product was directly used in the subsequent step after removal of the solvent.

Platination to Pt-TPTCHPr_4

Due to the impurities of the obtained product from the previous reaction step, the reaction had to be stopped after one hour and filtrated in order to remove insoluble side or decomposition products. After continuing with the platination process, the Pt(II) -complex was formed almost quantitatively after 90 minutes according to the absorption spectrum. The crude product was purified via column chromatography yielding a pure red powder. The structure was confirmed using MALDI-TOF and ^1H NMR measurements.

Aromatisation to Pt–TPTBPBr₄

The last step of the porphyrin synthesis was the oxidation of the Pt–TPTCHPBr₄ to form the Pt(II)-benzoporphyrin using DDQ as oxidizing agent. Quantitative conversion was observed after 15 min according to UV-Vis spectra. A major issue in this reaction was the very bad solubility of the product, therefore the work up procedure had to be conducted in very diluted solutions. This problem occurred after removal of the solvent, which caused that the product hardly dissolved at all. It is already known that TBP suffer from low solubility [42]. One reason could be that the extended π -system and the occurring polarization due to the introduced bromine cause very strong π -stacking effects [43]. The product was validated via MALDI-TOF and ¹H NMR measurements.

Suzuki Coupling to Pt–TPTBPStyr₄

Due to poor solubility the Suzuki-coupling was performed as a highly diluted heterogeneous reaction. The idea was that replacing the bromine with the styrene group would reduce the π -stacking due to steric effects and therefore the dye would dissolve better. The solubility did actually improve which made column chromatography possible. This was necessary because of different degrees of styrene modification. In addition the side product yielded by Heck-cross coupling was removed (Fig.5.2). The obtained product contained four styrene groups according to MALDI-TOF.

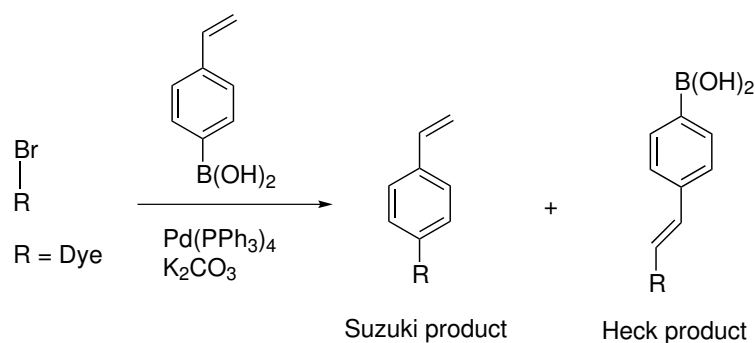


Figure 5.2: Possible products using Pd(PPh₃)₄ for C-C cross coupling reaction

This method results in a very pure product. However, due to the solubility problems and the numerous reaction steps requiring dry solvents and inert atmosphere, the simpler template method was carried out. In order to avoid solubility problems, t-butyl groups were introduced

at the peripheral positions.

5.1.2 Template Synthesis

Usually the template synthesis uses phthalimide as one of the starting materials [41], but by using dicyanobenzene instead, the reaction takes place more readily at lower temperatures (280 °C instead of 320 °C) and shorter reaction time. All reaction steps were monitored using UV-Vis spectroscopy.

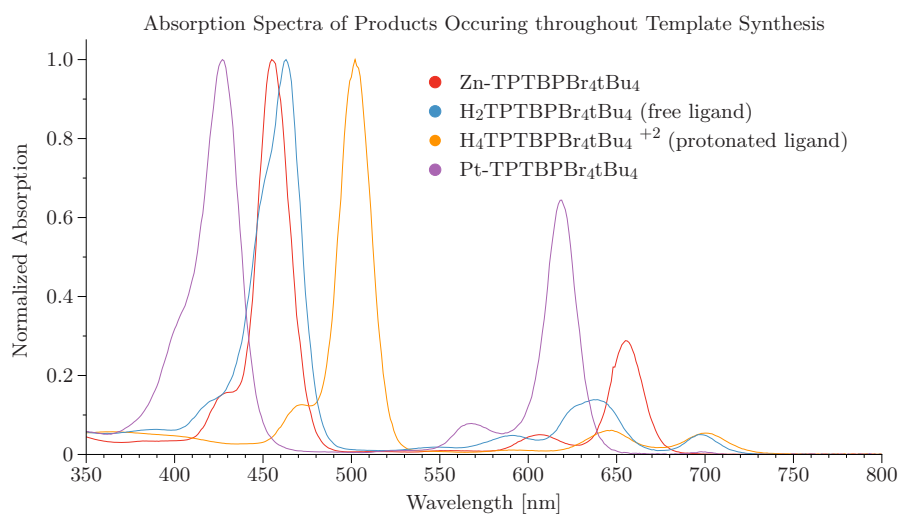


Figure 5.3: Summary of absorption spectra of different products during template synthesis

Synthesis of Zn-TPTBPtBu₄Br₄ and demetalation to H₂TPTBPtBu₄Br₄

Phenylacetic acid and 4-tert-butylphthalonitrile can be purchased in large quantities. Zinc-phenylacetate was obtained by an exchange reaction of ZnO and phenylacetic acid. The equivalent of starting material was optimized in a way that the main product of the template synthesis is TPTBP and only little azaporphyrin side product is formed. Side products can be easily removed by means of column chromatography. The yield (7%) is acceptable with respect to the costs and working time.

The demetalation reaction step is quantitatively and is easily conductible.

Platination to Pt–TPTBPtBu₄Br₄

The platination of the complex can be considered as the key step. The synthesis itself is discussed in more detail in section 5.1.3. The difference of other Pt-TPTBP is that after column chromatography, the product is very viscous and shows broad signals in the ¹H NMR between 2.1 - 2.4 ppm and 6.8 - 7.1 ppm. These are the areas where TMB shows characteristic signals. A possible reason might be encapsulated TMB between two dyes, which are linked together by π stacking effects, and their t-Bu groups, which sterically trap the TMB in between these dimers. After heating the viscous product to 350 °C under high vacuum in a round flask with a cold finger, a highly viscous film is depositing on the finger, a crystalline, pure product remains. TPTBP obtained by template synthesis can suffer from impurities like additional benzyl groups due to the harsh reaction conditions. Using the modified method with lower temperatures and introduction of sterically demanding t-butyl groups prevent such impurities. This was confirmed by MALDI-TOF and ¹H NMR data.

Suzuki coupling to different substituted derivatives Pt–TPTPtBu₄Br_xStyr_y

By using 1 eq of 4-vinylphenylboronic acid the synthesis results in a mixture of non-, mono-, di-styrene and Heck product dyes (4/3/2/1). These products can be separated by silica column chromatography. The di-styrene dye can be used as starting material for the synthesis of higher substituted indicators. By using 20 eq of 4-vinylphenylboronic acid the obtained product contained three to four styrene groups with relative intensities of 5:4 according to MALDI-TOF. This is sufficient for further cross-linking reactions. Although the product is a mixture, it will be referred to as "tetra-styrene dye" in this thesis.

By introducing styrene groups the Soret band is red-shifted and the extinction of the Q-band decreases, but is not bathochromically shifted.

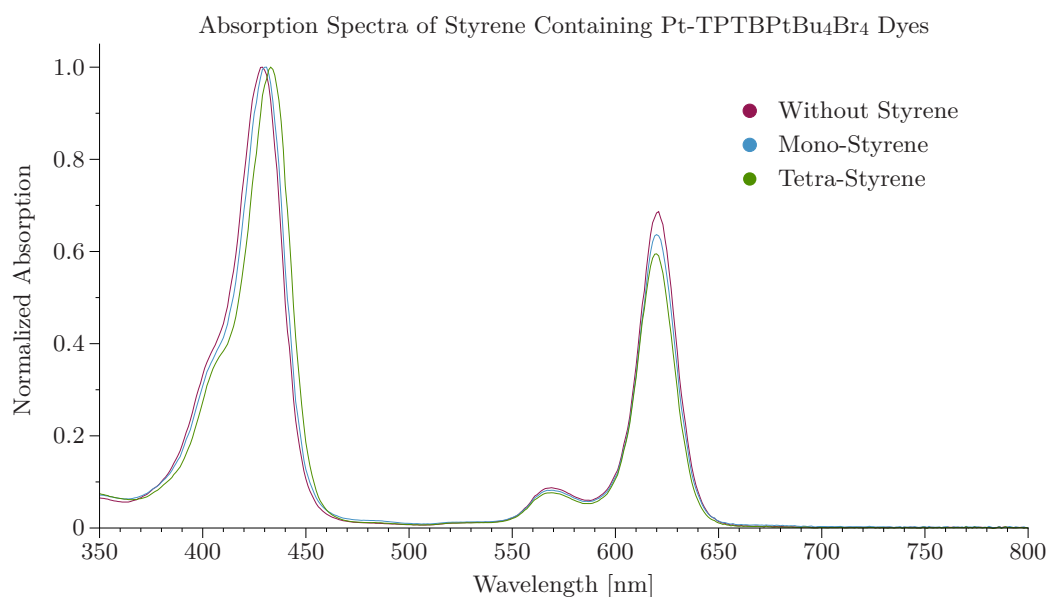


Figure 5.4: Absorption spectra of Suzuki modified Pt-TPTBP

5.1.3 Optimizing the Platination

Porphyrins which are not π -extended are in general platinated by refluxing PtCl_2 in degassed benzonitrile (BN) resulting in a square planar $\text{Pt}(\text{BN})_2\text{Cl}_2$ complex which enhances the solubility of the platinum reagent in the reaction medium[44] [45]. However, despite the increase in solubility, metalation of TBP proceeds very slowly and used to be thought of as impossible due to steric hindrances[46].

Therefore more complicated synthesis pathways were established in which the platination step was carried out on tetraphenyl-cyclohexenoporphyrin with subsequent oxidation to tetraphenyl-tetrabenzoporphyrin [47] (as shown in section 4.1).

This method cannot be used in the template method, because there is no adequate porphyrin intermediate. One method in order to conduct this reaction is to use $\text{Pt}(\text{BN})_2\text{Cl}_2$ in non-coordinating diphenylether instead of benzonitrile as a solvent [48]. Diphenylether is solid at RT and cannot be removed by vacuum. Using a different non-coordinating and non-protic solvent with a high boiling point in which the dye and Pt-precursor dissolves properly would simplify the reaction. 1,2,4-trimethylbenzene was shown to be suitable for this reaction [39].

Recently, a new method using Pt-acetate instead of $\text{Pt}(\text{BN})_2\text{Cl}_2$ as precursor was published[49].

Our consideration is that the complexation consists of a few important equilibriums. With each complexation HCl is generated (1), which consecutively protonates the free ligand (2). This protonation decreases the solubility of the dye in the solvent, complicating and preventing the metalation step of the complex (3). Therefore, different approaches in order to optimize the key reaction step were investigated.

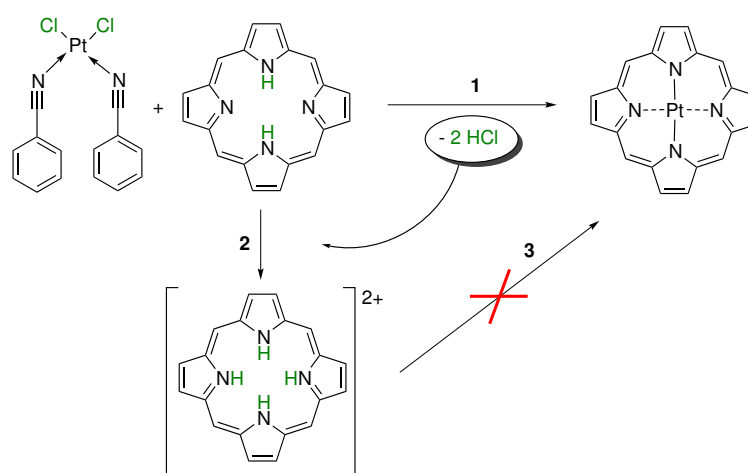


Figure 5.5: Scheme for platinumation step and possible protonation of the ligand

First, we tried to prevent the ligand from protonation by removing the formed H^+ using two different ways. Either by bubbling N_2 gas through the reaction mixture in order to remove the formed HCl or adding the base tri-*n*-butylamine (TBA) to catch the H^+ . As reference one reaction was done without N_2 or base.

Secondly the drop-wise addition of the ligand to the hot $\text{Pt}(\text{BN})_2\text{Cl}_2$ solution was investigated. The idea was to add free ligand in order to avoid the generation of protonated ligand. In reaction A, C and D 0.4 eq of pre-dissolved $\text{Pt}(\text{BN})_2\text{Cl}_2$ was added.

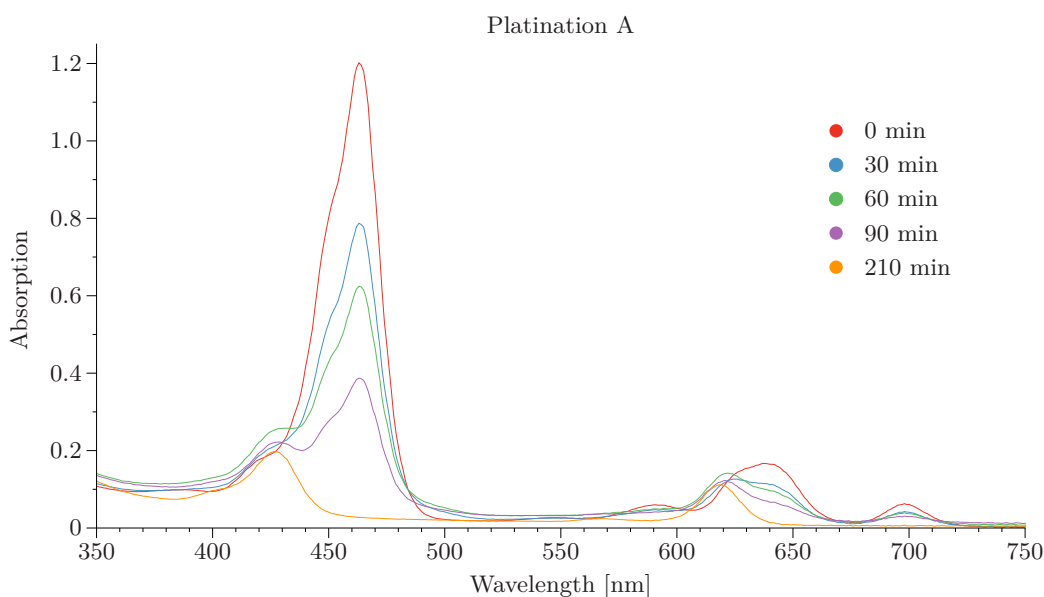


Figure 5.6: Reaction A) Without adding a base and without bubbling N_2 through the reaction mixture

Figure 5.6 shows that the platinum complex is not generated in presence of HCl. The lack of the acidic complex is unusual as well. One possible explanation is, that the acidic complex precipitates and therefore cannot be seen in the absorption spectrum. However, after cooling down the reaction mixture no precipitation could be observed. It is likely that the ligand was not stable in the used reaction conditions. Therefore, only the platinum complex which had formed at the beginning of the reaction could be observed. One possible explanation is that the ligand reacts with oxygen at such high temperatures.

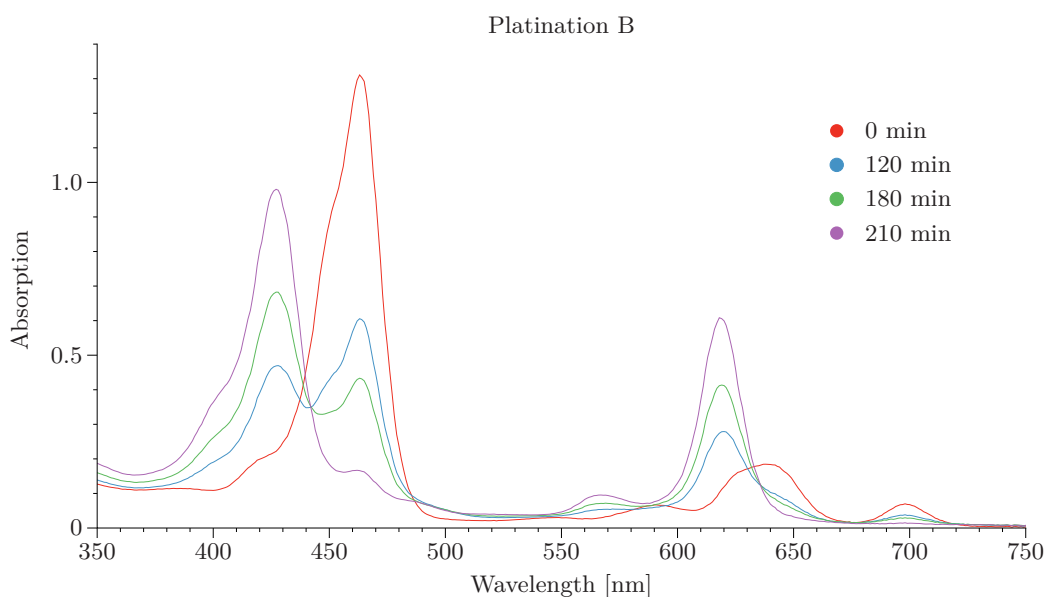


Figure 5.7: Reaction B) Without adding a base but bubbling N_2 through the reaction mixture

In method B also no acidic ligand was observed. With decreasing free ligand concentration, an increase of platinum complex was observed. Nevertheless, after the reaction was finished, the spectra indicates nearly quantitative yield. However due to bubbling N_2 through the mixture TMB evaporates and the reaction mixture gets more concentrated. Figure 5.27 shows absorption spectra with the right concentrations. By adding the Pt-precursor in smaller amounts (0.3 eq) at higher temperatures 70% yield were achieved. (section 4.2.3, page 36). The set up could have been improved by adding the Pt-precursor drop-wise. This was not possible as the precursor did not dissolve in the solvent at RT properly.

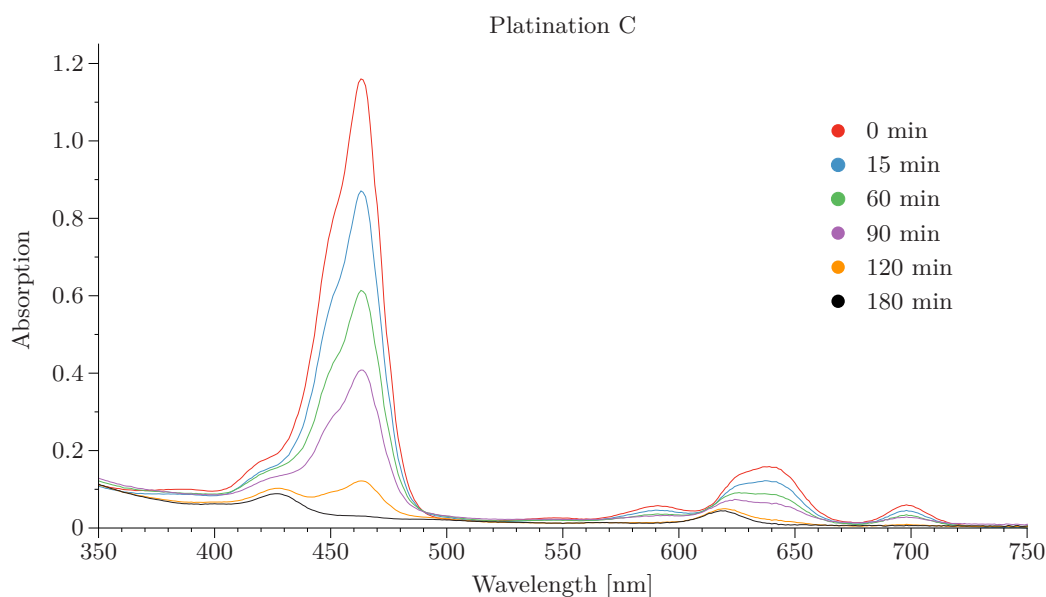


Figure 5.8: Reaction C) adding 2 eq base and without bubbling N_2 through the reaction mixture

By adding 2 eq TBA a decomposition of the ligand, no formation of the complex could be observed. Comparing A and C it can be concluded that without bubbling N_2 through the reaction mixture a decomposition of the ligand can occur.

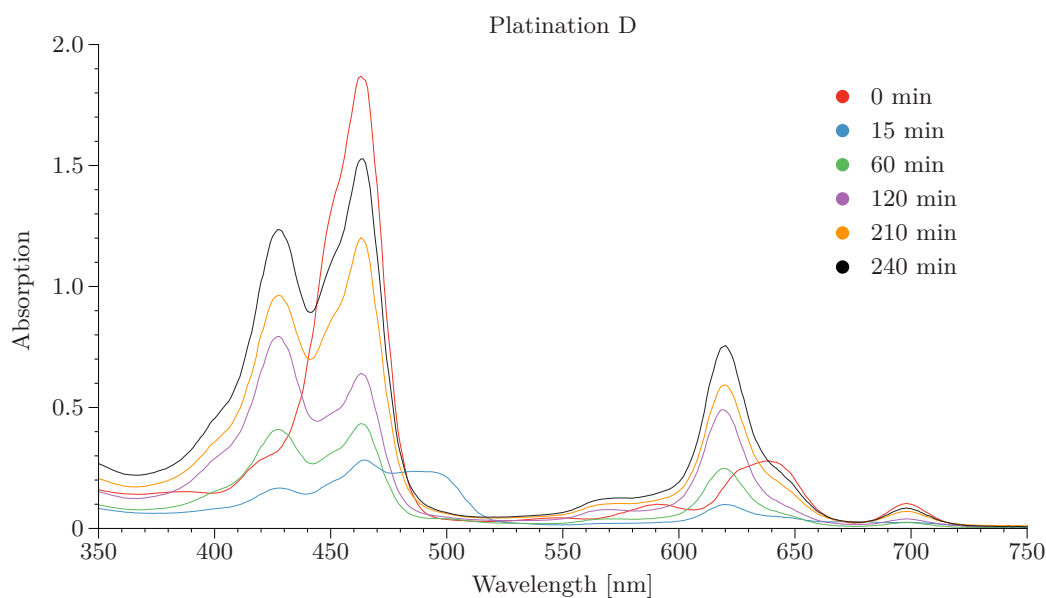


Figure 5.9: Reaction D) bubbling N_2 through the reaction mixture and adding the ligand dropwise to the Pt-precursor solution

When adding the ligand drop-wise to the hot Pt-precursor solution, some protonated ligand could be observed in the spectrum after 15 minutes. After that the drop rate was slowed down and the concentration of complex and ligand increased. After 240 minutes the reaction was stopped, but there was still reactive free ligand in the reaction. Apparently no ligand was destroyed with this method. It has to be noted that the volume of the reaction increases with time as 2/3 of the solvent is added throughout the reaction time, but the absorption spectra were recorded with the same sample volume.

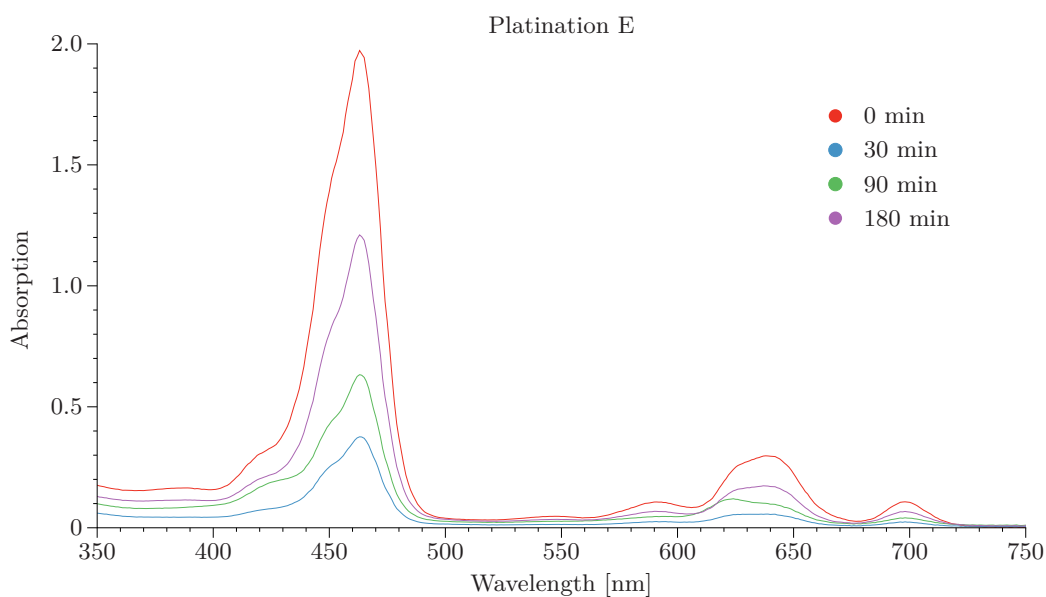


Figure 5.10: Reaction E) without bubbling N_2 and adding the ligand and 2eq base drop-wise to the Pt-precursor solution

By adding the ligand and the base drop-wise, the formation of the platinum complex is suppressed. In comparison to method C in which the platinum is added to the ligand - base mixture, less decomposition of the ligand is observed.

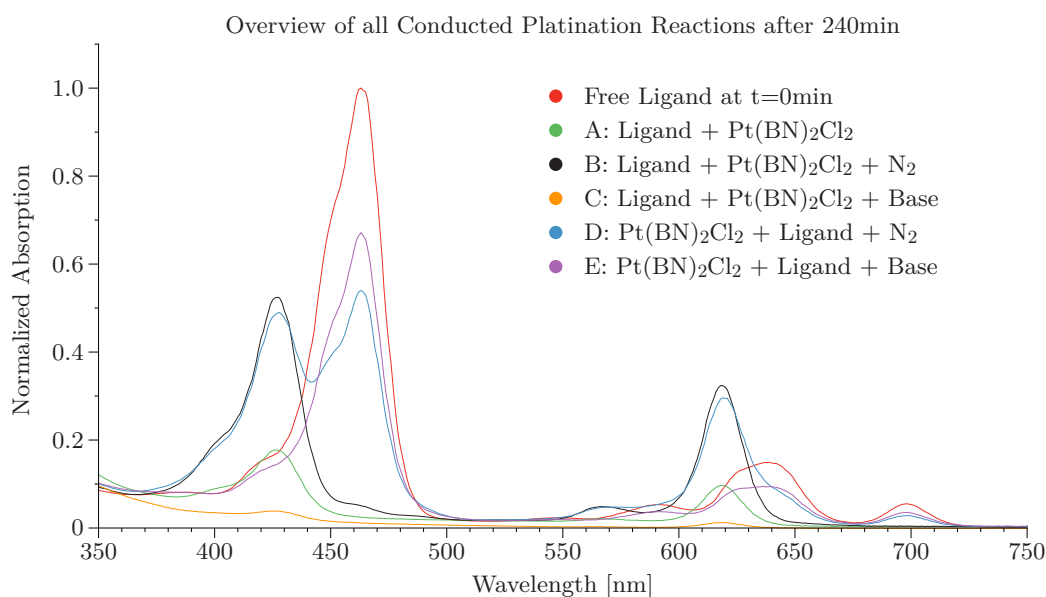


Figure 5.11: Normalized absorption spectra of the different finished reaction

In figure 5.27 all the methods are plotted normalized with respect to the absorption of the free ligand at the start of the reaction. The reactions with base are not promising, because either the ligand is destroyed or the reaction does not occur. It is known that Pt(BN)₂Cl₂ can be attacked nucleophilically by primary and secondary amines and alcohols[50] [51]. Pd(BN)₂Cl₂ reacts with the TBA[52] as well. Thus, it can be assumed that TBA reacts with the Pt-homologous too and deactivates it. This causes no platinum complex to be formed. A more promising approach is bubbling N₂ through the reaction to remove HCl in an inert atmosphere. Reaction D is most promising, as it yields comparable amounts of platinum complex like method B in the end, whilst there is still the same amount of free ligand available to react.

5.2 Dye Characterization

5.2.1 Absorption- and Emissionspectra

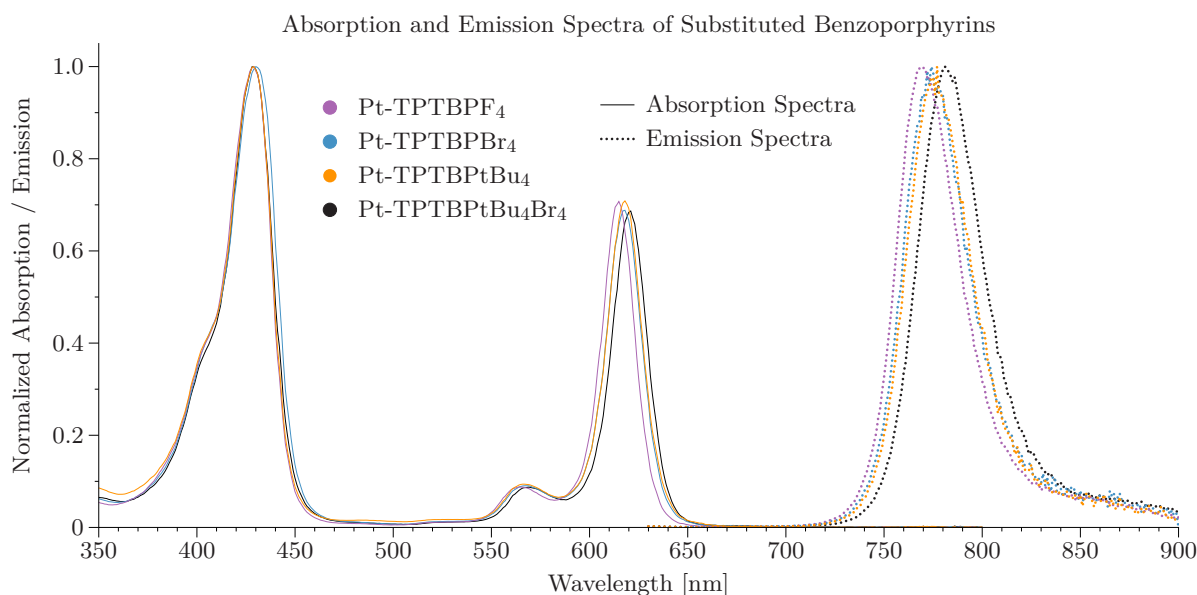


Figure 5.12: Normalized absorption and emission spectra of different Pt-TPTBP indicators

Absorption spectra were recorded in DCM and emission spectra in toluene. The spectra show that the absorption in the Soret-band remains more or less the same when varying the substitutes of the dye. The Q-band however is changed. The introduction of bromines or t-butyl groups results in a bathochromic shift of 3 nm. The dye with both groups causes a shift of 6 nm compared to Pt-TPTBPF₄. Many substitutes at the porphyrin can force it out of its planar structure causing a red shift [53]. Emission spectra show the same order only with larger shifts to the red (6 nm). The extinction coefficients and the shape are not influenced by the substituents.

Table 5.1: Photophysical properties of different Pt-TPTBP dyes

Indicator	λ_{abs} [nm]	molar absorption $\cdot 10^{-3}$ [L·mol ⁻¹ · cm ⁻¹]	λ_{em} [nm]	τ_0 [μ s]	ref.
Pt-TPTBPtBu ₄ Br ₄	429, 621	244, 150	783	56	this work
Pt-TPTBPBr ₄	431, 618	330,196	775	46	[39]
Pt-TPTBPtBu ₄	429, 618	330,196	775		this work
Pt-TPTBPF ₄	429, 615	212, 146	770	50	[21]

5.2.2 Influence of the t-Butyl Group

Due to the introduction of the t-butyl group the solubility of the dye changes. The results of the solubility experiments are listed in table 5.2. The results show, that the t-Bu groups have a tremendous effect on the solubility compared to Pt-TPTBPF₄. Since the solubility in n-butanol, DCM and cyclohexane is over 10 mg/ml, it can be assumed that the solubility is also >10 mg/ml in most commonly used organic solvents like THF, chloroform and toluene just to name a few. The solubility in TMB is very good, which has a positive influence on the platination reaction step as well.

Table 5.2: Solubility of the dyes in different solvents at 25 °C

Solvent	Pt-TPTBPtBu ₄ Br ₄ [mg/ml]	Pt-TPTBPF ₄ [mg/ml]
Methanol	0.1	not measurable
Isopropyl alcohol	2.3	0.008
Ethanol	2.2	0.2
n-Butanol	9.6	0.03
Cyclohexane	>10	0.03
DCM	>10	2.9
Trimethylbenzene	>10	1.9

5.2.3 Photobleaching

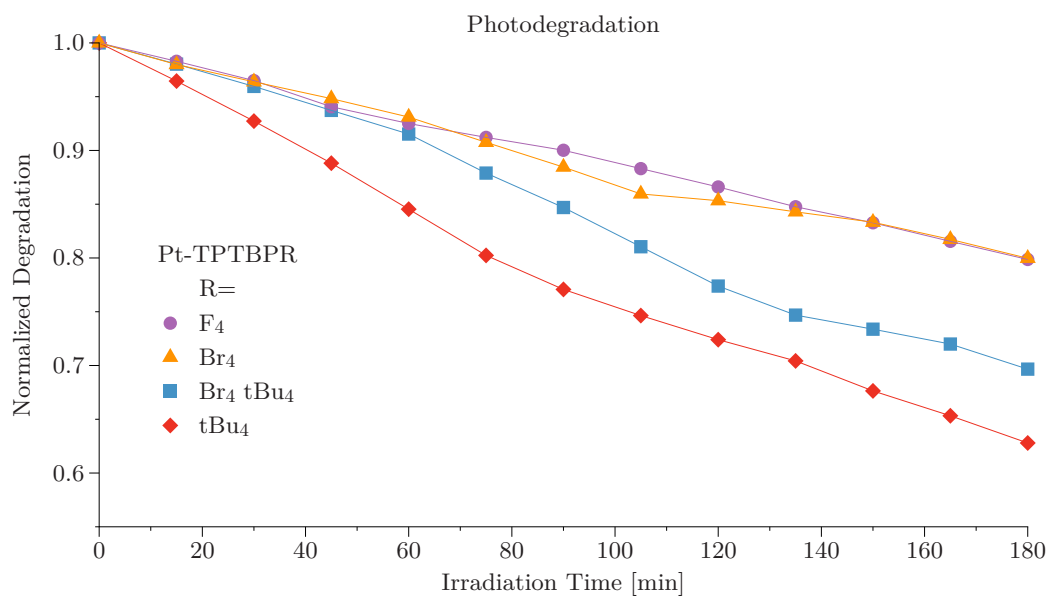


Figure 5.13: Normalized degradation of different porphyrin dyes

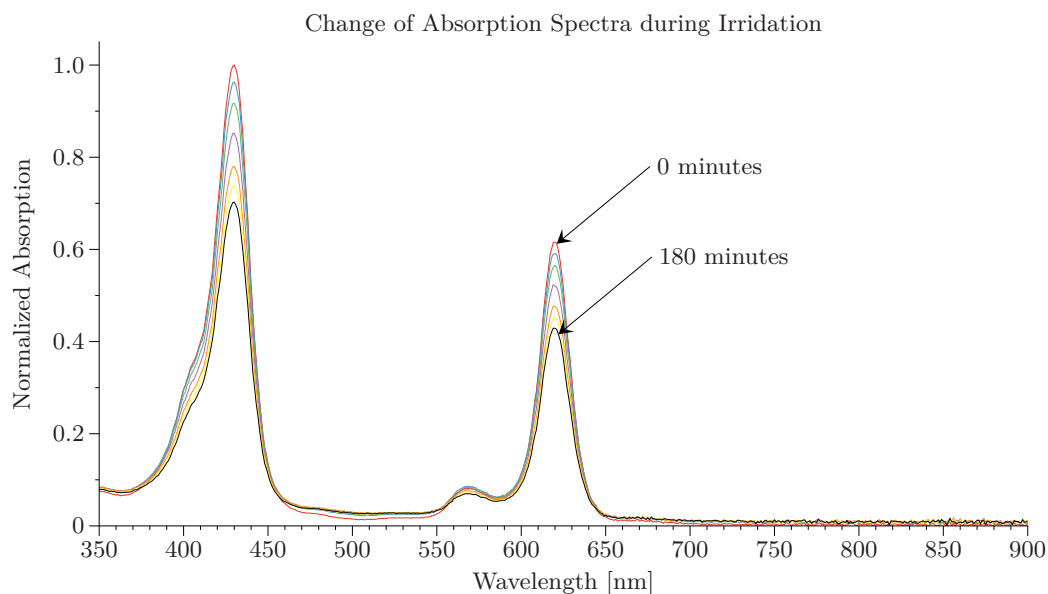


Figure 5.14: Absorption spectra during irradiation

The photostability of the dye is of particular interest for practical applications. Especially in those cases where high light densities are used or measurements are performed for prolonged time.

Photodegradation occurs mainly due to singlet oxygen production upon quenching. This singlet oxygen reacts with the dye in the ground state resulting in products, which are typically not luminescent [23]. Previous studies have indicated that the substituents affect the redox behaviour of the porphyrin ring because of electronic effects and non-planar deformations of the macro cycle induced by crowding at the porphyrin periphery [54][55].

By this experiment information about the relationship of the structure of a luminescent dye and its stability against photodegradation may be obtained.

After 180 min of irradiation $\approx 20\%$ of bromo and fluoro substituted porphyrin is already destroyed. Pt-TPTBPtBu₄Br₄ ($\approx 30\%$) and Pt-TPTBPtBu₄ ($\approx 40\%$) indicates that introducing t-Bu groups decrease the photostability. It is already known that electron withdrawing substitutes like fluorine have a positive influence on the photostability[21]. Therefore it can be assumed that electron pushing substitutes, like t-butyl groups enhance the oxidative decomposition as they decrease the reduction potential. However, the benzoporphyrin indicator dyes are all highly photostable compared to for example commercially available octaethylporphyrins [56].

5.3 Sensor Materials

The platinum catalysed hydrosilylation of vinyl terminated siloxanes (backbone BB) with hydride functional siloxanes (crosslinker CL) is the basis for preparing the silicone rubber sensor matrix. A variety of basic functionalized polysiloxanes can be commercially obtained. $\text{Pt-TPTBPtBu}_4\text{Br}_x\text{Styr}_y$ was used for all sensor foils. Due to the styrene groups of the modified indicator dye, it is possible to bind it to the polymer matrix covalently by the reaction of the dye with the hydride containing polysiloxane. A possible combination of dye, crosslinker and backbone is shown in Fig.5.15. Using silicone rubber yields in a highly gas permeable matrix for the oxygen sensor. Therefore, the sensor can be used for measuring trace oxygen concentrations.

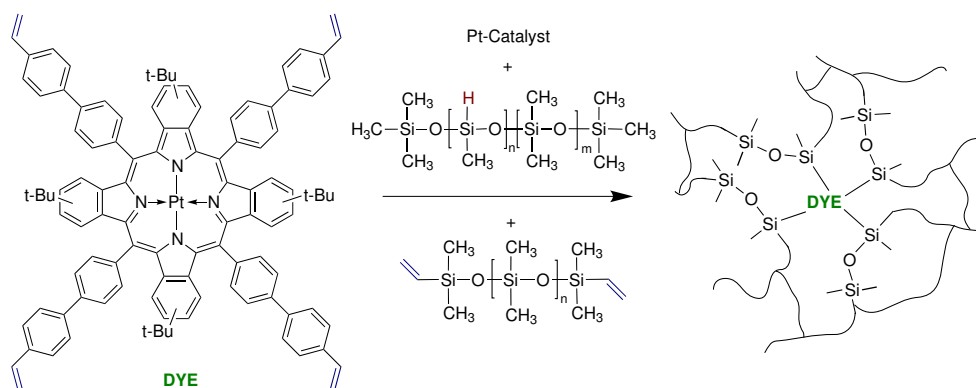


Figure 5.15: Reaction scheme for preparing the silicone matrix with covalently linked indicator dye

Due to the covalent linking of the dye it is possible to prevent leaching and aggregation, which is caused by migration of the dye in the matrix, which would seriously compromise the performance of an optical sensor over time.

One goal of this thesis was to change the sensitivity of the sensor material by applying different substituted polysiloxanes. We were able to use three different crosslinkers: a hydride terminated polysiloxane (a) and two hydride containing co-polymers with different amounts of hydride and molecular weight (b) (Fig.5.16). Although the dihydride is not a crosslinker per definition (it is able to make linear polymers), it will be stated as crosslinker throughout this thesis.

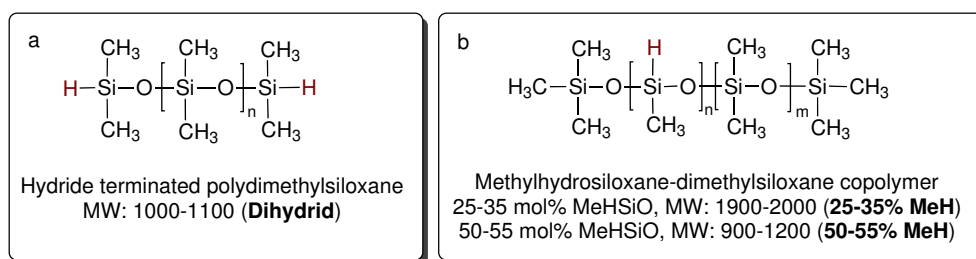


Figure 5.16: Different hydride functionalised polysiloxane crosslinkers (CL)

Six different vinyl terminated polysiloxanes were used as backbones, whereby two of them only differ in molecular weight. The effect of the side groups of the polymer should influence the free volume of the silicone rubber and therefore change the sensitivity (Fig.5.17).

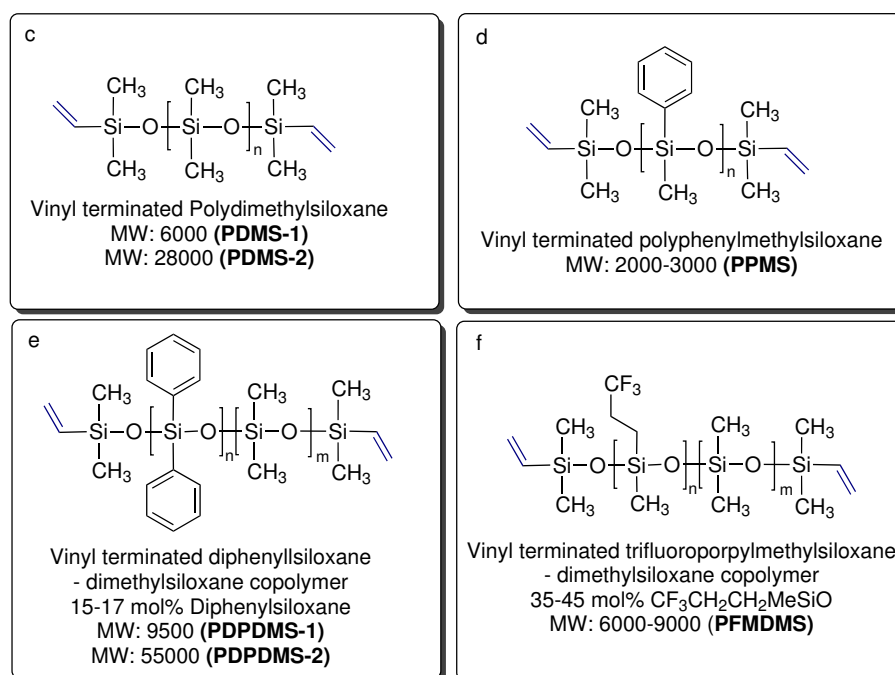


Figure 5.17: Different vinyl terminated polysiloxane backbones (BB)

The sensor layers were generally prepared as described in section 4.4.1. First, the styrene modified dye (0.5w%) was allowed to react with the crosslinker to ensure that the dye was covalently bound to the matrix. Afterwards, the backbone was added and the cocktail was knife-coated. The used quantities for each silicone foil are listed in table 4.2 on page 41.

5.3.1 The Dye in Different Media

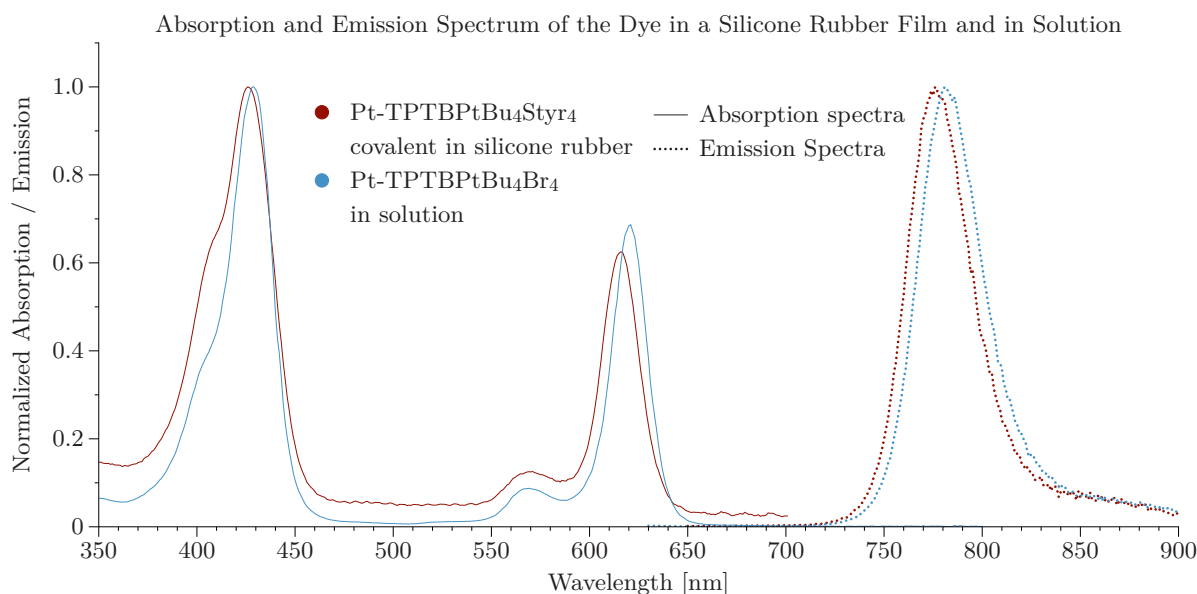


Figure 5.18: Normalized absorption and emission spectra of the dye in different media

Figure 5.18 shows, that covalent linking of the dye in the silicone rubbers has no major influence on the absorption and emission spectra. The indicator in the silicone rubber foil shows a broad shoulder at the Soret-band. The Q-band shows a lower extinction at the covalent coupled dye, which can be attributed to the missing Br groups as already seen in Fig. 5.4 on page 48. Additionally, the silicone foil shows a hypsochromic shift of the Q-band and the emission spectra which may be attributable to the more rigid environment of the dye.

5.3.2 Influence of Pot-Time and Knife Coating

One key factor of preparing the sensor is the time between adding the backbone and knife coating. The pot time of the cocktail was only a few minutes at RT as the reaction takes place rapidly. Usually, it is possible to control the pot life by adding a retarder, which deactivates the Pt-catalyst for a certain time. By using the retarder, the sensor foils showed very different τ_0 values and it was not possible, to make sensor foils reproducible. Due to that, all sensor foils were prepared without an retarder.

When producing two sensors from the same cocktail, it could be observed that the one which

was knife coated a few seconds later had longer lifetimes and K_{SV} values (Tab. 5.3). These observations are neither beneficial to handling nor to the reproducibility of the sensor preparation. To increase the pot life the cocktail was cooled down to -18°C in the freezer before and after adding the backbone. With this method, the cocktail remains viscous for a longer time and the sensor foils turn out to be more reproducible. A cocktail after 10 minutes in the freezer (after adding the backbone) has the same sensor performance as a cocktail that was cooled down for 60 minutes or more. It was also possible, to use a cocktail after 3 days in the freezer.

Table 5.3: Influence of pot-time and knife coating on SV-fitting parameters

Sensor	Indicator	Backbone	Crosslinker	eq CL	τ_0 [μs]	K_{SV1} [$h\text{Pa}^{-1}$]	f
Not cooled I	Tetra-styrene	PDMS-2	25-35% MeH	1.5	54.0	0.152	0.975
Not cooled II	Tetra-styrene	PDMS-2	25-35% MeH	1.5	55.9	0.169	0.977
10 min freezer	Tetra-styrene	PDMS-2	25-35% MeH	1.5	54.5	0.150	0.974
60 min freezer	Tetra-styrene	PDMS-2	25-35% MeH	1.5	54.9	0.152	0.973

5.3.3 Mono and Tetra-Styrene Dyes with Different Crosslinkers

In this experiment, the influence of mono-and tetra styrene dyes in different crosslinkers was investigated. Tetra-styrene can act as a crosslinker whilst mono-styrene can more easily move in the rubber.

As backbone PDMS-2 was used and three crosslinkers with both the mono-and tetra-styrene dye sensors were prepared. Sensor foils with dihydride, 3 eq crosslinker were used as the foil was mechanically unstable with just 1.5 eq. The different calibration curves are plotted in Fig.5.19 and sensor parameters are listed in table 5.4.

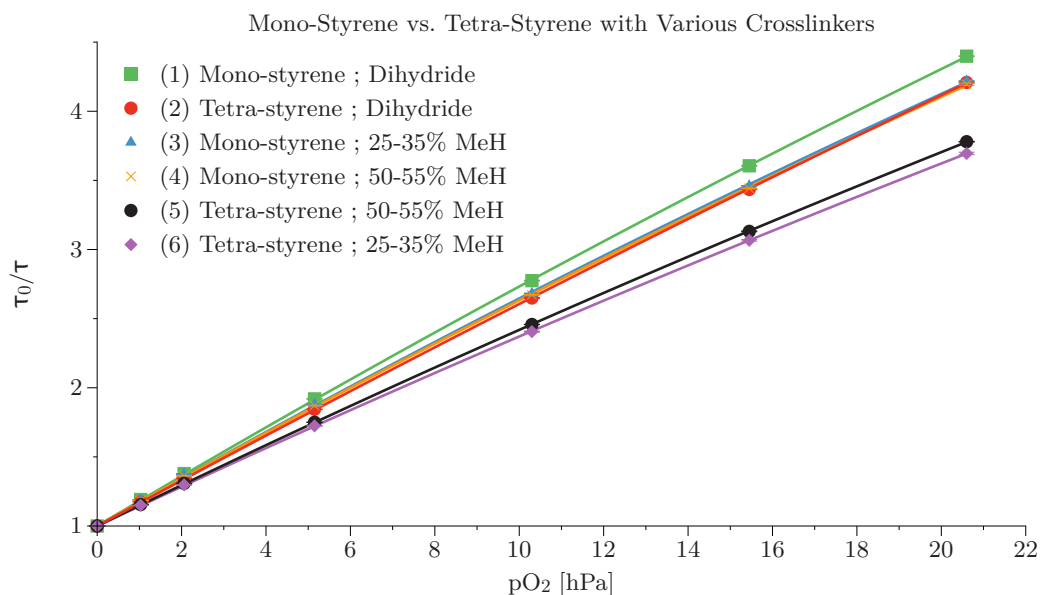


Figure 5.19: Mono-styrene vs. tetra-styrene with different crosslinkers

Table 5.4: SV-Fitting parameters of mono- and tetra-styrene dyes with different crosslinkers

Nr.	Indicator	Backbone	Crosslinker	eq CL	τ_0 [μ s]	K_{SV1} [hPa^{-1}]	f
(1)	Mono-styrene	PDMS-2	Dihydride	3	61.5	0.187	0.973
(2)	Tetra-styrene	PDMS-2	Dihydride	3	65.1	0.169	0.981
(3)	Mono-styrene	PDMS-2	25-35% MeH	1.5	61.7	0.179	0.969
(4)	Mono-styrene	PDMS-2	50-55% MeH	1.5	61.5	0.177	0.969
(5)	Tetra-styrene	PDMS-2	50-55% MeH	1.5	52.2	0.154	0.966
(6)	Tetra-styrene	PDMS-2	25-35% MeH	1.5	54.5	0.148	0.968

All sensors with dihydride crosslinker or mono-styrene dye have a higher τ_0 and are slightly more sensitive compared to 25-35 % MeH and 50-55 % MeH crosslinkers or tetra-styrene dye. This can be attributed to more free volume in the silicone rubber due to less crosslinking. Tetra-styrene in dihydride is an exception with the highest τ_0 . It can be assumed that using dihydride keeps the backbone in distance to the dye and therefore the free volume around the dye is increased, whilst mono-styrene dye can move easily in the silicone rubber. The other two crosslinkers be-

have similarly, whether using mono-or tetra-styrene.

It can be concluded that changing the crosslinker does not radically affect the sensitivity. Using mono-styrene dye yields in higher lifetimes, but the sensor foils suffer from lower mechanical stability as mono-styrene does not act as a crosslinker.

5.3.4 Influence of Different Amounts of Used Crosslinker

Different amounts of crosslinker were used for PDMS-2 as backbone, 25-35 % MeH as crosslinker and 0.5 w% tetra-styrene dye respectively to the amount of crosslinker and backbone together. According to the SV-Plots (Tab.5.5) using higher crosslinker ratios yields in slightly more sensitive sensors because of more free volume in the silicone rubber. However, no dramatic change of τ_0 and K_{SV} can be obtained, meaning this set up is very robust against the change of crosslinker concentration.

A faster curing of the silicone rubber with an increasing concentration of the crosslinker could not be noticed.

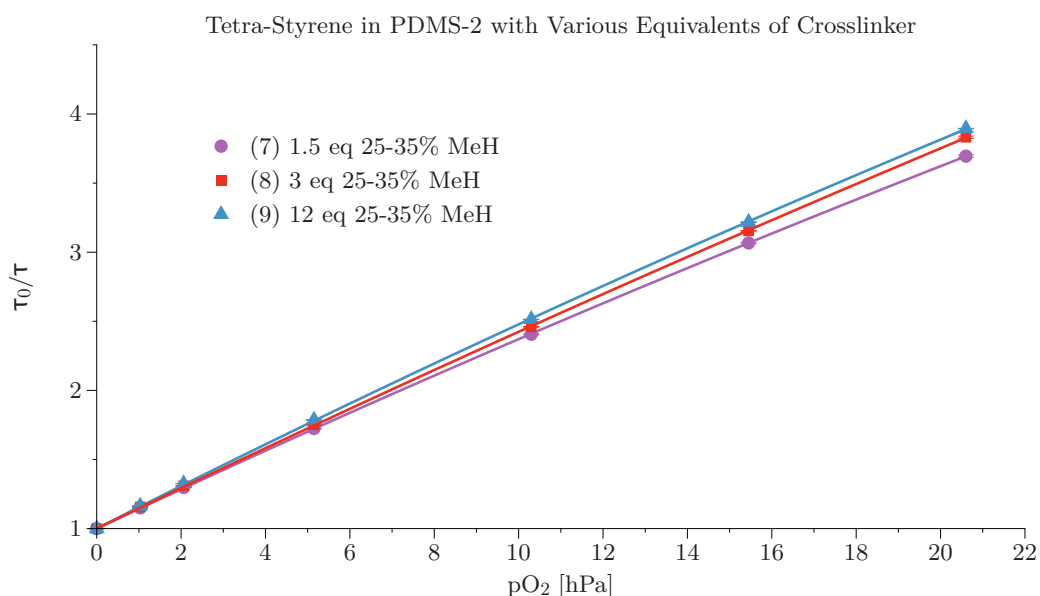


Figure 5.20: Tetrastylene with various equivalent of crosslinker

Table 5.5: SV-Fitting parameters of tetrastylene with different equivalent of crosslinker

Nr.	Indicator	Backbone	Crosslinker	eq CL	τ_0 [μ s]	K_{SV1} [hPa^{-1}]	f
(7)	Tetra-styrene	PDMS-2	25-35% MeH	1.5	54.5	0.148	0.968
(8)	Tetra-styrene	PDMS-2	25-35% MeH	3	54.7	0.151	0.976
(9)	Tetra-styrene	PDMS-2	25-35% MeH	12	56.7	0.161	0.967

The previous set up profits from the chemically similar structures of crosslinker and backbone. Therefore, polydiphenyl-dimethyl-siloxane (PDPDMS-2) backbone was cross-linked with different equivalents of dihydride or 25-35 % MeH crosslinker (Fig.5.20). Interestingly, the amount of used crosslinker has no significant impact. The main difference yields from the chemical structure of the crosslinker. Using dihydride results in longer τ_0 than highly crosslinking 25-35 % MeH (as already seen in section 5.3.3). To conclude, using more equivalents of cross-linker does not influence the sensor performance, but can increase the mechanical stability of the silicone rubber, especially by using dihydride crosslinker.

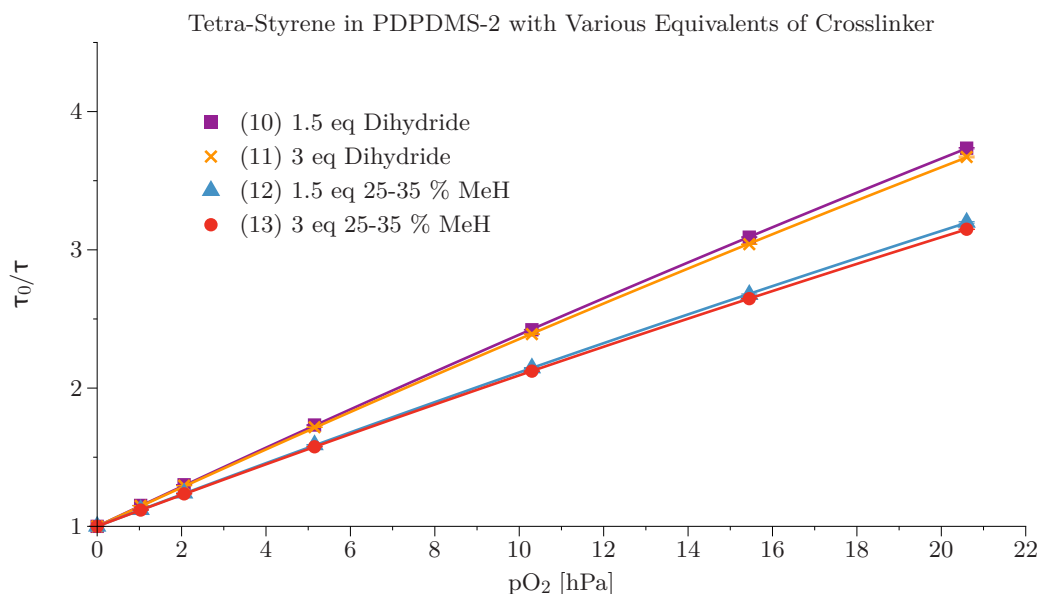


Figure 5.21: Different equivalent of crosslinker using PDPDMS backbone

Table 5.6: SV-Fitting parameters of tetra-styrene in PDPDMS and different amount of crosslinker

Nr.	Indicator	Backbone	Crosslinker	eq CL	τ_0 [μs]	K_{SV1} [hPa^{-1}]	f
(10)	Tetra-styrene	PDPDMS-2	Dihydride	1.5	58.1	0.149	0.970
(11)	Tetra-styrene	PDPDMS-2	Dihydride	3	57.2	0.146	0.969
(12)	Tetra-styrene	PDPDMS-2	25-35% MeH	1.5	47.5	0.121	0.963
(13)	Tetra-styrene	PDPDMS-2	25-35% MeH	3	50.0	0.119	0.961

5.3.5 Influence of Different Backbones

Throughout these experiments differently substituted backbones were used in combinations with various crosslinkers in order to change the sensitivity. However, not every set up yielded in measurable sensor foils because of poor mechanical stability. In order to overcome this problem, the concentration of used crosslinker was adapted. According to the experiments in section 5.3.4, this should not have a dramatic influence.

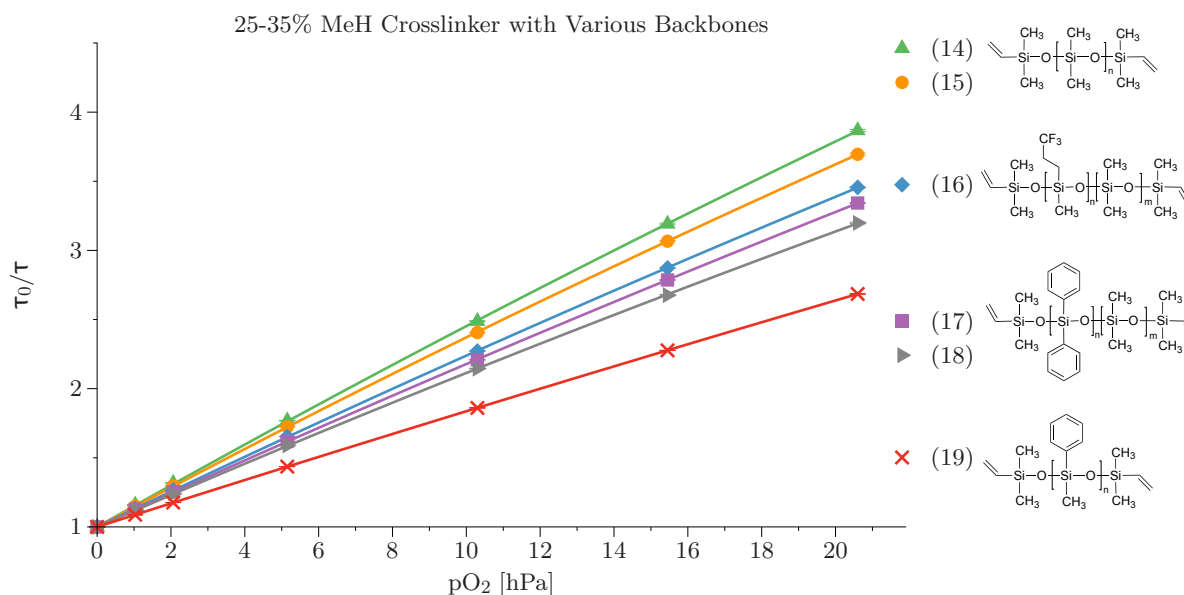


Figure 5.22: Tetra-styrene dye with 25-35% MeH crosslinker and different backbones

Table 5.7: SV Fitting parameters of 25-35% MeH crosslinker and different backbones

Nr.	Indicator	Backbone	Crosslinker	eq CL	τ_0 [μs]	K_{SV1} [hPa^{-1}]	f
(14)	Tetra-styrene	PDMS-1	25-35% MeH	1.5	54.5	0.156	0.972
(15)	Tetra-styrene	PDMS-2	25-35% MeH	1.5	54.5	0.148	0.968
(16)	Tetra-styrene	PDPDMS-1	25-35% MeH	3	56.2	0.133	0.970
(17)	Tetra-styrene	PFMDMS	25-35% MeH	6	52.0	0.119	0.961
(18)	Tetra-styrene	PDPDMS-2	25-35% MeH	3	47.5	0.121	0.963
(19)	Tetra-styrene	PPMS	25-35% MeH	1.5	53.4	0.088	0.975

The change of the sensitivity of the sensor corresponds to the predictions in literature [57]. The gas permeability coefficient decreases as increasingly bulky functional groups are substituted in the polymer side chain. This decrease is mainly due to a decline in diffusivity, which is caused by increasing rigidity of the polymer backbone and the decreasing free volume available for diffusion [58]. Moreover, the solubility of oxygen gas decreases with increasing substitutes. Polydimethylsiloxane with a MW of 6000 (PDMS-1) showed the highest K_{SV} value. With increasing molecular weight, the sensitivity decreases which can be attributed to the flexibility of the chain and longer distances between crosslinkers, which is subsequently reducing the free volume in the rubber. The same effect occurs with poly-diphenyl-co-dimethyl siloxane (PDPDMS). Polyphenylmethyl (PPMS) shows the lowest sensitivity of these backbones as it is not a copolymer like PDPDMS (15-17 mol% diphenyl groups) or poly-trifluoropropyl-methylco-dimethylsiloxane (PFMDMS) (35-45 mol% trifluoropropyl groups). These copolymers all show similar sensitivities.

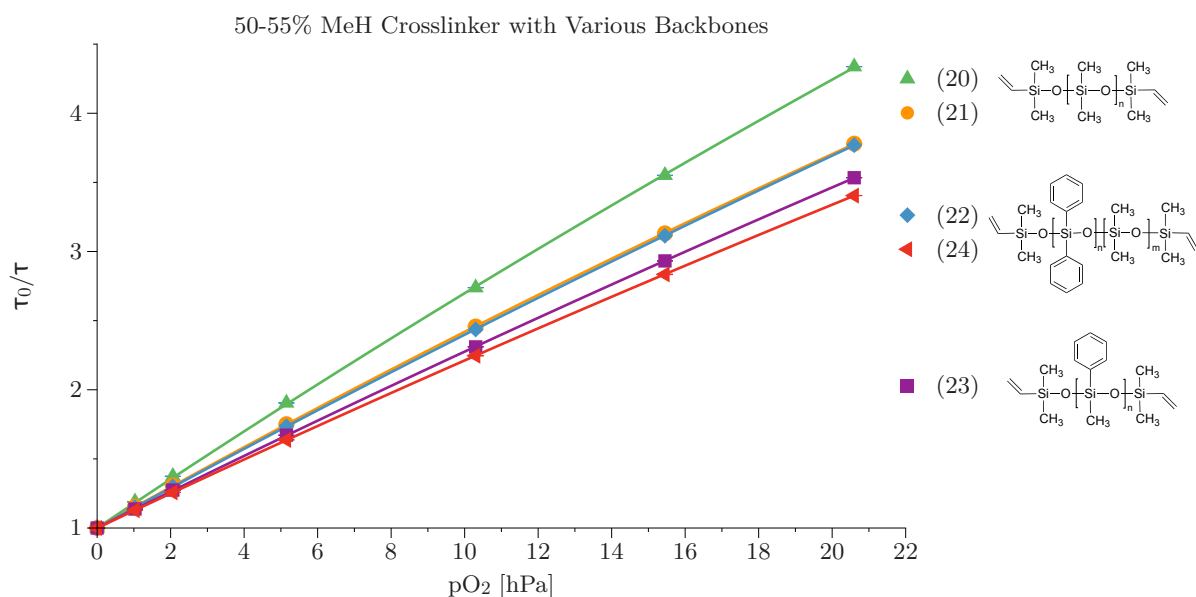


Figure 5.23: Tetra-styrene in 50-55%H crosslinker and different backbones

Table 5.8: SV Fitting parameters of 45-55% MeH crosslinker and different backbones

Nr.	Indicator	Backbone	Crosslinker	eq CL	τ_0	K_{SV1}	f
					[μ s]	[hPa^{-1}]	
(20)	Tetra-styrene	PDMS-1	50-55% MeH	3	58.9	0.183	0.973
(21)	Tetra-styrene	PDMS-2	50-55% MeH	3	52.2	0.154	0.967
(22)	Tetra-styrene	PDPDMS-1	50-55% MeH	3	54.5	0.149	0.973
(23)	Tetra-styrene	PPMS	50-55% MeH	3	57.6	0.136	0.973
(24)	Tetra-styrene	PDPDMS-2	50-55% MeH	3	47.9	0.129	0.971

Using a cross-linker with more mol% hydride shows the similar order of sensitivity, although in this case the bulkier backbones show higher K_{SV} values. For some reason, the fluorinated polysiloxane backbone (PFMDMS) showed a surprisingly low τ_0 value and was therefore not further investigated.

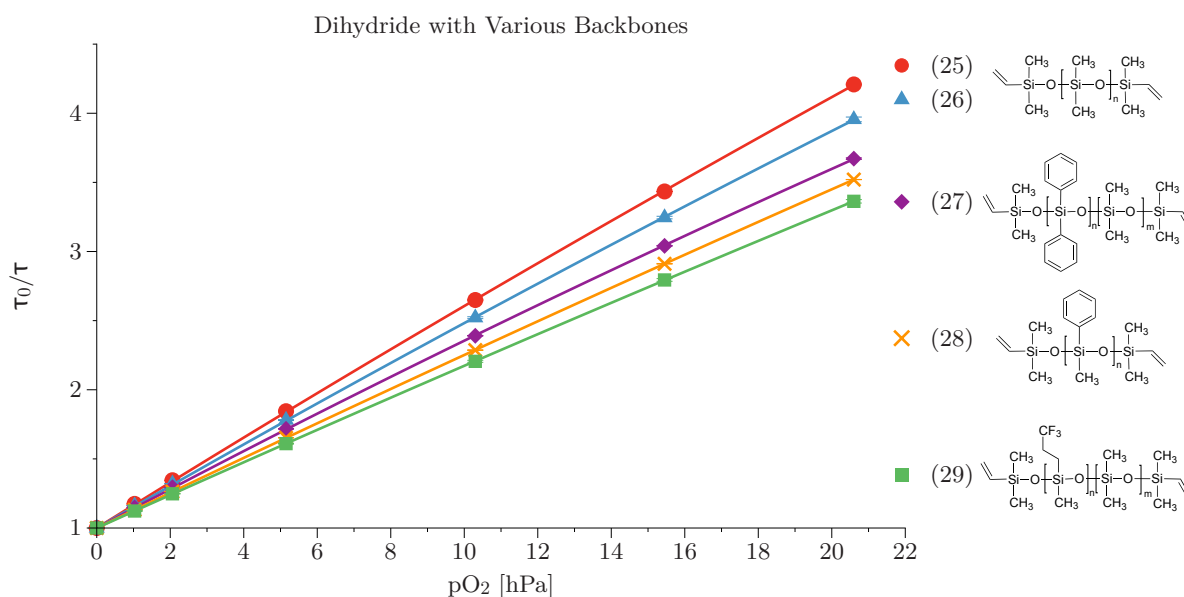


Figure 5.24: Tetra-styrene in dihydride crosslinker and different backbones

Table 5.9: SV Fitting parameters of dihydride crosslinker and different backbones

Nr.	Indicator	Backbone	Crosslinker	eq CL	τ_0 [μ s]	K_{SV1} [hPa^{-1}]	f
(25)	Tetra-styrene	PDMS-1	Dihydride	3	65.0	0.168	0.980
(26)	Tetra-styrene	PDMS-2	Dihydride	1.5	63.0	0.156	0.978
(27)	Tetra-styrene	PDPDMS-2	Dihydride	3	57.2	0.146	0.969
(28)	Tetra-styrene	PPMS	Dihydride	1.5	55.3	0.130	0.983
(29)	Tetra-styrene	PFMDMS	Dihydride	3	52.0	0.122	0.982

Using dihydride crosslinker usually yields in higher τ_0 values and the sensors are slightly more sensitive. This can be attributed to the high free volume in the silicone rubber. A huge drawback is the low mechanical stability of the sensor foils which could not be improved by applying more crosslinker. Adding a highly crosslinking agent like 50-55% MeH might improve the mechanical stability without negatively influencing the high τ_0 values. To proof that, further investigations would be necessary.

Conclusion

The preparation of the trace oxygen sensors with this two component addition method to obtain silicone rubber is a very robust method. All the different backbones and crosslinkers generate trace sensors in a similar dynamic range. By using the dihydride crosslinker or mono-styrene dye, very high τ_0 values can be achieved. The preferred setup though is the PDMS-2 with the 25-35 % MeH crosslinker, and tetra styrene dye, because of several reasons:

- sensor foils show high mechanical stability
- cocktail have a very good viscosity for knife coating
- sensor layers are homogeneous
- cocktail can be kept in freezer for at least 3 days
- τ_0 is acceptable

Using tetra styrene dye is also preferable, as the synthesis and purification of mono-styrene dye is more time-consuming.

Limit of Detection

The limit of detection is calculated using the linear Stern-Volmer equation (2.7). For the preferred sensor setup, a τ_0 of 54.5 μs is measured using phase fluorimetry at 4000 kHz frequency. This means, a ϕ value of 53.8° is measured. The smallest change of signal which is reliable is 0.1°. By calculating the τ value at 53.7° and using the Stern-Volmer equation with an K_{SV} value of 0.148 hPa^{-1} , a limit of detection of 0.0248 hPa is calculated.

5.3.6 Leaching Experiment

For the leaching experiment, a sensor (mono-styrene in 25-35 % MeH crosslinker and PDMS-2) was extracted for 48 hours in a 1/1 mixture of THF/EtOH in which the dye shows a very good solubility. Afterwards the sensor was dried for 12 hours at 60 °C and the sensor was calibrated again.

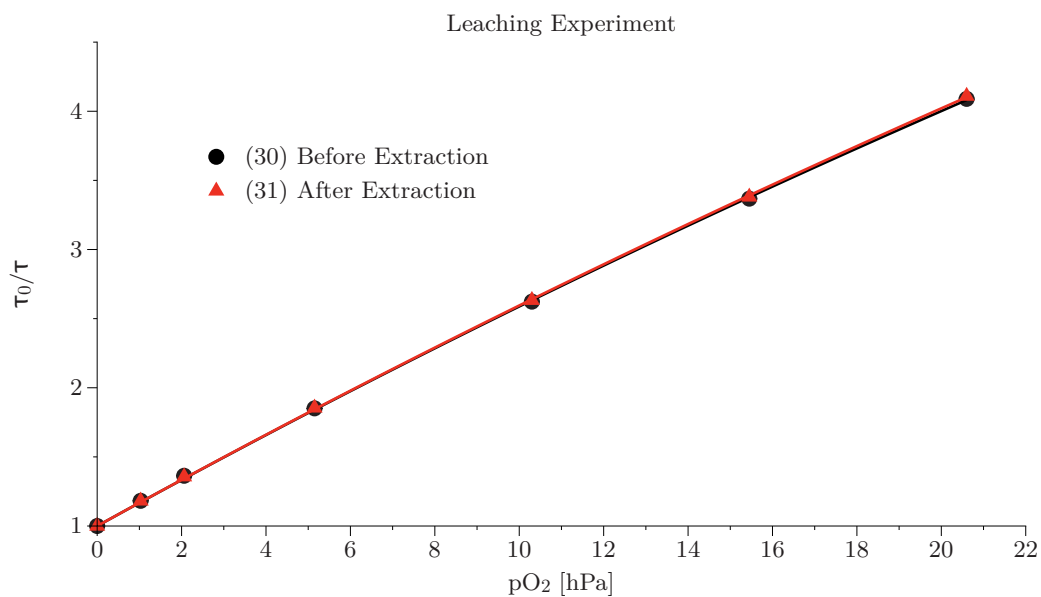


Figure 5.25: Leaching experiment of mono-styrene in 25-35% MeH crosslinker and PDMS-2 backbone

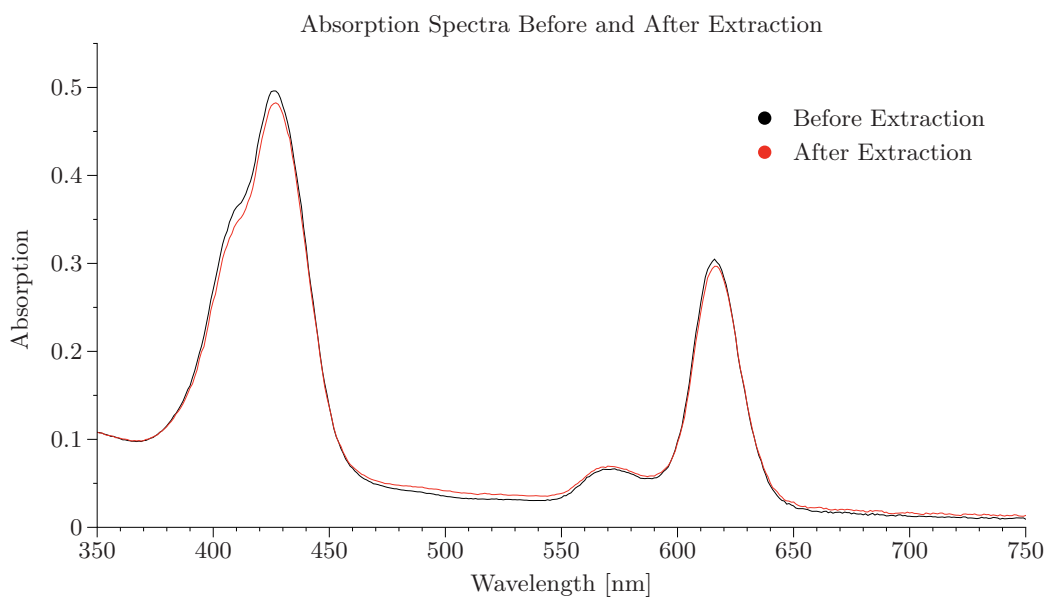


Figure 5.26: Absorption spectra of the sensor foil before and after extraction

Table 5.10: SV Fitting parameters of the sensor foil before and after extraction experiment

Nr.	Indicator	Backbone	Crosslinker	eq CL	τ_0 [μs]	K_{SV1} [hPa^{-1}]	f
(30)	Mono-styrene	PDMS-2	25-35% MeH	1.5	60.3	0.175	0.965
(31)	Mono-styrene	PDMS-2	25-35% MeH	1.5	60.3	0.175	0.966

The τ_0 and K_{SV} values did not change due to extraction. The absorption spectra of the sensor remained the same as well, which means that no dye was washed out which is the proof of covalent immobilization. By extraction of a silicone foil with non-styrene modified dye like Pt-TPTBPtBu₄Br₄, leaching of the indicator can be observed immediately.

5.3.7 Temperature Dependency of the Sensor

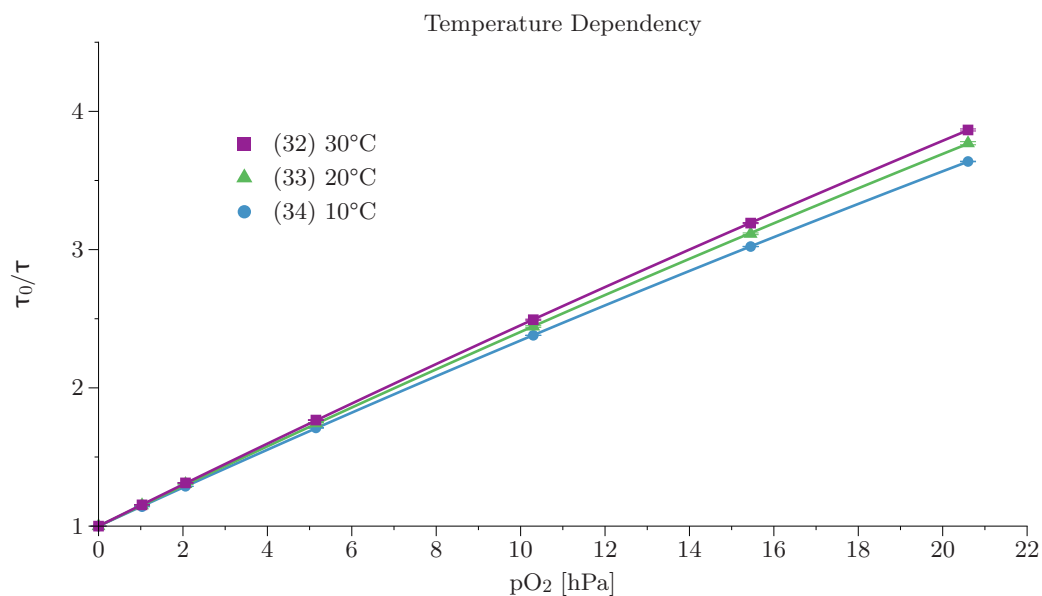


Figure 5.27: Temperature dependency of tetra-styrene in 25-35% MeH crosslinker and PDMS-2 backbone

Table 5.11: SV Fitting parameters of temperature dependency experiment

Nr.	Indicator	Backbone	Crosslinker	eq CL	τ_0 [μs]	K_{SV1} [hPa^{-1}]	f
(32) 10°C	tetra-styrene (1w %)	PDMS-2	25-35% MeH	12	56.5	0.156	0.972
(33) 20°C	tetra-styrene (1w %)	PDMS-2	25-35% MeH	12	56.0	0.153	0.970
(34) 30°C	tetra-styrene(1w %)	PDMS-2	25-35% MeH	12	55.5	0.146	0.967

A sensor foil consisting of 1 w% tetra-styrene dye, PDMS-2. and 12 eq 25-35 % MeH was used for this experiment. Calibrations were recorded at 10°C , 20°C and 30°C in order to receive information about the temperature dependency of the sensor.

The decay time without oxygen decreases with increasing temperature. This can be attributed to thermal quenching. However, the sensitivity increases with rising temperature due to increased oxygen diffusion in the silicone matrix.

5.3.8 Comparison with Other Trace Oxygen Sensors

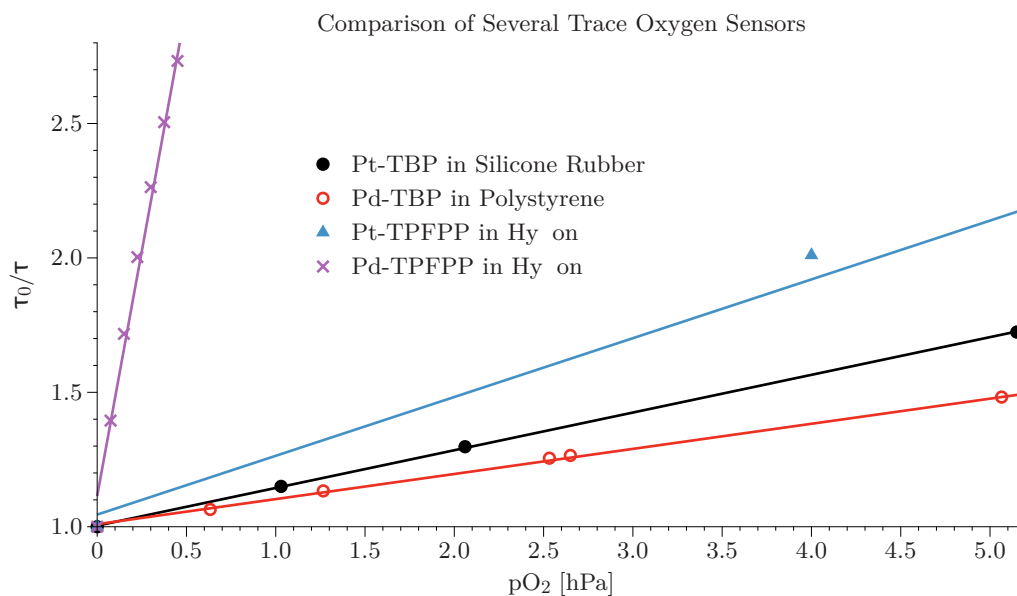


Figure 5.28: Comparison of different trace oxygen sensors

Table 5.12: SV Fitting parameters of different trace oxygen sensors

Sensor	K_{SV1} [hPa^{-1}]	R^2
Pt-TBP in Silicone Rubber	0.140	0.99985
Pd-TBP in Polystyrene	0.093	0.99917
Pt-TPFPP in Hyflon	0.219	0.99208
Pd-TPFPP in Hyflon	3.645	0.99507

Different trace oxygen sensors are plotted in Fig. 5.28. A linear SV-Fit was used. Hyflon is a perfluorinated polymer with a very high oxygen gas permeability. Using it together with an indicator dye which possesses long decay times yields in a highly sensitive sensor with a K_{SV} of $3.645 hPa^{-1}$ which can be used for ultra trace oxygen sensing. By applying Pt(II)-porphyrin in Hyflon the sensitivity decreases to a K_{SV} of $0.219 hPa^{-1}$ and is in a similar dynamic range as the new silicone rubber sensors. However, as Hyflon is perfluorinated it is difficult to immobilize an indicator without aggregation of the dye.

Pd-TBP in polystyrene is the standard trace oxygen sensor and is also commercially available. It is less sensitive and the SV-Plot is not as linear as Pt(II)-TBP in the highly permeable silicone rubber. Furthermore, using Pt(II)-TBP has the advantage of higher brightness which yields in a better signal to noise ratio.

5.3.9 Immobilisation Without Backbone

The immobilization of the tetra-styrene dye was investigated using only the dihydride crosslinker. With this method, it would be possible to produce very thin sensor foils, which show very short response times.

Between the two hydride groups are 12-13 Si-O units which is considered to be enough distance to avoid intermolecular interactions between the indicators. The dye (1 mg) was dissolved in 100 μ l chloroform, 4.8 eq dihydride (42.2 μ l) and 1 mg catalyst were added. The solution was spin coated on a glass slide as the viscosity was too low for knife coating (4000 rpm for 30 seconds). After drying in the oven at 60 °C for 12 hours, a τ_0 of 30 μ s was measured. This can be explained by aggregation of the indicator.

5.3.10 Reaction With Monohydridpolysiloxane

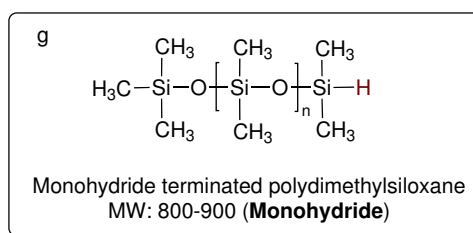


Figure 5.29: Monohydrid terminated polysiloxane

In this experiment it was tried to increase the solubility of the indicator dye in the silicone matrix by functionalizing it with a monohydride polysiloxane(g). This means that the dye is not covalently bond to the matrix.

The monohydride has a length of 9-10 Si-O groups which should be sufficient in order to enhance the solubility. 3 mg of the tetra-styrene dye was dissolved in 600 μl chloroform. Monohydride (13 μl) and 1 mg catalyst were added. The reaction mixture was stirred for 24 hours. A sensor foil with 0.5 w% of the reacted dye, 3 eq 25-35 % MeH crosslinker and PDMS-2. backbone was prepared. After drying in the oven at 60 °C for 24 hours, a τ_0 of 22.6 μs was measured. This indicates that the dye aggregates in the silicone rubber and that covalent immobilization is required.

5.4 Application of the New Sensor Material - Wine Bottles

One of the possible applications of the new trace sensors is the measurement of oxygen in wine bottles. Wine is usually sold in brown or green colored bottles as the color is a crucial factor, influencing the photo-degradation of wine as different wavelengths of light are transmitted, depending on the color of the glass[59][60].

The color of the glass results from iron(II)-oxide or chrom(III)-oxid. One major problem of the optical measurement through wine bottles is the luminescence of Cr^{3+} -ions which interferes with the luminescence of the used oxygen indicator dye[61]. Furthermore, the weak transmission through the glass can be problematic.

5.4.1 Transmission Spectra of Wine Bottles

Fig.5.30 shows that flint glass has a high transmission over 400 nm which makes the excitation and the emission of the oxygen indicator dye possible.

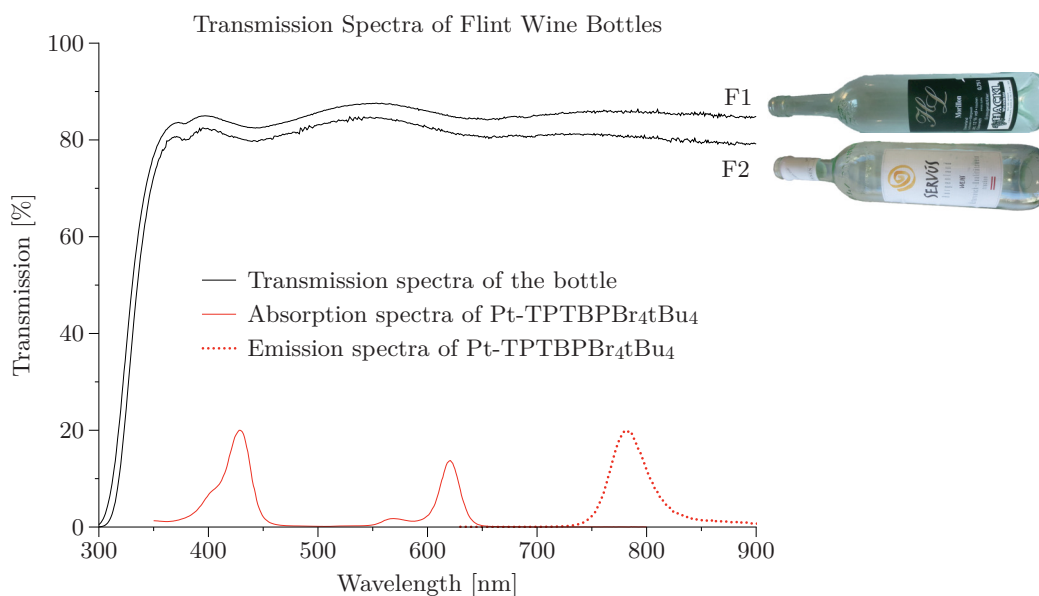


Figure 5.30: Transmission spectra of flint wine bottles

Measuring through green colored glass is more problematic because of the weak transmission around 650 nm, which is bad as the sensor dye is excited in the Q-band at around 620 nm (Fig.??). Although, the emission area of the indicator profits from a higher transmission at

around 780 nm the transmission at the excitation wavelength is still quite low in comparison to flint glass.

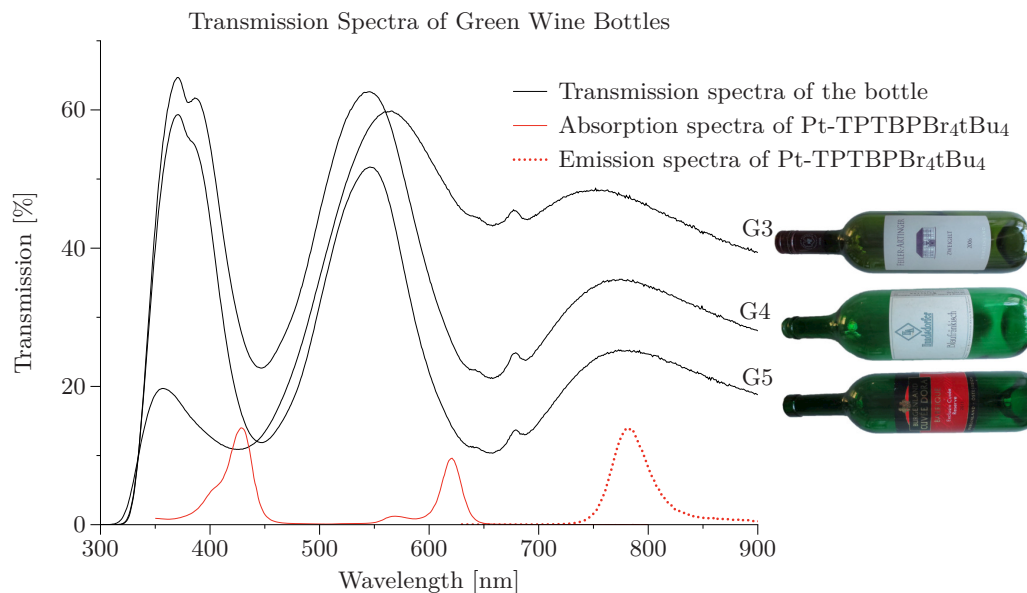


Figure 5.31: Transmission spectra of green wine bottles

It is possible to excite the benzoporphyrin indicator dye at the Q-band through brown glass (Fig.5.32). However, with increasing wavelength a decrease of the transmission of the glass occurs, which causes a decline of the emission intensity. This makes measurements through brown bottles quite difficult.

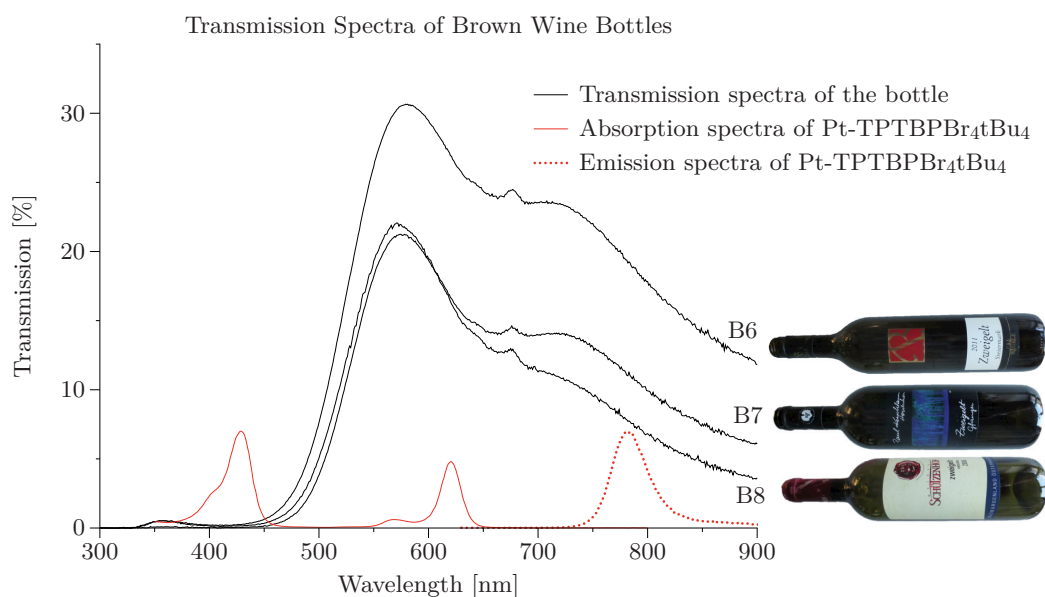


Figure 5.32: Transmission spectra of brown wine bottles

5.4.2 Excitation and Emission Spectrum

Fig.5.33 shows the excitation and the emission spectrum of Cr³⁺ of the green glass and in comparison the absorption and emission spectrum of the new silicone rubber sensor foil. All glass samples showed the same excitation/emission spectrum. The spectra shows that the used dye is not fully suitable for measuring through wine-bottles as their excitation and emission overlap. However, the new trace sensor with Pt(II)-porphyrin has a high Q.Y. and therefore it was tried to measure through the wine bottles.

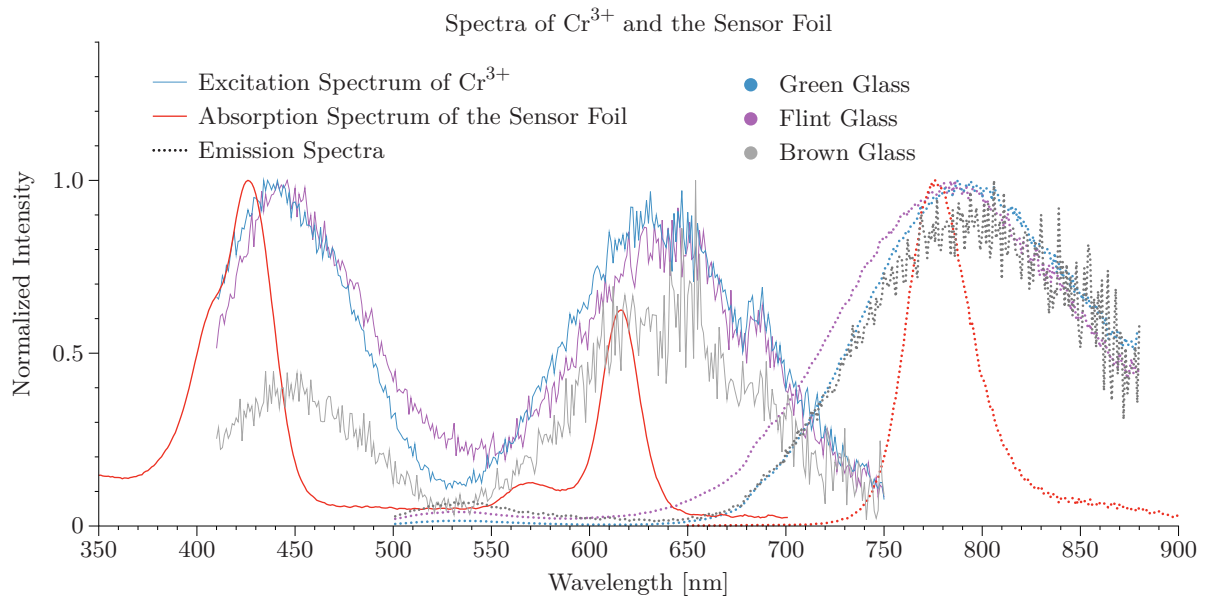


Figure 5.33: Excitation/emission spectra of the different glasses and absorption/emission spectrum of a silicone rubber sensor foil

5.4.3 Single Photon Counting

Single photon counting (SPC) measurements were conducted to determine the luminescence lifetime of the different glasses. A mono-exponential fit was used. Excitation was performed at 450 nm and emission was measured at 740 nm.

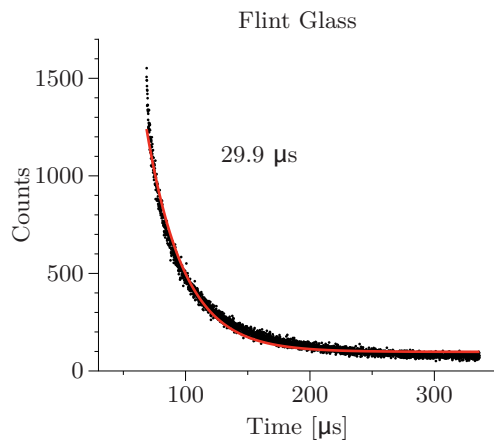


Figure 5.34: SPC of flint glass

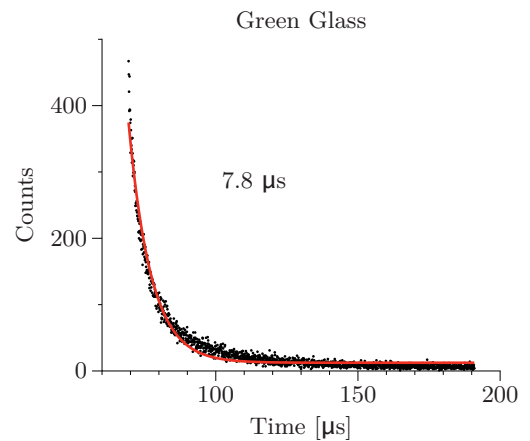


Figure 5.35: SPC of green glass

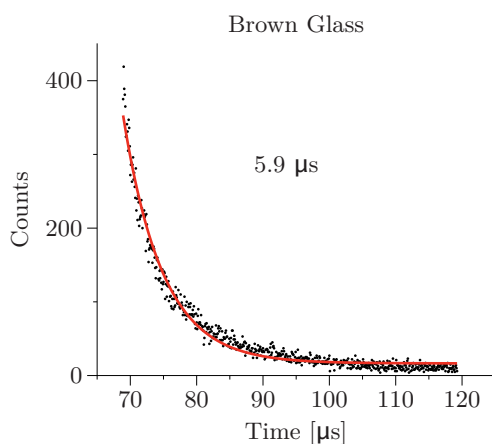


Figure 5.36: SPC of brown glass

The flint glass shows longer lifetimes in comparison to the colored wine bottles. This can be attributed to a high concentration of Cr^{3+} -ions in green and brown bottles. Therefore self quenching can occur.

5.4.4 Measuring Through Wine Bottles

A sensor foil was prepared as described in section 4.4.2. The foil was additionally coated with a TiO_2 layer to enhance backscattering of the light which leads to increased signal intensities. The 0.5 mm x 0.5 mm foil was attached to the glass surface on two positions (neck and wall) using silicone E4 because of heterogenous thickness of the glass (Fig.5.37). The neck of the bottle is generally thicker than the side-wall of the bottle.



Figure 5.37: Two sensor spots placed inside a wine bottle

Afterwards, the background of the bottle and τ_0 of the sensor were measured using a Na_2SO_3 solution. The measuring device was a Pyro-Science Firesting mini with a set LED intensity of 100 % and modulation frequency of 4000 Hz. All results are listed in table 5.13: The obtained ϕ with included background compensation (BG comp.), ϕ values without BG comp. and the background of the bottle itself. In general, ϕ values of over 50° are useful, processable data.

Table 5.13: Results from measuring through different colored wine bottles in Na_2SO_3

Sample	With BG comp.				Without BG comp.				Background			
	Neck		Wall		Neck		Wall		Neck		Wall	
	ϕ [°]	Int [mV]	ϕ [°]	Int [mV]	ϕ [°]	Int [mV]	ϕ [°]	Int [mV]	ϕ [°]	Int [mV]	ϕ [°]	Int [mV]
F1	51.3	270	51.3	270	50.8	1370	50.8	1270	33.9	32	30.4	26
F2	51.6	236	51.8	266	50.9	1030	51.3	1315	29.7	27	29.1	17
G3	48.0	100	50.9	260	40.4	138	47.0	283	12.5	39	12.4	31
G4	52.1	93	52.1	175	37.0	167	40.6	220	12.5	39	14.9	67
G5	48.3	8	51.1	70	48.1	46	37.2	107	9.1	41	9.1	37
B6	50.4	31	51.3	51	50.0	28	50.9	58	8.2	9	8.1	9
B7	46.0	6	51.4	65	28.7	13	47.3	70	7.2	7	7	7
B8	51.3	15	51.3	260	33.7	23	49.2	118	8.6	11	8.6	10

The background measurements of the flint bottles show high ϕ values compared to green and brown glass. This can be attributed to traces of Cr^{3+} -ions in the glass. ϕ values of the background in green bottles are lower, because self quenching occurs in this high concentrations of Cr^{3+} . This results are comparable to SPC measurements.

However, it was shown that conducting background compensation is necessary in order to measure through wine bottles. From the results it can be concluded that measurements through the wall are better suitable than measurements through the neck, as the glass is thicker and therefore low intensities were obtained. The excitation and emission wavelength of the optical indicator dye is not fully suitable and has to be optimized in order to obtain better signals.

6 Conclusion

In this thesis, two different synthesis methods to obtain functionalized Pt(II)-tetraphenyl tetra-benzoporphyrins for optical oxygen sensors were investigated. In both approaches, bromine groups were introduced to the meso-phenyl group yielding a Pt(II)-tetra(4-bromophenyl)benzoporphyrin (Pt-TPTBPBr₄). This bromine group can then undergo the Suzuki cross coupling in order to introduce styrene groups which can be used for covalent immobilization to the polymer sensor matrix.

First, the conventional method called Lindsey-Condensation was conducted. The current synthetic protocol relies on preparation of cyclohexenoporphyrins, their platination and their subsequent aromatization. This synthesis method yields very pure product, but due low solubility problems of the dye and many reaction steps which require dry solvents and inert atmosphere, a simpler method is carried out. To avoid solubility problems, t-butyl groups were introduced.

The template synthesis benefits from its cheap starting materials and few reaction steps in order to obtain the final product. One key step of this method is the platination of the dye, which was also investigated during this thesis. The new dye with containing t-butyl groups showed good solubility in most solvents and also excellent photostability. Using Suzuki-Cross coupling it was possible to produce mono- and tetra-styrene modified porphyrin dyes.

By applying the catalytic hydrosilation reaction it was possible to covalently immobilize the dye in different silicone rubbers, using different hydride containing polysiloxanes as crosslinker and vinyl terminated polysiloxanes as backbone. The produced sensor materials show very linear Stern-Volmer plots between 0 and 20 hPa with K_{SV} values between 0.183 and 0.088 hPa^{-1} and can therefore be used as trace-oxygen sensors. Furthermore it was tried to change the sensors' sensitivity by using different substituted polysiloxanes, but no drastic changes were observed, indicating that this system is very robust.

The new developed sensor material was tested for its suitability for oxygen measurements through colored wine bottles. The low transmission of the glass and luminescence of color

6 Conclusion

giving Cr^{3+} -ions aggravate the measurement. Measuring through the bottle wall was possible because of the thinner glass compared with the bottle neck. s

7 References

- [1] Philipp Babilas, Philipp Lamby, Lukas Prantl, Stephan Schreml, Ernst Michael Jung, Gregor Liebsch, Otto S Wolfbeis, Michael Landthaler, Rolf-Markus Szeimies, and Christoph Abels. Transcutaneous pO₂ imaging during tourniquet-induced forearm ischemia using planar optical oxygen sensors. *Skin research and technology*, 14(3):304–11, August 2008.
- [2] Xudong Ge, Michael Hanson, Hong Shen, Yordan Kostov, Kurt a Brorson, Douglas D Frey, Antonio R Moreira, and Govind Rao. Validation of an optical sensor-based high-throughput bioreactor system for mammalian cell culture. *Journal of biotechnology*, 122(3):293–306, April 2006.
- [3] Andrew Mills. Oxygen indicators and intelligent inks for packaging food. *Chemical Society reviews*, 34(12):1003–11, December 2005.
- [4] H Humele and A Stangelmayer. Oxygen Ingress Measurement into PET Bottles using Optical-Chemical Sensor Technology. *Monatsschrift fuer Brawissenschaft*, 60(December):5–15, 2006.
- [5] P.N. Revsbech, L.H. Larsen, J. Gunderson, T. Dalsgaard, O. Ulloa, and B. Thamdrup. Determination of ultra-low oxygen concentrations in oxygen minimum zones by the STOX sensor. *Limnol Oceanographic Methods*, 7(():371–381, 2009.
- [6] Bernard Valeur. *Molecular Fluorescence*. Wiley-VCH Verlag GmbH, Weinheim, FRG, December 2001.
- [7] Peter Gruendler. *Chemische Sensoren*. Springer Berlin Heidelberg, xi edition, 2004.
- [8] Colette McDonagh, Conor S Burke, and Brian D MacCraith. Optical chemical sensors. *Chemical reviews*, 108(2):400–22, February 2008.
- [9] Sergey M Borisov and Otto S Wolfbeis. Optical biosensors. *Chemical reviews*, 108(2):423–61, February 2008.
- [10] Yutaka Amao. Probes and Polymers for Optical Sensing of Oxygen. *Microchimica Acta*, 143(1):1–12, September 2003.

- [11] E. R. Carraway, J. N. Demas, B. a. DeGraff, and J. R. Bacon. Photophysics and photochemistry of oxygen sensors based on luminescent transition-metal complexes. *Analytical Chemistry*, 63(4):337–342, February 1991.
- [12] Michela Quaranta, Sergey M Borisov, and Ingo Klimant. Indicators for optical oxygen sensors. *Bioanalytical reviews*, 4(2-4):115–157, December 2012.
- [13] Ingo. Klimant and Otto S. Wolfbeis. Oxygen-Sensitive Luminescent Materials Based on Silicone-Soluble Ruthenium Diimine Complexes. *Analytical Chemistry*, 67(18):3160–3166, September 1995.
- [14] Andrew Mills and Mark Thomas. Fluorescence-based Thin Plastic Film Ion-pair Sensors for Oxygen. *Analyst*, 122(January):63–68, 1997.
- [15] Delyle Eastwood and Martin Gouterman. Porphyrins XVIII - Luminescence of (Co), (Ni), Pd , Pt Complexes. *Journal of Molecular Spectroscopy*, 35(-):359–375, 1979.
- [16] Klaus Koren, Sergey M Borisov, Robert Saf, and Ingo Klimant. Strongly Phosphorescent Iridium(III)-Porphyrins - New Oxygen Indicators with Tuneable Photophysical Properties and Functionalities. *European journal of inorganic chemistry*, 2011(10):1531–1534, April 2011.
- [17] Joy E Rogers, Kiet A Nguyen, David C Hufnagle, Daniel G Mclean, Weijie Su, Kristi M Gossett, Aaron R Burke, Sergei A Vinogradov, Ruth Pachter, and Paul A Fleitz. Observation and Interpretation of Annulated Porphyrins : Studies on the Photophysical Properties of meso- Tetraphenylmetalloporphyrins. *Journal of Physical Chemistry A*, 107(51):11331–11339, 2003.
- [18] S M Borisov, G Nuss, and I Klimant. Red Light-Excitable Oxygen Sensing Materials Based on Platinum (II) and Palladium (II) Benzoporphyrins. *Analytical chemistry*, 80(24):9435–9442, 2008.
- [19] Siu-Wai Lai, Yuan-Jun Hou, Chi-Ming Che, Hei-Leung Pang, Kwok-Yin Wong, Chi K Chang, and Nianyong Zhu. Electronic spectroscopy, photophysical properties, and emission quenching studies of an oxidatively robust perfluorinated platinum porphyrin. *Inorganic chemistry*, 43(12):3724–32, June 2004.

-
- [20] Peter C Alford, Michael J Cook, Anthony P Lewis, Glenn S G Mcauliffe, Vladimir Skarda, Andrew J Thomson, John L Glasper, and David J Robbins. Luminescence Properties of Ring-substituted 1,10-Phenanthroline Tris-complexes of Ruthenium(II). *Journal of the Chemical Society, Perkin Transactions 2*, -(-):705–709, 1985.
- [21] S.M. Borisov, G. Nuss, W. Haas, R. Saf, M. Schmuck, and I. Klimant. New NIR-emitting complexes of platinum(II) and palladium(II) with fluorinated benzoporphyrins. *Journal of Photochemistry and Photobiology A: Chemistry*, 201(2-3):128–135, January 2009.
- [22] Xu-Dong Wang and Otto S Wolfbeis. Fiber-optic chemical sensors and biosensors (2008-2012). *Analytical chemistry*, 85(2):487–508, January 2013.
- [23] Barbara Enko, Sergey M Borisov, Johannes Regensburger, Wolfgang Bäumlner, Georg Gescheidt, and Ingo Klimant. Singlet oxygen-induced photodegradation of the polymers and dyes in optical sensing materials and the effect of stabilizers on these processes. *The journal of physical chemistry. A*, 117(36):8873–82, September 2013.
- [24] Otto S. Wolfbeis. Materials for fluorescence-based optical chemical sensors. *Journal of Materials Chemistry*, 15(27-28):2657, 2005.
- [25] Maria C DeRosa, Peter J Mosher, Glenn P a Yap, K-S Focsaneanu, Robert J Crutchley, and Christopher E B Evans. Synthesis, characterization, and evaluation of [Ir(ppy)₂(vpy)Cl] as a polymer-bound oxygen sensor. *Inorganic chemistry*, 42(16):4864–72, August 2003.
- [26] Gelest. Reactive Silicones: Forging new polymer links. In *Silicon Compound: Silanes & Silicones*, pages 488–506. 2013.
- [27] Volker Damrath. Chemie und Technologie der Silicone II. *Chemie in unserer Zeit*, 23(3):86–99, 1989.
- [28] Bharathibai Basu, A. Thirumurugan, A.R. Dinesh, C. Anadan, and K.S. Rajam. Optical oxygen sensor coating based on the fluorescence quenching of a new pyrene derivative. *Sensors and Actuators B: Chemical*, 104(1):15–22, January 2005.
- [29] Mohamad Riduwan Ramli, Muhammad Bisyrul Hafi Othman, Azlan Arifin, and Zulkifli Ahmad. Cross-link network of polydimethylsiloxane via addition and condensation (RTV)

- mechanisms. Part I: Synthesis and thermal properties. *Polymer Degradation and Stability*, 96(12):2064–2070, December 2011.
- [30] Huarui He, Robert J. Fraatz, Marc J.P. Leiner, Margit M. Rehn, and James K. Tusa. Selection of silicone polymer matrix for optical gas sensing. *Sensors and Actuators B: Chemical*, 29(1-3):246–250, October 1995.
- [31] R.N. Meals. Homogeneous Catalysis of Hydrosilation by Transition Metals. *Advances in Organometallica*, 17(.):407, 1979.
- [32] Christoph Elschenboich. *Organometallicchemie*, volume 55. Teubner Studienbücher Chemie, 6 edition, 2008.
- [33] Larry N Lewis, Judith Stein, Yan Gao, and Robert E Colborn. Platinum Catalysts Used in the Silicones Industry. *Platinum Metals Review*, 41(2):66–75, 1997.
- [34] Klaus Koren, Sergey M Borisov, and Ingo Klimant. Stable optical oxygen sensing materials based on click-coupling of fluorinated platinum(II) and palladium(II) porphyrins-A convenient way to eliminate dye migration and leaching. *Sensors and actuators. B, Chemical*, 169(5):173–181, July 2012.
- [35] Yanqing Tian, Bradley R Shumway, and Deirdre R Meldrum. A New Crosslinkable Oxygen Sensor Covalently Bonded into Poly(2-hydroxyethyl methacrylate)-CO-Polyacrylamide Thin Film for Dissolved Oxygen Sensing. *Chemistry of Material*, 22(6):2069–2078, March 2010.
- [36] Sergey M Borisov, Philipp Lehner, and Ingo Klimant. Novel optical trace oxygen sensors based on platinum(II) and palladium(II) complexes with 5,10,15,20-meso-tetrakis-(2,3,4,5,6-pentafluorophenyl)-porphyrin covalently immobilized on silica-gel particles. *Analytica chimica acta*, 690(1):108–115, March 2011.
- [37] I.E Efremova, M. I. Vakulenko, K. A. Lysenko, I. S. Bushmarinov, L. V. Lapshina, G. A. Berkova, and V. M. Berestovitskaya. Reactions of 1-nitrocyclohexene with N,N-binucleophiles. *Russian Journal of General Chemistry*, 80(-):2298–2305, 2010.
- [38] Carsten Borek, Kenneth Hanson, Peter I Djurovich, Mark E Thompson, Kristen Aznavour, Robert Bau, Yiru Sun, Stephen R Forrest, Jason Brooks, Lech Michalski, and Julie Brown.

- Highly efficient, near-infrared electrophosphorescence from a Pt-metalloporphyrin complex. *Angewandte Chemie (International ed. in English)*, 46(7):1109–12, January 2007.
- [39] Lukas Hutter. Masterthesis - On Covalent Immobilisation of Indicators in Optical Oxygen Sensors. 2012.
- [40] Jonathan S. Lindsey, Irwin C. Schreiman, Henry C. Hsu, Patrick C. Kearney, and Anne M. Marguerettaz. Rothemund and Adler-Longo reactions revisited: synthesis of tetraphenylporphyrins under equilibrium conditions. *The Journal of Organic Chemistry*, 52(5):827–836, March 1987.
- [41] Sergei a. Vinogradov and David F. Wilson. Metallotetrabenzoporphyrins. New phosphorescent probes for oxygen measurements. *Journal of the Chemical Society, Perkin Transactions 2*, 2(1):103, 1995.
- [42] Olga S Finikova, Andrei V Cheprakov, and Sergei A Vinogradov. Synthesis and luminescence of soluble meso-unsubstituted tetrabenzo- and tetranaphtho[2,3]porphyrins. *The Journal of organic chemistry*, 70(23):9562–72, November 2005.
- [43] Christopher A Hunter and Jeremy K M Sanders. The Nature of pi-pi Interactions. *Journal of the Chemical Society*, 112(2):5525–5534, 1990.
- [44] Olga S Finikova, Ping Chen, Zhongping Ou, Karl M Kadish, and Sergei a Vinogradov. Dynamic Quenching of Porphyrin Triplet States by Two-Photon Absorbing Dyes: Towards Two-Photon-Enhanced Oxygen Nanosensors. *Journal of photochemistry and photobiology. A, Chemistry*, 198(1):75–84, January 2008.
- [45] Johann W Buchler, Christine Dreher, and Gerhard Herget. Vilsmeier-Formylierung von Metallporphyrinen mit Co(II), Ni(II), Pd(II), Pt(II), Cu(II), Zn(II), Co(III) , Cr(III) , Mn(III)’, Fe(III), Al(III), Si(IV) und Pt(IV) in Abhaengigkeit vom Zentralmetall. In *Liebigs Ann. Chem*, volume -, chapter Metallkomp, pages 43–54. 1988.
- [46] Marcus Baumann and Adrian Waldner. Process for the preparation of palladium benzoporphyrins and platinum or palladium cyclohexenoporphyrins, intermediates, and an oxygen sensor comprising platinum or palladium cyclohexenoporphyrin, 2001.

- [47] Olga S Finikova, Andrei V Cheprakov, and Sergei A Vinogradov. Synthesis and Luminescence of Soluble meso-Unsubstituted Tetrabenzo- and Tetranaphtho [2,3] porphyrins. *Journal of Organic Chemistry*, 70(23):9562–9572, 2005.
- [48] Sergey M. Borisov and Ingo Klimant. Efficient metallation in diphenylether. A convenient route to luminescent platinum(II) complexes. *Dyes and Pigments*, 83(3):312–316, December 2009.
- [49] Jonathan R Sommer, Abigail H Shelton, Anand Parthasarathy, Ion Ghiviriga, John R Reynolds, and Kirk S Schanze. Photophysical Properties of Near-Infrared Phosphorescent π -Extended Platinum Porphyrins. *Chemistry of Materials*, 23(-):5269–5304, 2011.
- [50] Christopher A. Amodio and Kevin B. Nolan. Reactions of Coordinated Nitriles. Nucleophilic Attack by Amines on cis-Dichlorobisbenzotrileplatinum(II). *Inorganica Chimica Acta*, 3(113):27–30, 1986.
- [51] Rino a. Michelin, Mirto Mozzon, and Roberta Bertani. Reactions of transition metal-coordinated nitriles. *Coordination Chemistry Reviews*, 147:299–338, January 1996.
- [52] Robert McCrindle, George Ferguson, Gilles J Arsenault, and Alan J McAlees. Reaction of Tertiary Amines with Bis(benzonitrile)dichloro-palladium(II). formation and Crystal Structure Analysis of Di-chloro-dichlorobis[N,N-di-isopropylimino]ethyl-C]dipalladium(II). *Journal of the Chemical Society, Chemical Communications*, -(10):571–572, 1983.
- [53] Jeremy S Evans and Ronald L Musselman. Red shifting due to nonplanarity in alkylporphyrins: solid-state polarized UV-vis spectra and ZINDO calculations of two nickel(II)octaethylporphyrins. *Inorganic chemistry*, 43(18):5613–29, September 2004.
- [54] Craig J Medforth, Raid E Haddad, Cinzia M Muzzi, Neal R Dooley, Laurent Jaquinod, David C Shyr, Daniel J Nurco, Marilyn M Olmstead, Kevin M Smith, Jian-Guo Ma, and John a Shelnut. Unusual aryl-porphyrin rotational barriers in peripherally crowded porphyrins. *Inorganic chemistry*, 42(7):2227–41, April 2003.
- [55] Xing-Zhi Song, Walter Jentzen, Laurent Jaquinod, Richard G. Khoury, Craig J. Medforth, Song-Ling Jia, Jian-Guo Ma, Kevin M. Smith, and John a. Shelnut. Substituent-Induced Perturbation Symmetries and Distortions of meso-tert-Butylporphyrins. *Inorganic chemistry*, 37(9):2117–2128, May 1998.

-
- [56] Sang-kyung Lee and Ichiro Okura. Photostable Optical Oxygen Sensing Material : Platinum Tetrakis (pentafluorophenyl) porphyrin Immobilized in Polystyrene. *Analytical Communications*, 34(June):185–188, 1997.
- [57] Chi-Long Lee, Harry L. Chapman, Martin E. Cifuentes, Kenneth M. Lee, Linda D. Merrill, Katherine L. Ulman, and Krishnaswamy Venkataraman. Effects of polymer structure on the gas permeability of silicone membranes. *Journal of Membrane Science*, 38(1):55–70, July 1988.
- [58] S. A.. Stern, V. M. Shah, and B. J. Hardy. Structure-permeability relationships in silicone polymers. *Journal of Polymer Science Part B: Polymer Physics*, 25(6):1263–1298, June 1987.
- [59] Chantal Maury, Andrew C Clark, and Geoffrey R Scollary. Determination of the impact of bottle colour and phenolic concentration on pigment development in white wine stored under external conditions. *Analytica chimica acta*, 660(1-2):81–6, February 2010.
- [60] Hua Li, Anque Guo, and Hua Wang. Mechanisms of oxidative browning of wine. *Food Chemistry*, 108(1):1–13, May 2008.
- [61] H. Aizawa, T. Katsumata, Y. Kiyokawa, T. Nishikawa, T. Sasagawa, S. Komuro, T. Morikawa, H. Ishizawa, and E. Toba. Evaluation of Cr-doped yttrium aluminum garnet crystals for hybrid fiber-optic thermometer application. *Measurement*, 39(2):147–152, February 2006.

List of Tables

2.1	Photophysical properties of different Pt-TPTBP dyes	18
2.2	Permeability rates of commonly used sensor matrices [10]	20
4.1	Summary of different set ups for the platination reaction	39
4.2	Used quantities for each sensor material	41
5.1	Photophysical properties of different Pt-TPTBP dyes	56
5.2	Solubility of the dyes in different solvents at 25 °C	56
5.3	Influence of pot-time and knife coating on SV-fitting parameters	62
5.4	SV-Fitting parameters of mono- and tetra-styrene dyes with different crosslinkers	63
5.5	SV-Fitting parameters of tetrastylene with different equivalent of crosslinker . .	65
5.6	SV-Fitting parameters of tetra-styrene in PDPDMS and different amount of crosslinker	66
5.7	SV Fitting parameters of 25-35% MeH crosslinker and different backbones	67
5.8	SV Fitting parameters of 45-55% MeH crosslinker and different backbones	68
5.9	SV Fitting parameters of dihydride crosslinker and different backbones	69
5.10	SV Fitting parameters of the sensor foil before and after extraction experiment .	72
5.11	SV Fitting parameters of temperature dependancy experiment	73
5.12	SV Fitting parameters of different trace oxygen sensors	74
5.13	Results from measuring through different colored wine bottles in Na_2SO_3	81

List of Figures

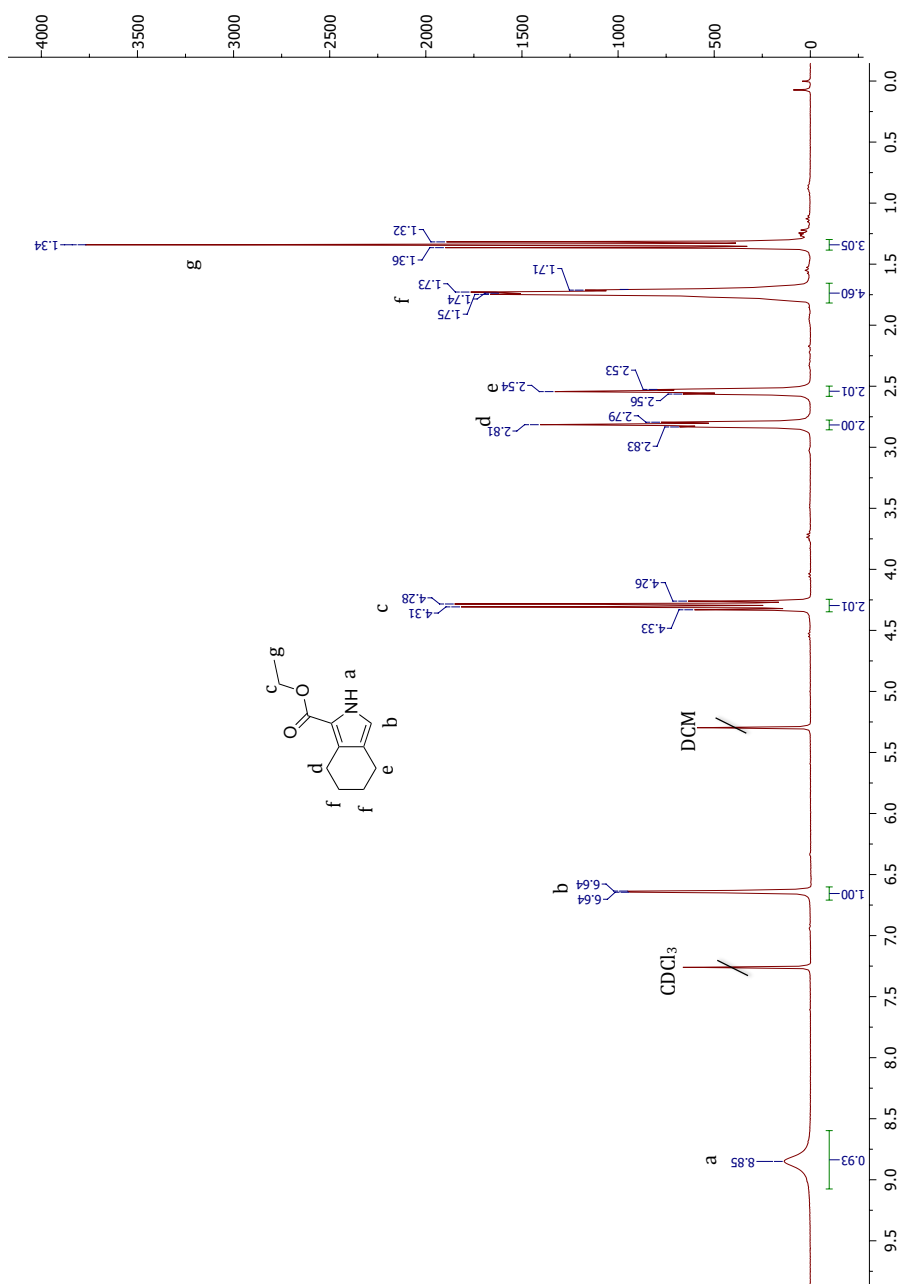
2.1	Franck-Condon principle	4
2.2	Jablonski-Diagram	5
2.3	Scheme for internal conversion	6
2.4	Scheme for intersystem crossing	7
2.5	Scheme for fluorescence	7
2.6	Scheme for phosphorescence	8
2.7	Scheme for delayed fluorescence	8
2.8	Different quenching mechanisms	10
2.9	Principle of an optical oxygen sensor	13
2.10	Phasefluorimetry	15
2.11	Commonly used Oxygen Indicators	18
2.12	Normalized absorption and emission spectra for commonly used optical oxygen sensors	18
2.13	RTV1 Silicones	21
2.14	RTV2 Silicones - condensation	21
2.15	RTV2 Silicones - addition	22
2.16	Hydrosilation	22
2.17	Catalytic cycle of hydrosilation reaction	23
2.18	Different ways of immobilization	24
4.1	Reaction scheme for 1-nitro-2-iodocyclohexan	27
4.2	Reaction scheme for 1-nitrocyclohexen	27
4.3	Reaction scheme for 2H-isoindol-4,5,6,7-tetrahydro-1-carboxylic acid ethyl ester	28
4.4	Reaction scheme for 4,5,6,7-tetrahydroisoindol	29
4.5	Reaction scheme for $H_2TPTCHPBr_4$	29
4.6	Reaction scheme for $Pt-TPTCHPBr_4$	31

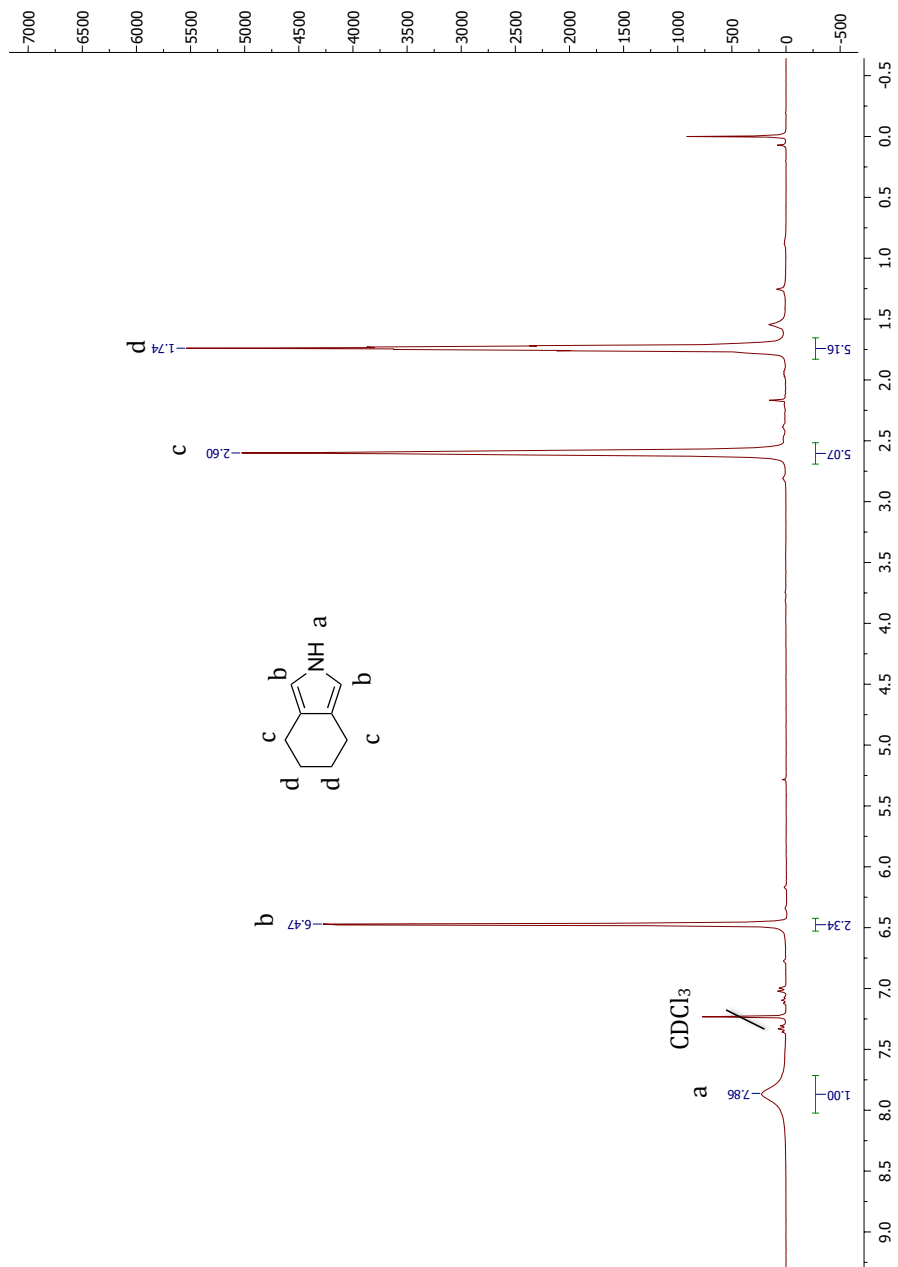
4.7	Reaction scheme for Pt-TPTBPBr ₄	32
4.8	Reaction scheme for Pt-TPTBPStyr ₄	33
4.9	Reaction scheme for Zn-TPTBPtBu ₄ Br ₄	34
4.10	Reaction scheme for H ₂ TPTBPtBu ₄ Br ₄	35
4.11	Reaction scheme for Pt-TPTBPtBu ₄ Br ₄	36
4.12	Reaction scheme for Pt-TPTBPtBu ₄ Br ₃ Styr	37
4.13	Reaction scheme for PtTPTBPtBu ₄ Styr ₄	38
5.1	Normalized absorption spectra of the different products occurring during Lindsey method	44
5.2	Possible products using Pd(PPh ₃) ₄ for C-C cross coupling reaction	45
5.3	Summary of absorption spectra of different products during template synthesis .	46
5.4	Absorption spectra of Suzuki modified Pt-TPTBP	48
5.5	Scheme for platination step and possible protonation of the ligand	49
5.6	Reaction A) Without adding a base and without bubbling N ₂ through the reaction mixture	50
5.7	Reaction B) Without adding a base but bubbling N ₂ through the reaction mixture	51
5.8	Reaction C) adding 2 eq base and without bubbling N ₂ through the reaction mixture	52
5.9	Reaction D) bubbling N ₂ through the reaction mixture and adding the ligand drop-wise to the Pt-precursor solution	52
5.10	Reaction E) without bubbling N ₂ and adding the ligand and 2eq base drop-wise to the Pt-precursor solution	53
5.11	Normalized absorption spectra of the different finished reaction	54
5.12	Normalized absorption and emission spectra of different Pt-TPTBP indicators . .	55
5.13	Normalized degradation of different porphyrin dyes	57
5.14	Absorption spectra during irritation	57
5.15	Reaction scheme for preparing the silicone matrix with covalently linked indicator dye	59
5.16	Different hydride functionalised polysiloxane crosslinkers (CL)	60
5.17	Different vinyl terminated polysiloxane backbones (BB)	60
5.18	Normalized absorption and emission spectra of the dye in different media	61
5.19	Mono-styrene vs. tetra-styrene with different crosslinkers	63

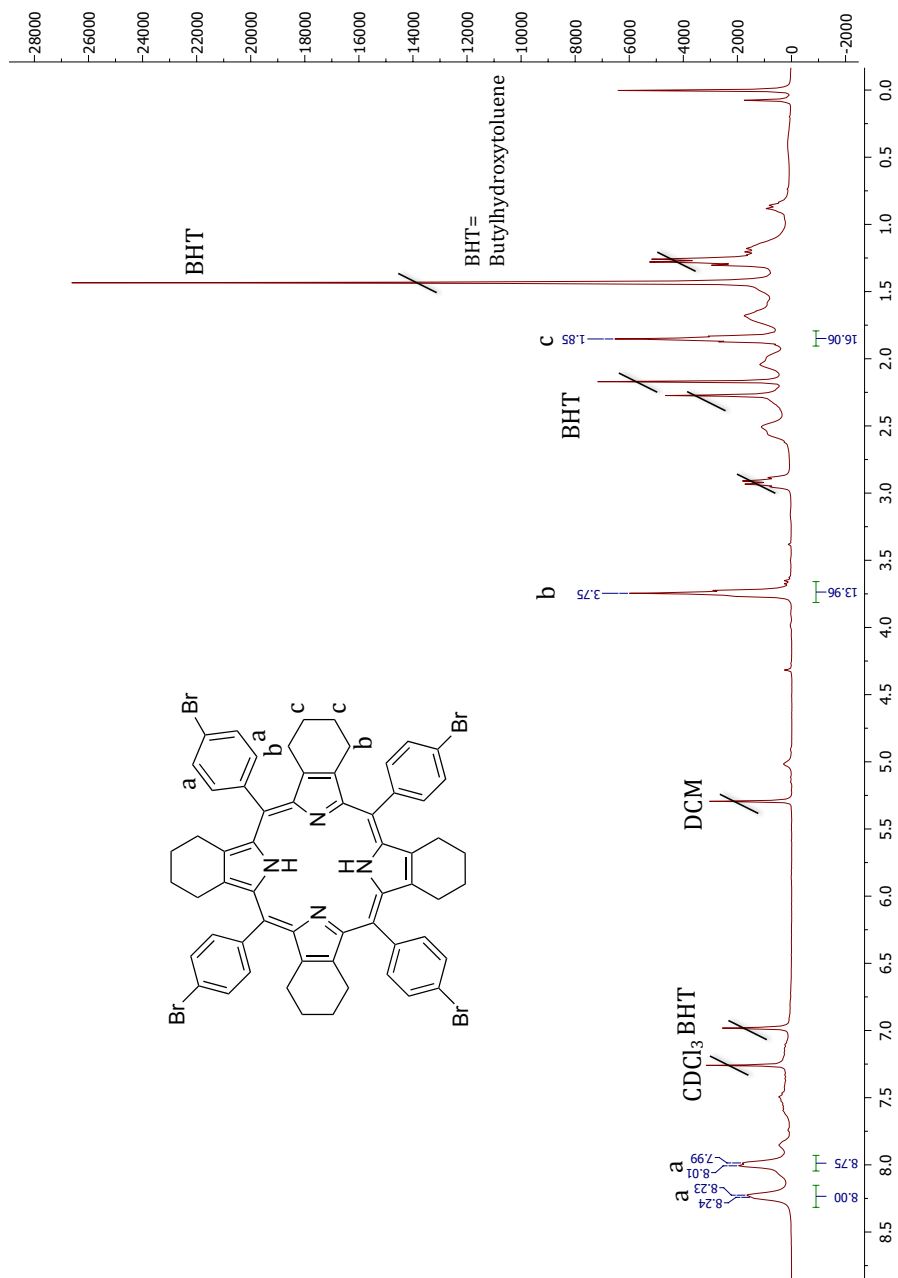
5.20	Tetrastylene with various equivalent of crosslinker	64
5.21	Different equivalent of crosslinker using PDPDMS backbone	65
5.22	Tetra-styrene dye with 25-35% MeH crosslinker and different backbones	66
5.23	Tetra-styrene in 50-55%H crosslinker and different backbones	68
5.24	Tetra-styrene in dihydride crosslinker and different backbones	69
5.25	Leaching experiment of mono-styrene in 25-35% MeH crosslinker and PDMS-2 backbone	71
5.26	Absorption spectra of the sensor foil before and after extraction	71
5.27	Temperature dependancy of tetra-styrene in 25-35 % MeH crosslinker and PDMS- 2 backbone	72
5.28	Comparison of different trace oxygen sensors	73
5.29	Monohydrid terminated polysiloxane	75
5.30	Transmission spectra of flint wine bottles	76
5.31	Transmission spectra of green wine bottles	77
5.32	Transmission spectra of brown wine bottles	78
5.33	Excitation/emission spectra of the different glasses and absorption/emission spec- trum of a siicone rubber sensor foil	79
5.34	SPC of flint glass	79
5.35	SPC of green glass	79
5.36	SPC of brown glass	80
5.37	Two sensor spots placed inside a wine bottle	80

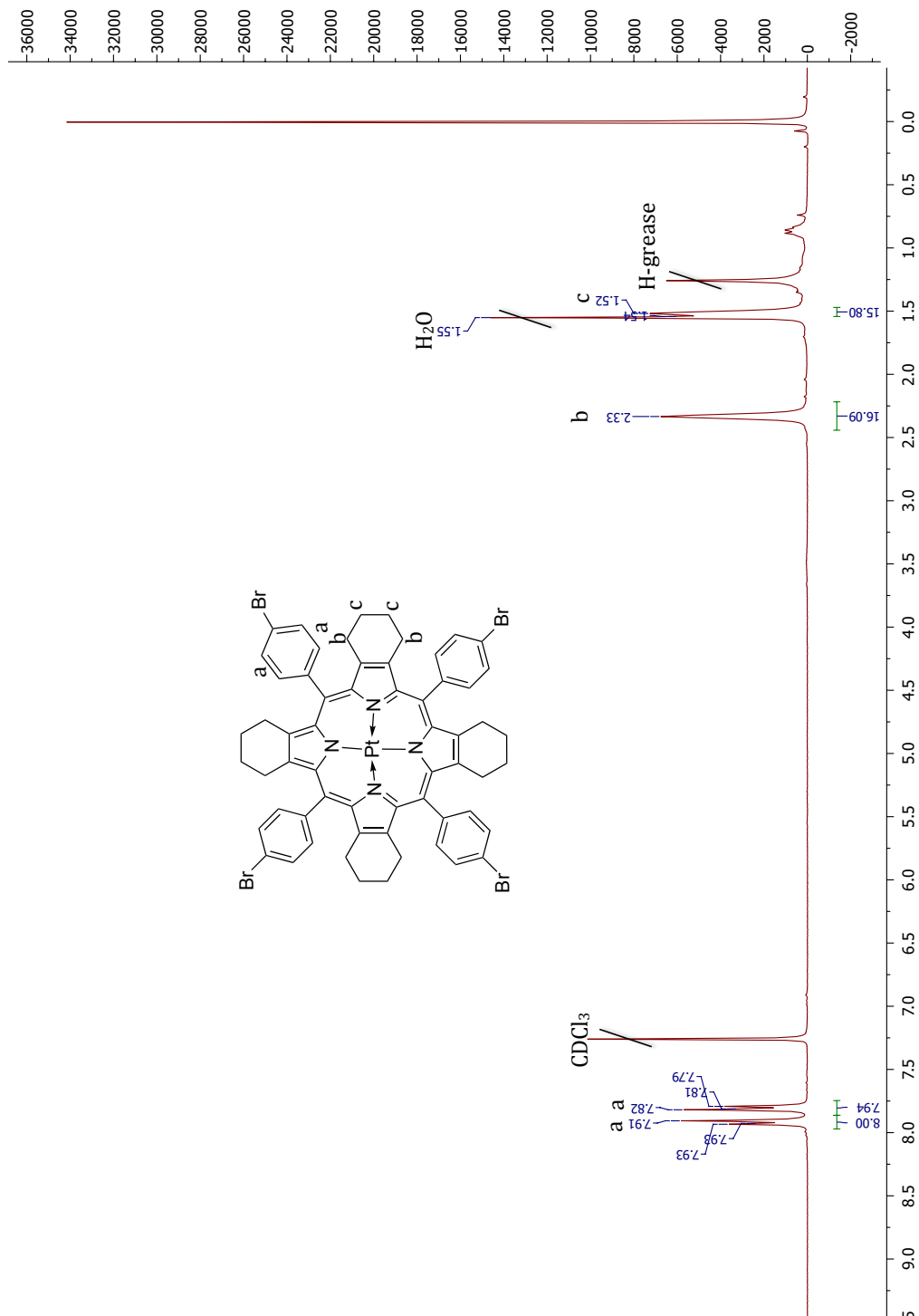
8 Appendix

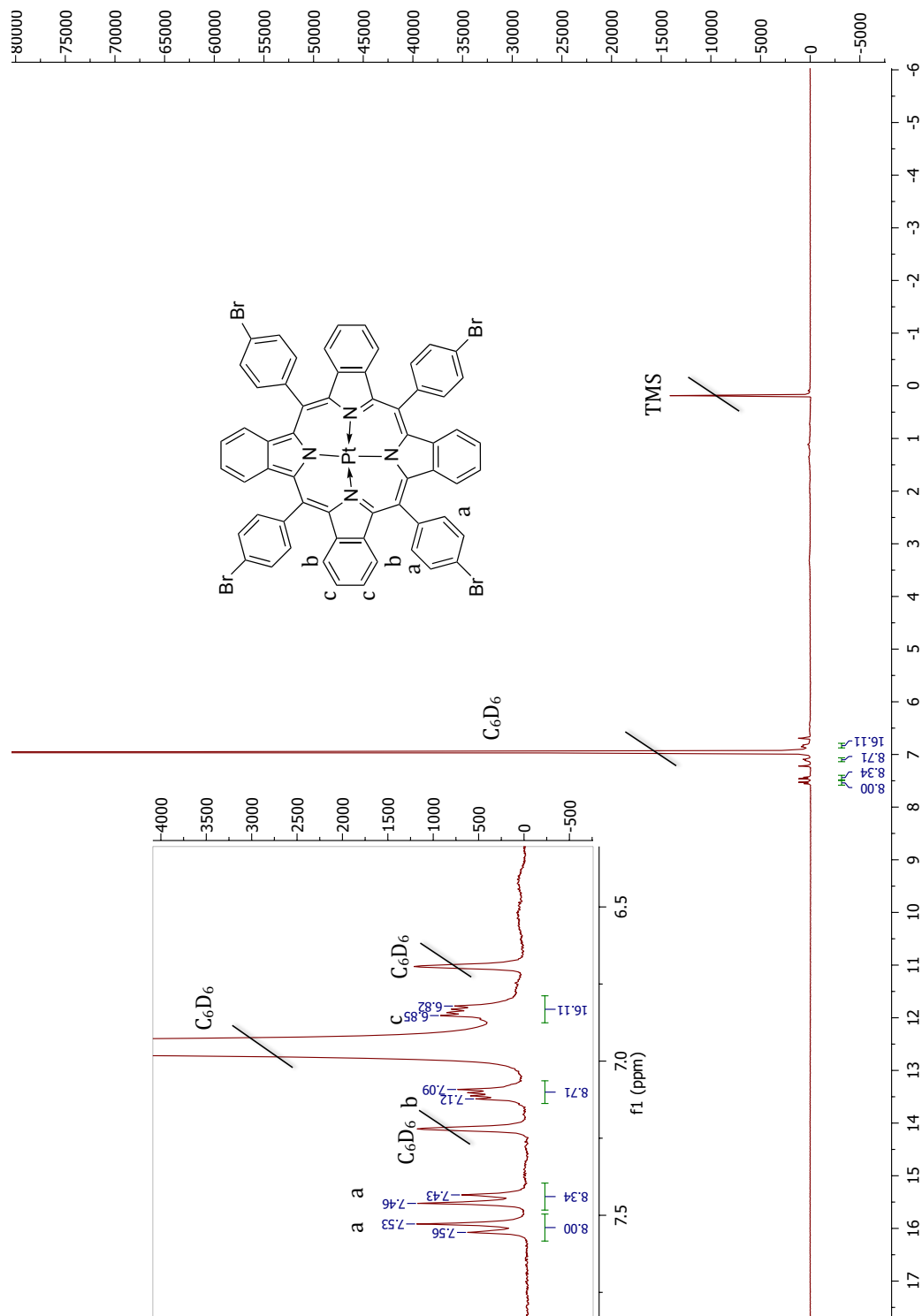
8.1 NMR Data

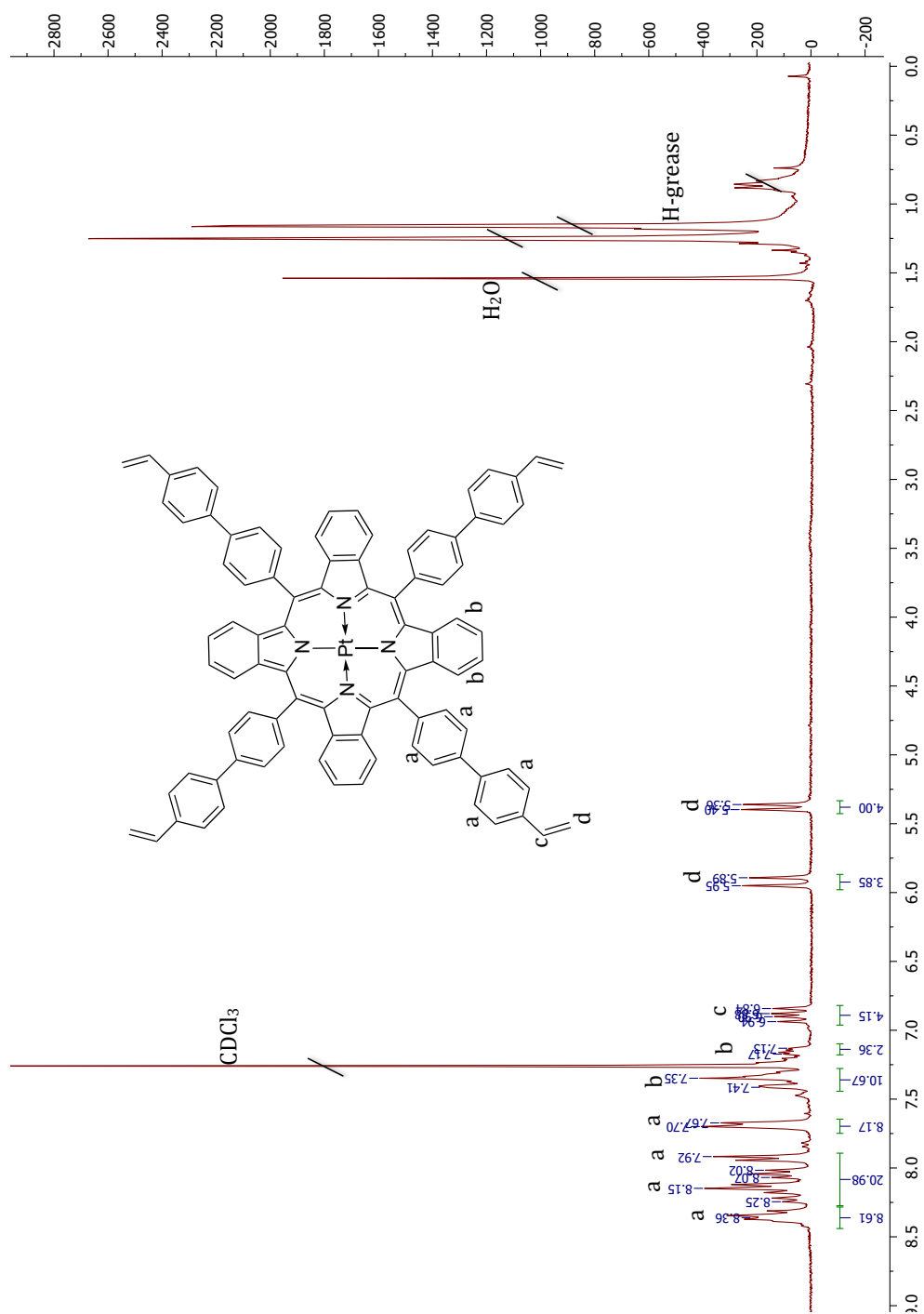


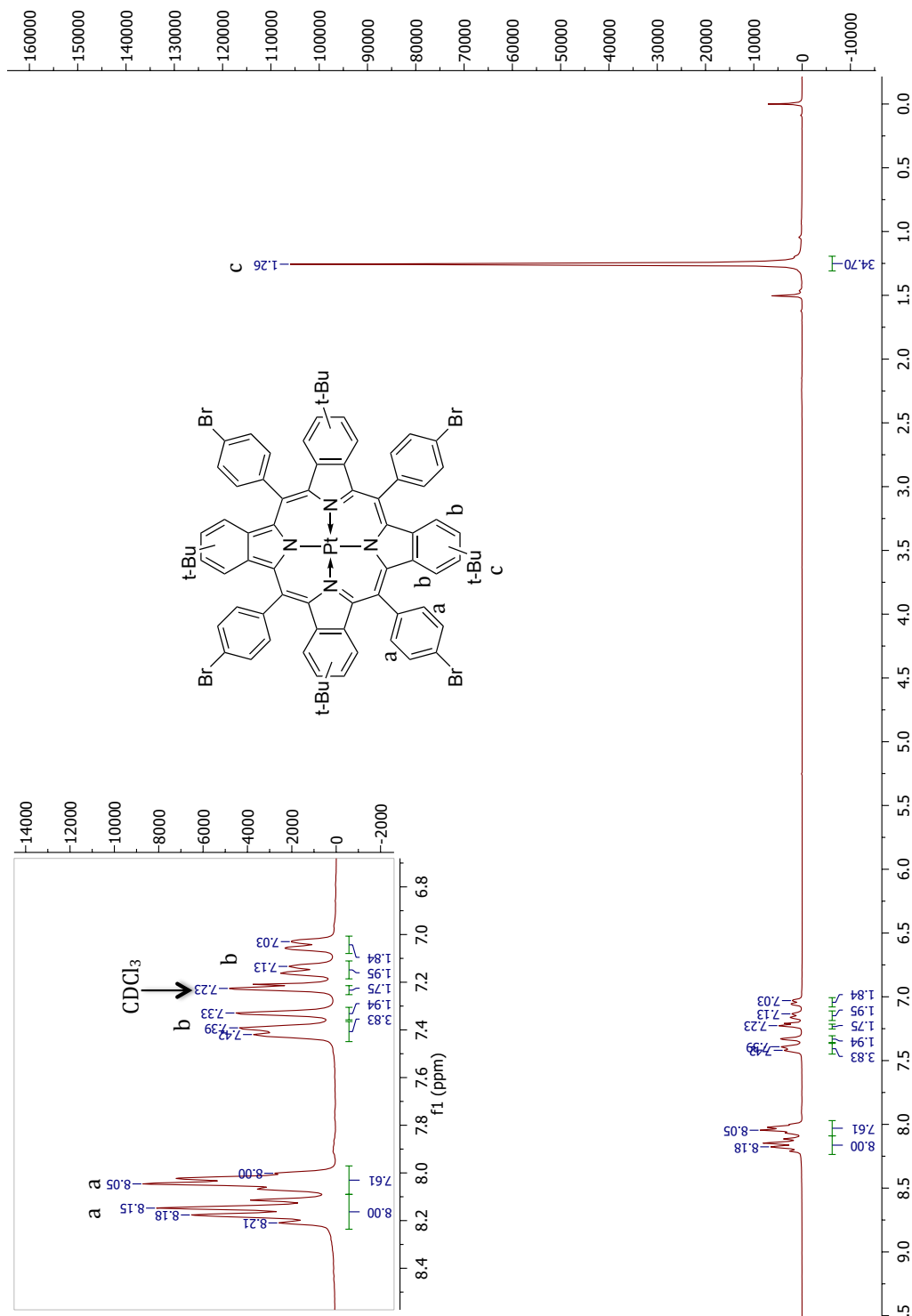


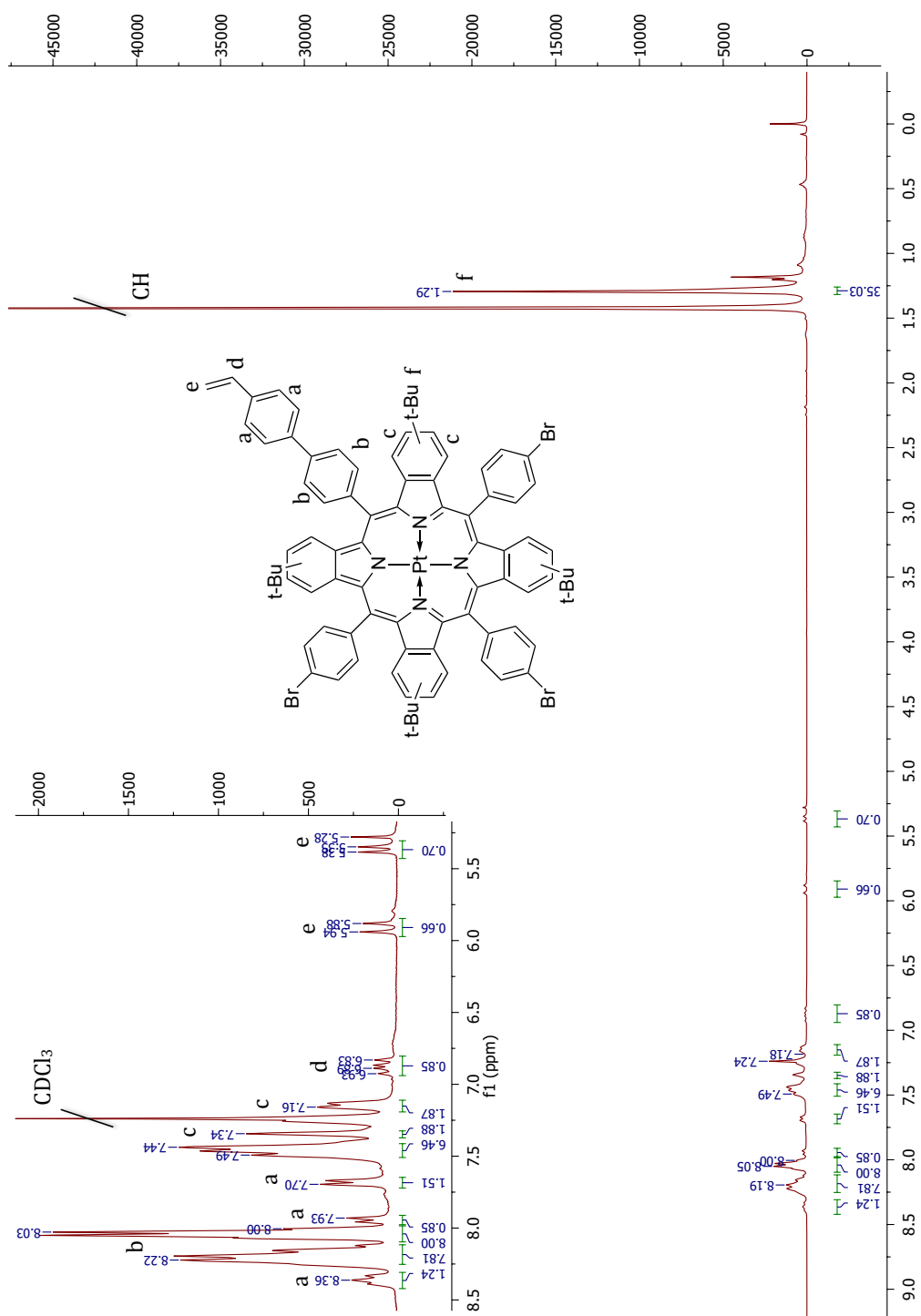


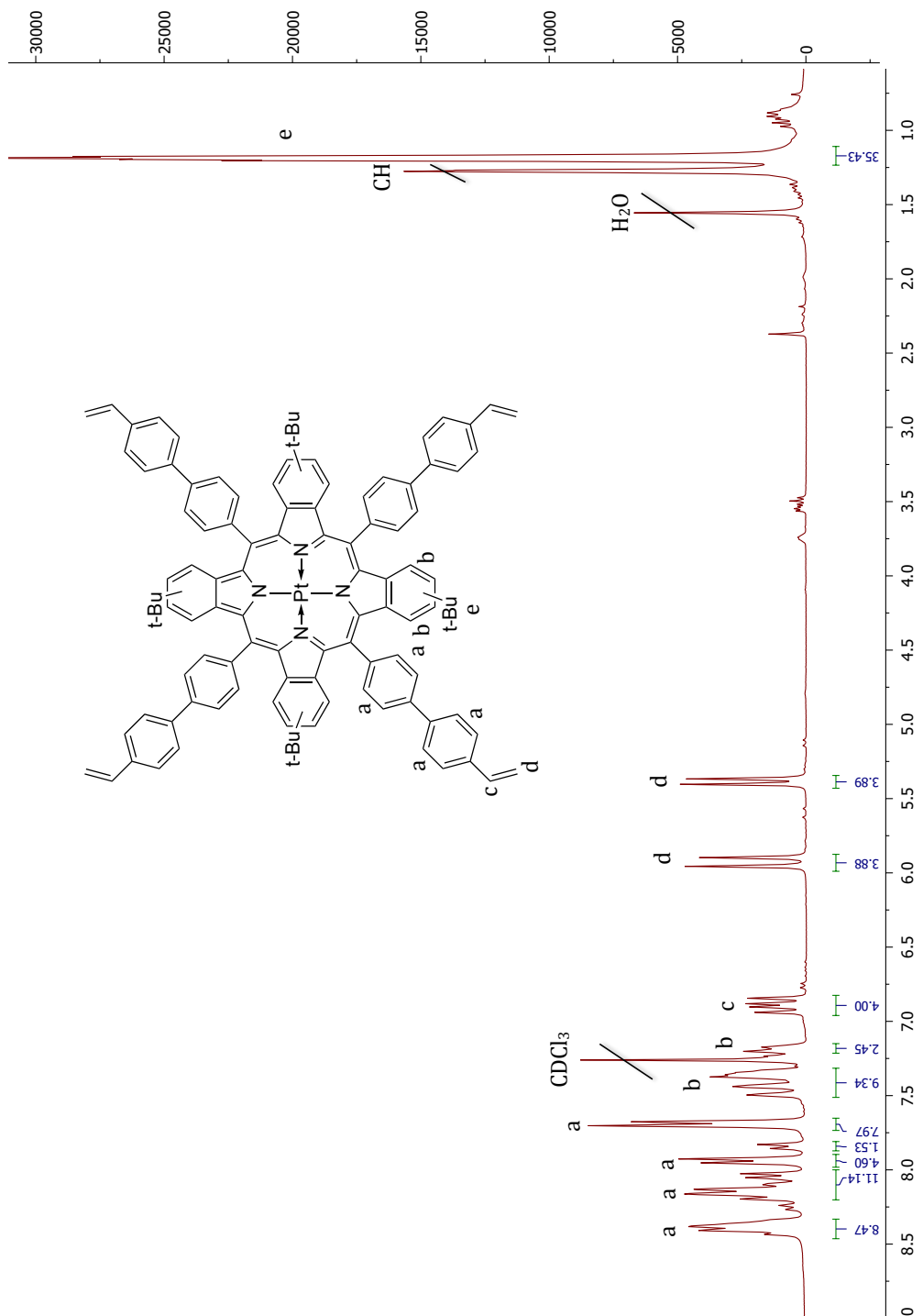








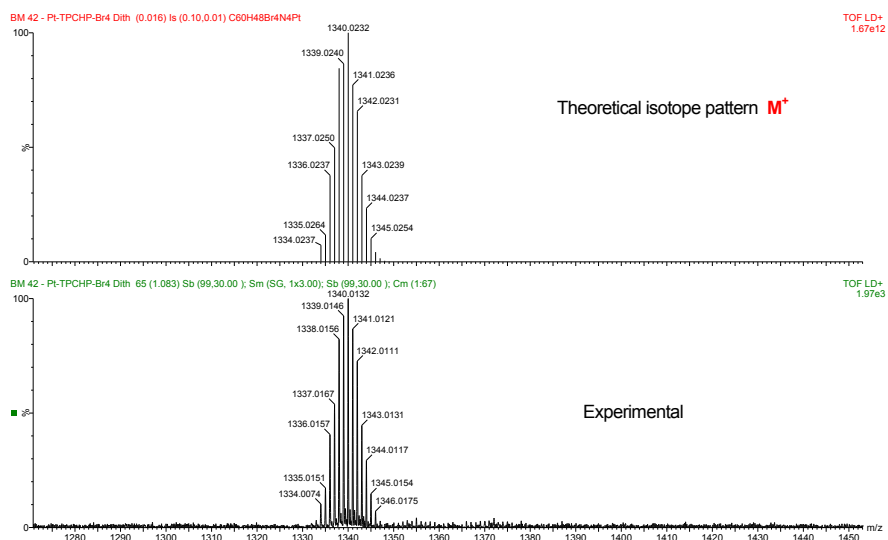
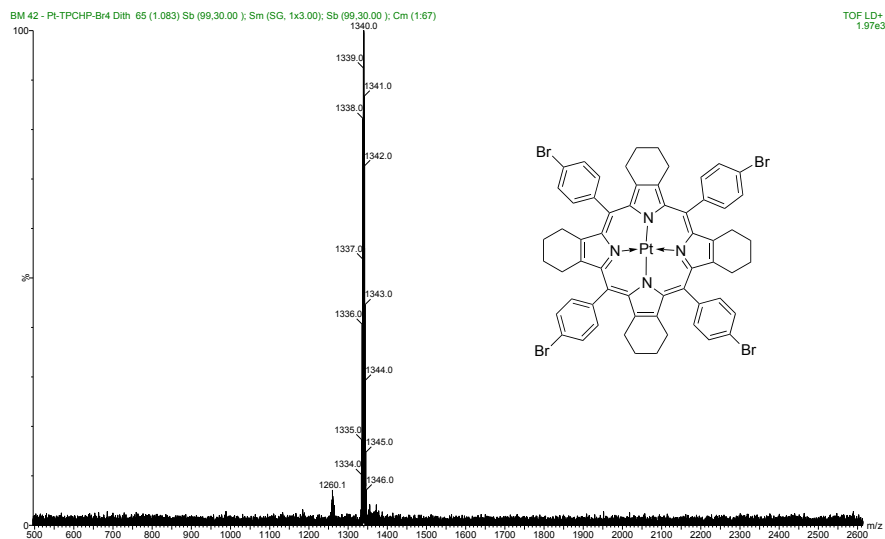




8.2 MALDI-TOF Data

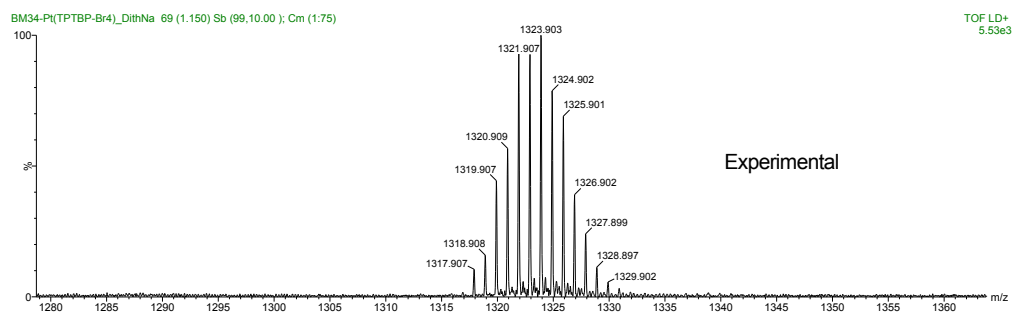
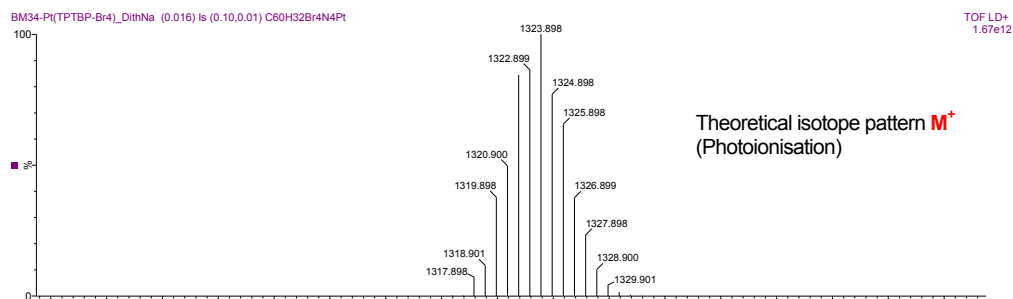
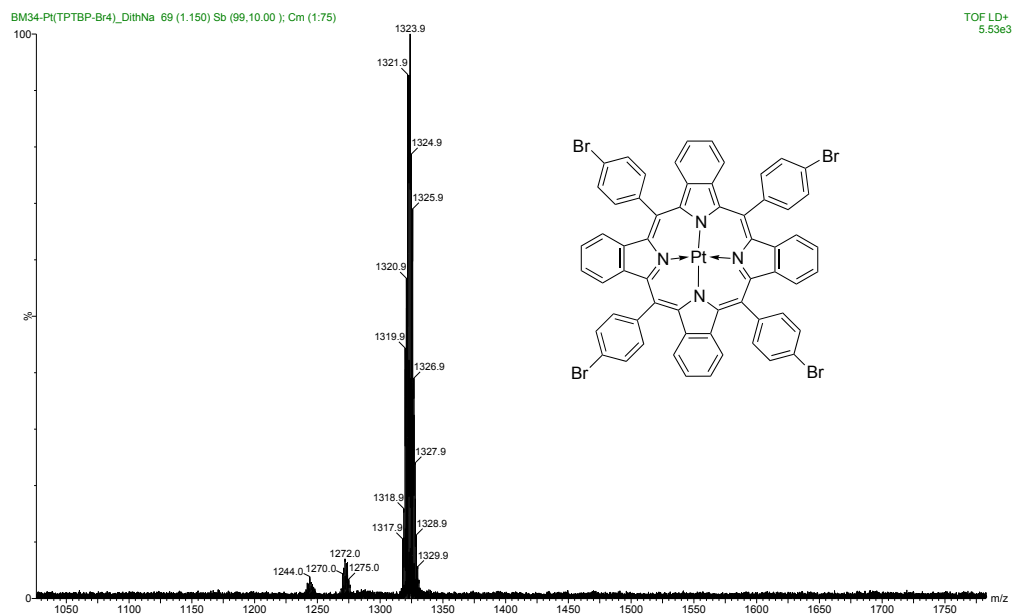
Sample: Pt-TPTCHPBr₄

Ionisation: MALDI/Dith



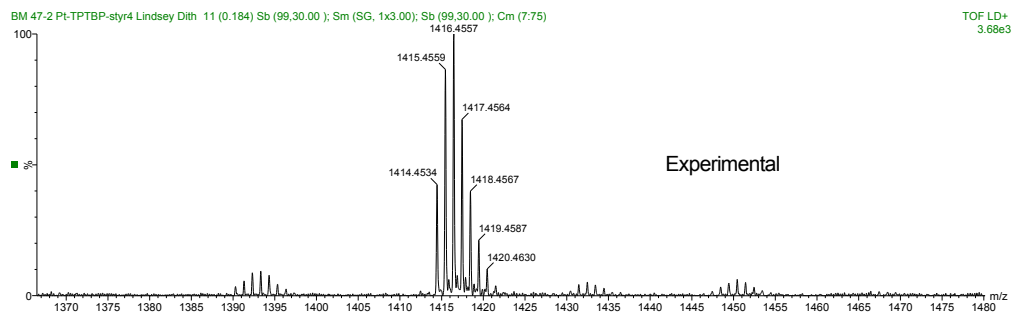
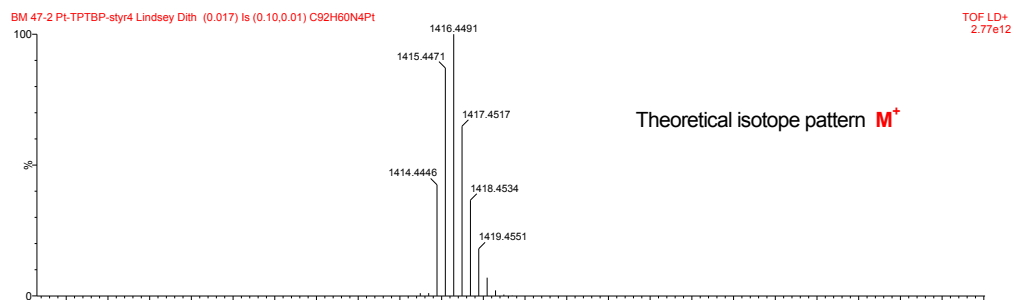
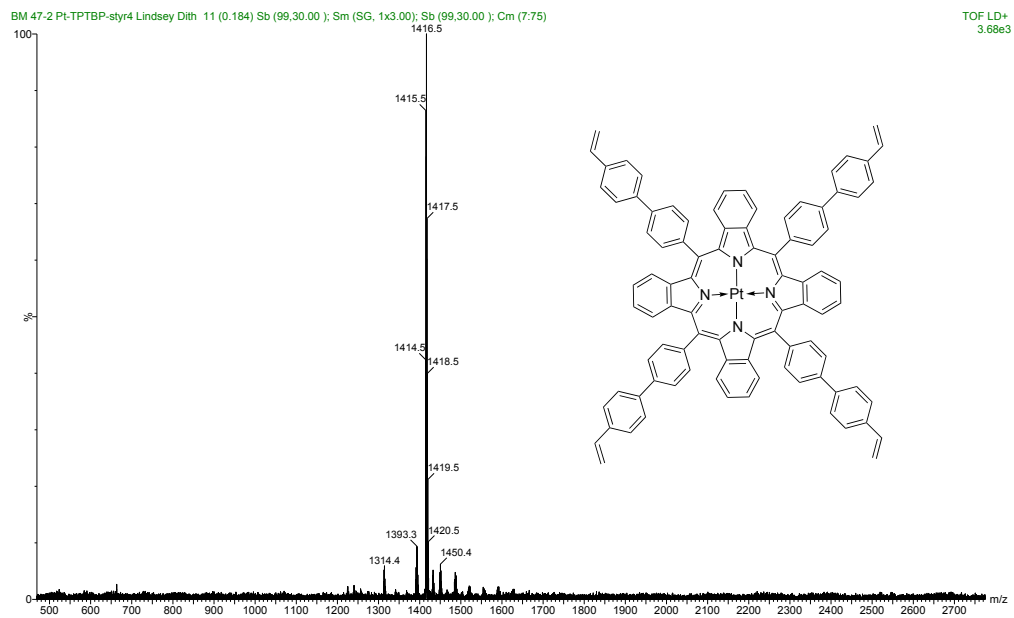
Sample: Pt-TPTBBr₄

Ionisation: MALDI/Dith



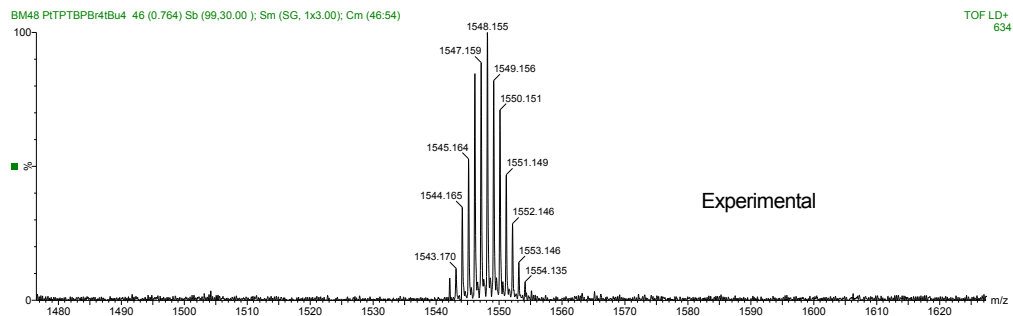
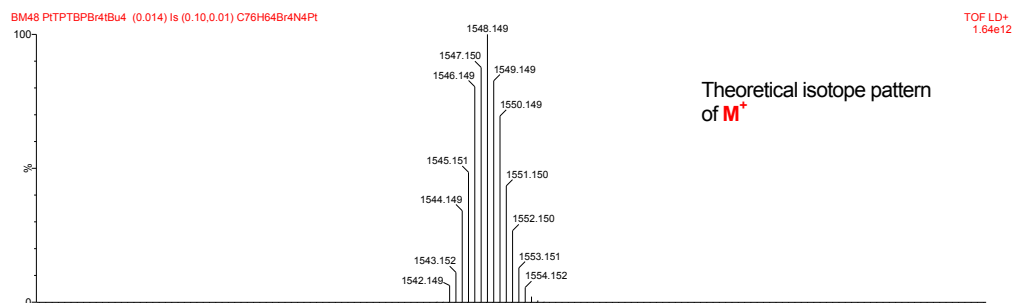
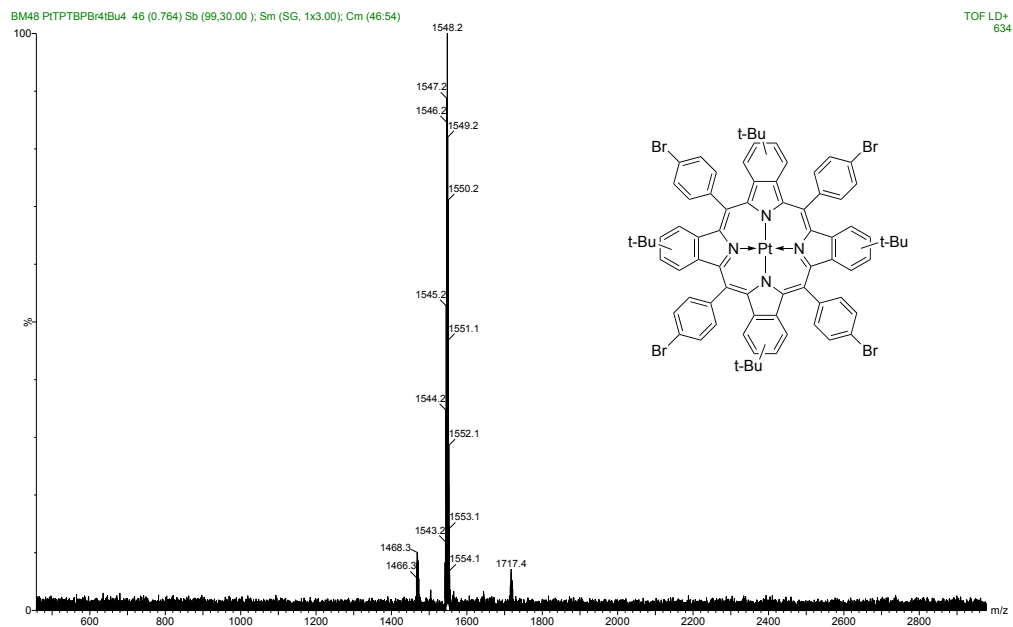
Sample: Pt-TPTBPStyr₄

Ionisation: MALDI/Dith



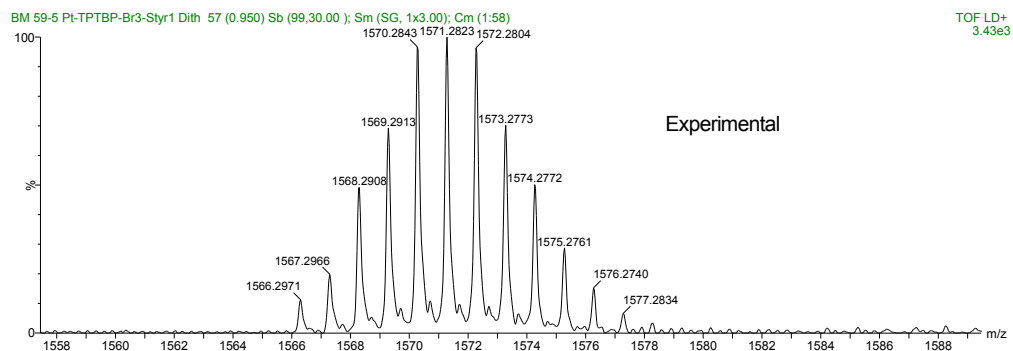
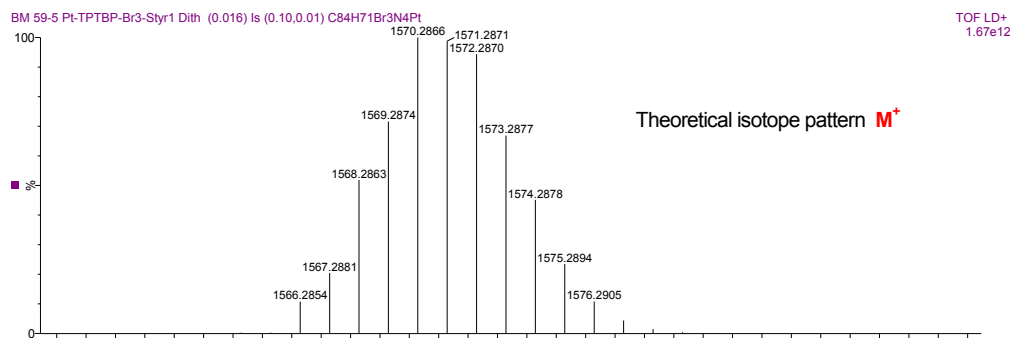
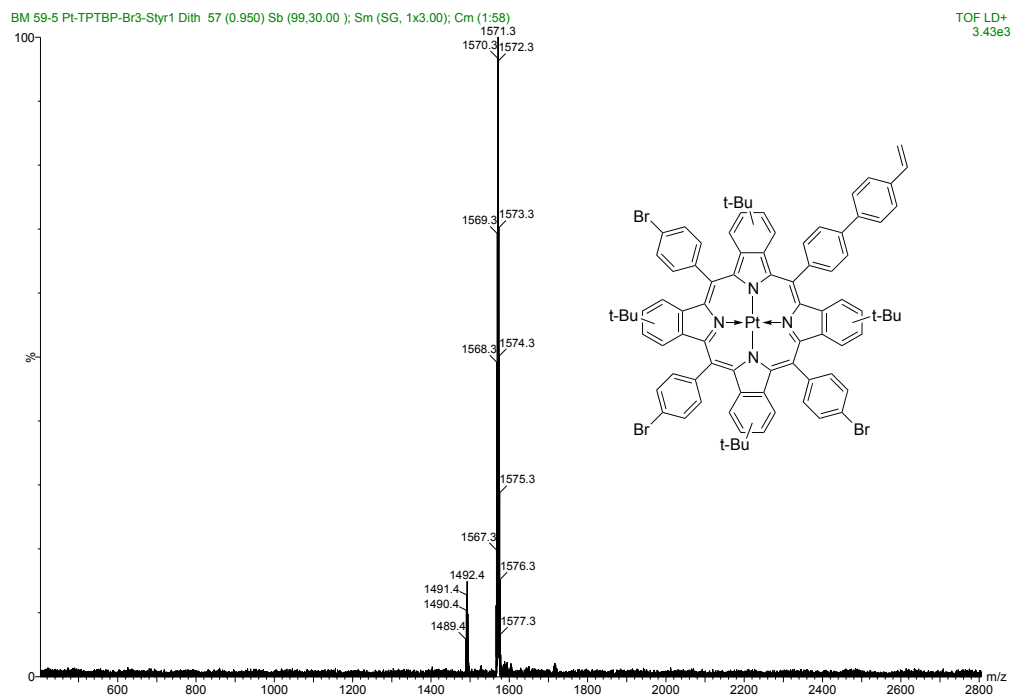
Sample: Pt-TPTBPtBu₄Br₄

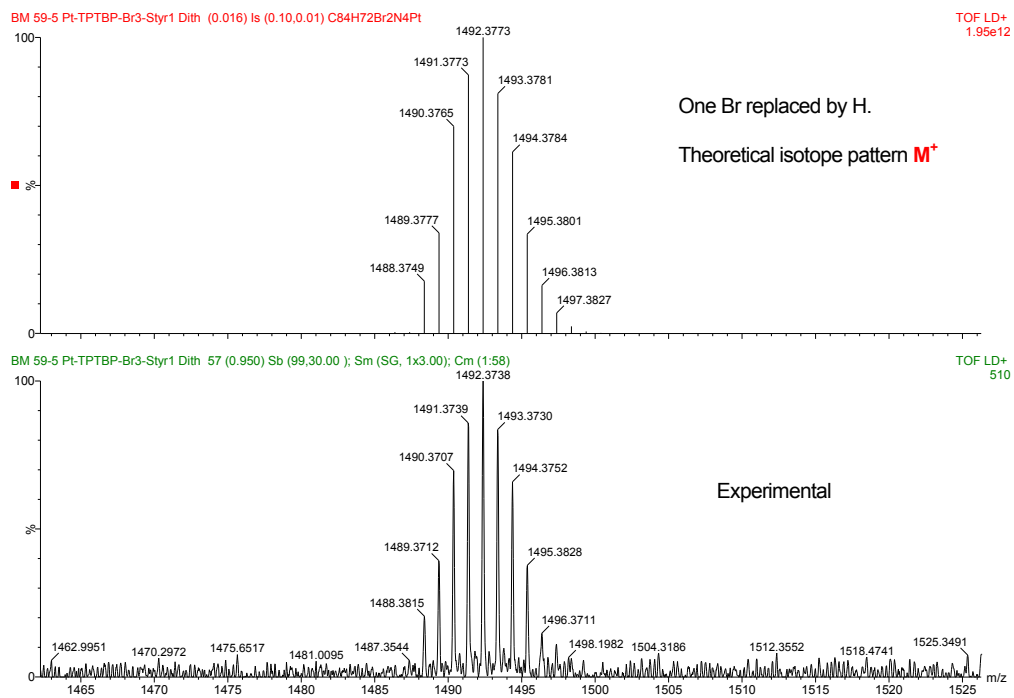
Ionisation: MALDI/DCTB



Sample: Pt-TPTBPtBu₄Br₃Styr

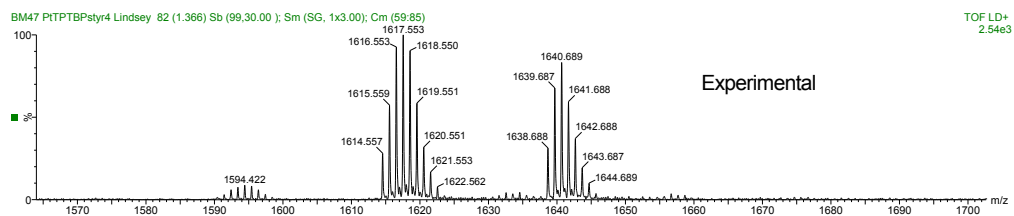
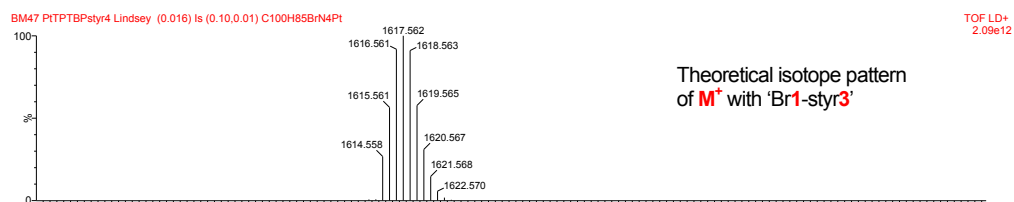
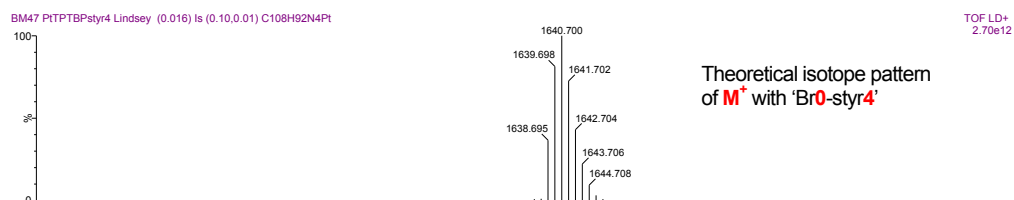
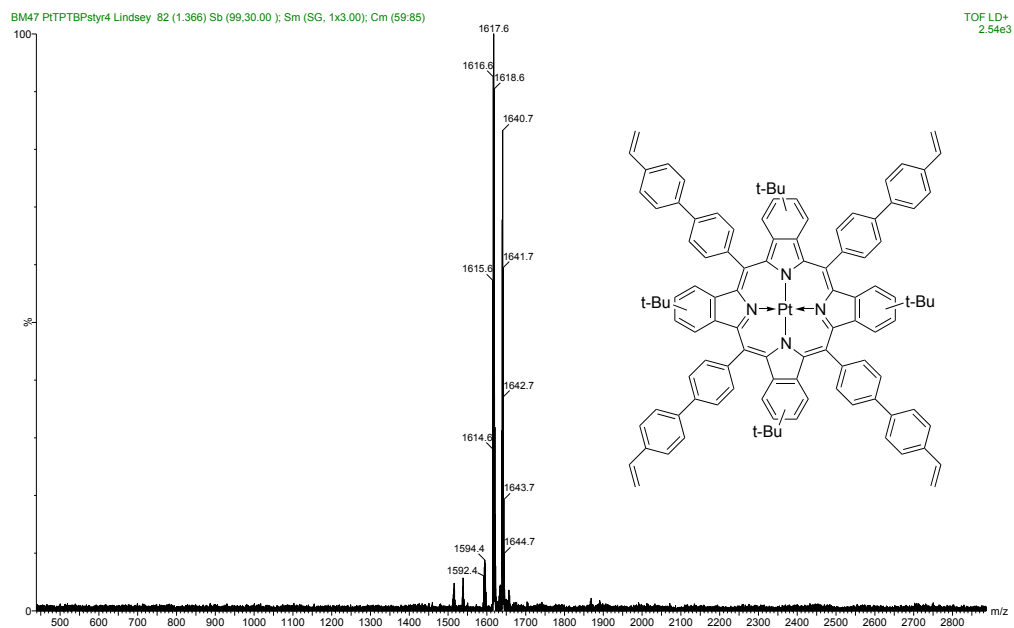
Ionisation: MALDI/Dith





Sample: Pt-TPTBPtBu₄Styr₄

Ionisation: MALDI/DCTB



8.3 List of Chemicals

Chemical	Supplier	CAS-Number
Acetone	Brenntag	67-64-1
Chloroform	Roth	67-66-3
Dichloromethane	VWR	75-09-2
Dichloromethan anhydrous	Sigma-Aldrich	75-09-2
Diethylether	Roth	60-29-7
N,N-Dimethylformamid anhydrous	Sigma-Aldrich	68-12-2
Ethylacetate	VWR	141-78-6
Ethanol	Brenntag	64-17-5
Tetrahydrofuran	VWR	109-99-9
Toluene	VWR	108-88-3
1,2,4-Trimethylbenzene	Sigma-Aldrich	95-63-6
Aluminium oxide neutral, 50-200µm	Acros	1344-28-1
Silica Gel	Acros	112926-00-8
Na ₂ SO ₄ anhydrous	VWR	7757-82-6
Boron trifluoride diethyl etherate	Sigma-Aldrich	109-63-7
Ethylisocyanoacetate	TCI	2999-46-4
Diazabicycloundecen	Sigma-Aldrich	6674-22-2
2,3-Dichlor-5,6-dicyano-1,4-benzochinon	Sigma-Aldrich	84-58-2
KOH 85 %	Roth	1310-58-3
NaNO ₂	Merck	7632-00-0
Na ₂ S ₂ O ₃	VWR	10102-17-7
Na ₂ SO ₃	VWR	7757-83-7
4-Bromophenylacetic acid	Sigma-Aldrich	1878-68-8
4-tert-Butylphthalonitrile	TCI	32703-80-3
HCl 37 %	VWR	7647-01-0
Tetrakis(triphenylphosphin)palladium	ABCR	14221-01-3
4-Vinylbenzeneboronic acid	ABCR	2156-04-9
K ₂ CO ₃	Roth	584-08-7

Chemical	Supplier	CAS-Number	Art.Nr
Polydimethylsiloxane, hydride terminated; visc. 7-10 cSt.	ABCR	70900-21-9	AB146376
(25-35% Methylhydrosiloxane) - dimethylsiloxane copolymer; visc. 25-35 cSt.	ABCR	68037-59-2	AB109380
(50-55% Methylhydrosiloxane) - dimethylsiloxane copolymer; visc. 10-15 cSt.	ABCR	68037-59-2	AB109381
Polydimethylsiloxane, monohydride terminated; visc. 5-9 cSt.	ABCR		AB250915
Polydimethylsiloxane, vinyl dimethylsiloxo terminated; visc. 1000 cSt.	ABCR	68083-19-2	AB109358
Polydimethylsiloxane, vinyl dimethylsiloxo terminated; visc. 100 cSt.	ABCR	68083-19-2	AB109356
(35-45% Trifluoropropylmethylsiloxane)-(dimethylsiloxane) vinyl terminated copolymer; vis. 12000-20000 cSt.	ABCR	68951-98-4	AB289269
Diphenylsiloxane - dimethylsiloxane vinyl terminated copolymer, visc. 500 cSt.	ABCR	68951-96-2	AB114256
Vinyl terminated dimethyl-diphenylsiloxane copolymer, visc. 4000-6000 cSt.	ABCR	68951-96-2	AB130287
Poly(phenylmethylsiloxane), vinyl terminated; visc. 300-600 cSt.	ABCR	225927-21-9	AB127690
Platinum-divinyltetramethyldisiloxane complex; 3-3.5% Platinum in vinyl terminated Polydimethylsiloxane	ABCR	68478-92-2	AB134321

8.4 Abbreviations

Ar	Argon
BB	Backbone
BG comp.	Background Compensation
CH	Cyclohexane
CL	Crosslinker
DBU	Diazabicycloundecen
DCM	Dichloromethane
DDQ	2,3-Dichlor-5,6-dicyano-1,4-benzochinon
DMF	N,N-Dimethylformamid
EE	Ethylacetate
EtOH	Ethanol
hPa	hecto Pascal
K_{SV}	Stern-Volmer Constant
LED	Light Emitting Diode
MALDI-TOF	Matrix-assisted laser desorption/ionization-Time of flight
$\text{Pd}(\text{PPh}_3)_4$	Tetrakis(triphenylphosphine)palladium(0)
$\text{Pt}(\text{BN})_2\text{Cl}_2$	Bis(benzonitrile)dichloroplatinum (II)
Q.Y.	Quantum Yield
RT	Room Temperature
SV	Stern-Volmer
TBA	Tri-n-butylamine
TBP	Tetrabenzoporphyrin
TEA	Triethylamine
THF	Tetrahydrofuran
TMB	1,2,4-Trimethylbenzene
TPTBP	Tetraphenyltetrabenzoporphyrin
UV-Vis	Ultraviolet-Visible
ϵ	Molar extinction coefficient
τ	Lifetime
ϕ	Phaseshift

25-35% MeH	(25-35% Methylhydrosiloxane) - dimethylsiloxane copolymer
50-55% MeH	(50-55% Methylhydrosiloxane) - dimethylsiloxane copolymer
Dihydride	Polydimethylsiloxane, hydride terminated
Monohydride	Polydimethylsiloxane, monohydride terminated
PDMS-1&2	Polydimethylsiloxane, vinyl dimethylsiloxy terminated
PDPDMS-1&2	Diphenylsiloxane - dimethylsiloxane vinyl terminated copolymer
PPMS	Poly(phenylmethylsiloxane), vinyl terminated
PFMDMS	(35-45% Trifluoropropylmethylsiloxane)- (dimethylsiloxane) vinyl terminated copolymer